The Characterization of 3D Printed Plastics Sterilized by Hydrogen Peroxide Vapour

By
Emil-Peter Sosnowski

A thesis submitted to
the Faculty of Graduate Studies
in partial fulfillment of
the requirements for the degree of
Master of Science

Department of Biosystems Engineering
University of Manitoba
Winnipeg, Manitoba

November 2016

Abstract

3D printers that precisely fuse plastic filament are enabling small companies to produce high-quality plastic products. Medical manufacturers apply this technology in the manufacture of custom medical devices and implants. However, the low-temperature plastic fusing process implies that post-production sterilization must also occur at a low temperature or destroy the precision of the pre-sterilized product. This study characterizes the effects of hydrogen peroxide vapour sterilization by a *STERIS® Amsco® V-PRO® maX* sterilizer on ASTM-compliant tensile samples of polylactic acid, polycaprolactone, and polycarbonate. Sterilization effects on the Young's modulus, ultimate tensile strength, and strain at ultimate tensile strength of the plastics were established against control samples. The sterilization process caused permanent physical deformations in polycaprolactone. Additionally, significant increases were observed in polycaprolactone and polycarbonate sample thickness, and in polycarbonate sample width. Furthermore, significant decreases in Young's modulus were found in all three materials, while ultimate tensile strength decreased in polycarbonate, and strain at ultimate tensile strength increased in polycaprolactone. The findings demonstrate that the materials can be considered compatible with hydrogen peroxide vapour sterilization, but products must be designed to accommodate for physical and mechanical changes that occur due to sterilization.

Acknowledgements

I would like to express my deepest gratitude to these individuals who have supported and guided me in my research; without you, I wouldn't have been able to accomplish what I have in my academic career.

- My advisor Dr. Jason Morrison, for providing me with help, guidance, and support over the past several years.
- Dr. David Herbert and Mark Hewko, for their roles as my advisory committee.
- The people at the Orthopaedic Innovation Centre for providing me with space and funding to conduct my research.
- Peter Trokajlo, Jorge Dourado, and the other students in the Herbert and Davis labs, who tolerated my endless questions and cries for help with the GPC.
- Tasneem Vahora, Mack Hayes, and Chris Harrysingh, who helped me get through all of this.
- Dr. Sandra Ingram for lending an ear (on several occasions), and providing valuable advice during difficult times.
- Melissa Rabb and Aaron Simoes for providing a quiet place to work, feedback, and flame-cooked hamburgers.
- Shannon Winters, for her exceptional patience and support.
- My Aunt Danuta, for supporting me during a difficult time in my academic career.
- My Mother and Father, for their unwavering support in my pursuit of knowledge; I'm sure dad would be proud of what I've accomplished.

This work is dedicated to my
Mother and late Father.

Table of Contents

Abstract ... ii

Acknowledgements ... iii

Table of Contents ... v

List of Tables ... vii

List of Figures ... xi

1 Introduction ... 1

1.1 Background ... 1

1.2 Scope and Objectives ... 3

1.3 Thesis Organization ... 4

1.4 Technical Background ... 5

1.4.1 3D Printing Technology ... 5

1.4.2 Applications of 3D Printing in Medicine ... 9

1.4.3 Material Biocompatibility ... 13

2 Literature Review ... 15

2.1 Mechanical Strength of Plastics ... 15

2.1.1 Mechanical Properties ... 15

2.1.2 Effects of Chemical Structure ... 19

2.2 Printable Plastics ... 21

2.2.1 Polylactic Acid ... 22

2.2.2 Polycaprolactone ... 23

2.2.3 Polycarbonate ... 25

2.3 Sterilization in Medical 3D Printing ... 26

2.3.1 Hydrogen Peroxide ... 28

2.3.2 Ethylene Oxide Gas ... 31

2.3.3 Radiation ... 32

2.3.4 Steam Sterilization ... 33

3 Materials and Methods ... 35

3.1 Sample Preparation ... 35

3.1.1 Printing Equipment and Materials ... 35

3.1.2 Test Specimens 36
3.1.3 Bulk Sterilization 39
3.1.4 Sample Conditioning 40
3.2 Image Processing 40
3.3 Mechanical Properties of Samples 41
4 Results 43
4.1 Physical Appearance 43
4.2 Dimensions and Mass 44
4.2.1 Sample Thickness 45
4.2.2 Sample Width 48
4.2.3 Sample Mass 52
4.3 Changes in Mechanical Properties 55
5 Discussion 59
5.1 Physical Changes 59
5.2 Decreases in Mechanical Strength 63
5.3 Designing for Sterilization 65
6 Conclusions and Recommendations 69
References 71
Appendix A 84
Appendix B 100

List of Tables

Table 1. Average thickness of n=10 PLA, PCL, and PC sterilized samples prior to sterilization and prior to conditioning. Standard deviations are reported in parentheses. Comparisons were performed through paired t-tests; bolding indicates statistical significance at the 95% confidence level. 45

Table 2. Average thickness of n=10 PLA, PCL, and PC sterilized samples prior to conditioning and prior to testing. Standard deviations are reported in parentheses. Comparisons were performed through paired t-tests; bolding indicates statistical significance at the 95% confidence level. 46

Table 3. Average thickness of n=10 PLA, PCL, and PC unsterilized control samples prior to conditioning and prior to testing. Standard deviations are reported in parentheses. Comparisons were performed through paired t-tests; bolding indicates statistical significance at the 95% confidence level. 46

Table 4. Average width of n=10 PLA, PCL, and PC sterilized samples prior to sterilization and prior to conditioning. Standard deviations are reported in parentheses. Comparisons were performed through paired t-tests; bolding indicates statistical significance at the 95% confidence level. 49

Table 5. Average width of n=10 PLA, PCL, and PC sterilized samples prior to conditioning and prior to testing. Standard deviations are reported in parentheses. Comparisons were performed through paired t-tests; bolding indicates statistical significance at the 95% confidence level. 49

Table 6. Average width of n=10 PLA, PCL, and PC unsterilized control samples prior to conditioning and prior to testing. Standard deviations are reported in parentheses. Comparisons were performed through paired t-tests; bolding indicates statistical significance at the 95% confidence level. 49

Table 7. Average mass of n=10 PLA, PCL, and PC sterilized samples prior to sterilization and prior to conditioning. Standard deviations are reported in parentheses. Comparisons were performed through paired t-tests; bolding indicates statistical significance at the 95% confidence level. 52

Table 8. Average mass of n=10 PLA, PCL, and PC sterilized samples prior to conditioning and prior to testing. Standard deviations are reported in parentheses. Comparisons were performed through paired t-tests; bolding indicates statistical significance at the 95% confidence level. 53

Table 9. Average mass of n=10 PLA, PCL, and PC unsterilized control samples prior to conditioning and prior to testing. Standard deviations are reported in parentheses. Comparisons were performed through paired t-tests; bolding indicates statistical significance at the 95% confidence level. 53

Table 10. Average of n=10 samples for Young's modulus (E), ultimate tensile strength (σ_{UTS}), and strain at the point of ultimate tensile strength (ε_{UTS}) in PLA, PCL, and PC. Statistically significant values from an ANOVA at a 95% confidence are bolded. 58

Table 11. Regression results for n=10 PLA sample thickness and width measurements. Standard errors are reported in parentheses; *, ** indicate statistical significance at the 95% and 99% confidence levels, respectively. 66

Table 12. Regression results for n=10 PCL sample thickness and width measurements. Standard errors are reported in parentheses; *, ** indicate statistical significance at the 95% and 99% confidence levels, respectively. 67

Table 13. Regression results for n=10 PC sample thickness and width measurements. Standard errors are reported in parentheses; *, ** indicate statistical significance at the 95% and 99% confidence levels, respectively. 68

Table 14. Initial dimensional measurements of PLA tensile samples, in accordance with Figure 7. Samples that were to be sterilized are identified in grey. 84

Table 15. Initial dimensional measurements of PCL tensile samples, in accordance with Figure 7. Samples that were to be sterilized are identified in grey. 85

Table 16. Initial dimensional measurements of PC tensile samples, in accordance with Figure 7. Samples that were to be sterilized are identified in grey. 86

Table 17. Measured mass, thickness, and width of PLA samples, pre-sterilization. Samples that underwent sterilization are identified in grey. 87

Table 18. Measured mass, thickness, and width of PLA samples, pre-conditioning. Samples that underwent sterilization are identified in grey. 88

Table 19. Measured mass, thickness, and width of PLA samples, pre-testing. Samples that underwent sterilization are identified in grey. 89

Table 20. Measured mass, thickness, and width of PCL samples, pre-sterilization. Samples that underwent sterilization are identified in grey. 90

Table 21. Measured mass, thickness, and width of PCL samples, pre-conditioning. Samples that underwent sterilization are identified in grey. 91

Table 22. Measured mass, thickness, and width of PCL samples, pre-testing. Samples that underwent sterilization are identified in grey. 92

Table 23. Measured mass, thickness, and width of PC samples, pre-sterilization. Samples that underwent sterilization are identified in grey. 93

Table 24. Measured mass, thickness, and width of PC samples, pre-conditioning. Samples that underwent sterilization are identified in grey. 94

Table 25. Measured mass, thickness, and width of PC samples, pre-testing. Samples that underwent sterilization are identified in grey. 95

Table 26. Young's modulus (E), ultimate tensile strength (σ_{UTS}), and strain at the point of ultimate tensile strength (ε_{UTS}) in PLA, as found through tensile testing. Samples that underwent sterilization are identified in grey. Average values for the control and sterilized samples are identified, with their corresponding p-values from an ANOVA. 96

Table 27. Young's modulus (E), ultimate tensile strength (σ_{UTS}), and strain at the point of ultimate tensile strength (ε_{UTS}) in PCL, as found through tensile testing. Samples that underwent sterilization are identified in grey. Average values for the control and sterilized samples are identified, with their corresponding p-values from an ANOVA. 97

Table 28. Young's modulus (E), ultimate tensile strength (σ_{UTS}), and strain at the point of ultimate tensile strength (ε_{UTS}) in PC, as found through tensile testing. Samples that

underwent sterilization are identified in grey. Average values for the control and sterilized samples are identified, with their corresponding p-values from an ANOVA. 98

Table 29. *STERIS® Amsco® V-Pro® maX* 'lumen cycle' chamber temperatures and pressures. The different stages of sterilization are separated by table shading. 99

List of Figures

Figure 1. FDM printers frequently begin by outlining objects, before filling them in with material. This example of a common raster fill is extruded in a back-and-forth pattern at a 45º angle (top), and is reversed for the following layer, producing an internal lattice structure within the object (bottom). Adapted from Agarwala et al. (1996). 7

Figure 2. Engineering stress-strain curve. The Young's Modulus, *E*, is shown as the slope of the elastic portion of the curve. The proportional limit, in blue, is the point at which the material is no longer elastic, and the material reaches its yield point, σ_Y, and ε_Y; some materials display a clearly-defined yield point, as seen from the red dotted portion of the curve. If yield must be calculated using the offset yield method, a line is drawn parallel to the elastic portion of the curve, offset by a chosen percentage of strain (often 0.2%), as shown by the green dotted line. The point ultimate tensile strength, σ_{UTS}, in red, is the point of maximum engineering stress before material failure. Strain at ultimate tensile strength, ε_{UTS}, is the measurement of strain at the point of ultimate tensile strength. Adapted from ASM International (2002). 18

Figure 3. The chemical structure of PLA. The ester group (red) is responsible for PLA's susceptibility to hydrolysis. Adapted from Engelberg and Kohn (1991). 23

Figure 4. The process of hydrolytic breakdown in PCL. In the presence of water, PCL degrades into low molecular weight chains. When *in vivo*, sufficiently shortened chains are consumed by macrophages, within which they are further broken down by acetyl coenzyme A. The molecular remnants are then eliminated from the body. Adapted from Woodruff and Hutmacher (2010). 24

Figure 5. The chemical structure of tyrosine-derived polycarbonate. The carbon-oxygen double bonds provide resistance to hydrolysis; components of the carbonate group, including the geminal ether groups (-O-), are identified in red, while the carbonyl group is identified in green. Adapted from Hooper, Cox, and Kohn (1997). 26

Figure 6. H_2O_2 vapour sterilization cycle. These systems require multiple cycles of liquid H_2O_2 injection, to ensure that sterilant concentration remains sufficient within the decontamination chamber. Adapted from Hultman et al. (2007). 30

Figure 7. An ASTM D638-Type IV tensile test sample. Key dimensions include gage width, $W_C = 6 \pm 0.05$ mm, length of narrow section, $L = 33 \pm 0.5$ mm, gage length, $G = 25 \pm 1.3$ mm, overall width, $WO = 19 + 6.4$ mm, overall length, LO = minimum 115 mm, and thickness, $T = 3.2 \pm 0.4$ mm (ASTM, 2013). 37

Figure 8. PCL (left) and PLA (right) samples were printed on a *Stratasys® Mojo™* 3D printer in batches of four samples at a time on Garolite, due to size limitations of the printer. 38

Figure 9. Top, Initial photograph of a PC sample; bottom, PC sample photograph, after perspective correction and sharpening transformations in ImageJ. This correction was carried out for the purposes of measurement collection. 41

Figure 10. Left, colour difference between PLA samples that were unsterilized control (top), and sterilized (bottom); right, PCL material deformation occurred in the sterilized samples (bottom), which was not present in the control samples (top). ... 44

Figure 11. Changes in PLA sample thickness at each stage of measurement, for the unsterilized control and sterilized samples. Average change is above each boxplot, with standard deviation reported in parentheses. Comparisons were performed through paired t-tests; an asterisk indicates statistical significance at the 95% confidence level. 47

Figure 12. Changes in PCL sample thickness at each stage of measurement, for the unsterilized control and sterilized samples. Average change is above each boxplot, with standard deviation reported in parentheses. Comparisons were performed through paired t-tests; an asterisk indicates statistical significance at the 95% confidence level. 47

Figure 13. Changes in PC sample thickness at each stage of measurement, for the unsterilized control and sterilized samples. Average change is above each boxplot, with standard deviation reported in parentheses. Comparisons were performed

through paired t-tests; an asterisk indicates statistical significance at the 95% confidence level. 48

Figure 14. Changes in PLA sample width at each stage of measurement, for the unsterilized control and sterilized samples. Average change is above each boxplot, with standard deviation reported in parentheses. Comparisons were performed through paired t-tests; an asterisk indicates statistical significance at the 95% confidence level. 50

Figure 15. Changes in PCL sample width at each stage of measurement, for the unsterilized control and sterilized samples. Average change is above each boxplot, with standard deviation reported in parentheses. Comparisons were performed through paired t-tests; an asterisk indicates statistical significance at the 95% confidence level. 51

Figure 16. Changes in PC sample width at each stage of measurement, for the unsterilized control and sterilized samples. Average change is above each boxplot, with standard deviation reported in parentheses. Comparisons were performed through paired t-tests; an asterisk indicates statistical significance at the 95% confidence level. 51

Figure 17. Changes in PLA sample mass at each stage of measurement, for the unsterilized control and sterilized samples. Average change is above each boxplot, with standard deviation reported in parentheses. Comparisons were performed through paired t-tests; an asterisk indicates statistical significance at the 95% confidence level. 54

Figure 18. Changes in PCL sample mass at each stage of measurement, for the unsterilized control and sterilized samples. Average change is above each boxplot, with standard deviation reported in parentheses. Comparisons were performed through paired t-tests; an asterisk indicates statistical significance at the 95% confidence level. 54

Figure 19. Changes in PC sample width at each stage of measurement, for the unsterilized control and sterilized samples. Average change is above each boxplot, with standard

deviation reported in parentheses. Comparisons were performed through paired t-tests; an asterisk indicates statistical significance at the 95% confidence level. 55

Figure 20. Engineering stress-strain curve, identifying the positions of ε_1 and ε_2 that define the linear region used to calculate Young's modulus (*E*). 56

Figure 21. Average stress-strain curves of n=10 unsterilized control and sterilized PC samples. The control curve is a solid line, while the sterilized curve is dashed. *E* is linearly regressed for the unsterilized control (blue), and sterilized (red, dashed) samples. Coloured dots represent the point of UTS for the unsterilized control (blue) and sterilized (red) stress-strain curves. 63

Figure 22. First PLA sample batch, printed Feb 5, 2016. 100

Figure 23. Second PLA sample batch, printed Feb 8, 2016. 100

Figure 24. Third PLA sample batch, printed Feb 8, 2016. 100

Figure 25. Fourth PLA sample batch, printed Feb 8, 2016..... 101

Figure 26. Fifth PLA sample batch, printed Feb 9, 2016. 101

Figure 27. First PCL sample batch, printed Jan 10, 2016. 101

Figure 28. Second PCL sample batch, printed Jan 11, 2016. 102

Figure 29. Third PCL sample batch, printed Jan 12, 2016. 102

Figure 30. Fourth PCL sample batch, printed Jan 13, 2016. 102

Figure 31. Fifth PCL sample batch, printed Feb 4, 2016..... 103

Figure 32. PC samples, printed Feb 25, 2016. 103

Figure 33. PC samples, printed Feb 25, 2016; close-up of sample 1..... 104

Figure 34. PC samples, printed Feb 25, 2016; close-up of samples 2 and 3. 104

Figure 35. PC samples, printed Feb 25, 2016; close-up of samples 3, 4, and 5. 105

Figure 36. PC samples, printed Feb 25, 2016; close-up of samples 5, 6, and 7. 105

Figure 37. PC samples, printed Feb 25, 2016; close-up of samples 6, 7, and 8. 106

Figure 38. PC samples, printed Feb 25, 2016; close-up of samples 9, 10, and 11. 106

Figure 39. PC samples, printed Feb 25, 2016; close-up of samples 11, 12, and 13. 107

Figure 40. PC samples, printed Feb 25, 2016; close-up of samples 13, 14, and 15. 107

Figure 41. PC samples, printed Feb 25, 2016; close-up of samples 16, 17, and 18. 108

Figure 42. PC samples, printed Feb 25, 2016; close-up of sample 19..... 108

Figure 43. PC samples, printed Feb 25, 2016; close-up of sample 20..... 109

1 Introduction

The topic of this thesis is to investigate the effects of sterilization on biocompatible, printable thermoplastics. The goal is to aid in the development of sterile 3D printing guidelines and practices. More specifically, the presented research investigates the effects of hydrogen peroxide vapour sterilization on the physical and mechanical properties of 3D printed polylactic acid, polycaprolactone, and polycarbonate. The results prove that this method of sterilization affects the size, mass and mechanical performance of some plastics.

This chapter introduces the role of 3D printing in the medical device manufacturing sector, the importance of sterility, and considerations that must be made when sterilizing plastics. The scope and objectives of this research are also outlined, and the layout of the thesis is described. Lastly, a technical overview of 3D printing, the role of this technology in the medical field, and the mechanisms of material biocompatibility are presented.

1.1 Background

Materials engineering researchers have developed plastics for use in medical applications (Langer & Tirrell, 2004). These developments have led to significant increases in material strength, durability, and biocompatibility (Langer & Tirrell, 2004). As a result, these materials have seen use in new and innovative medical applications: including medical device mould production, soft tissue replacements, artificial hearts, and joint implants (Langer & Tirrell, 2004; Peppas & Langer, 2014). A number of these materials have just begun to be used in medical manufacturing and in 3D printing, which for the purposes of this thesis are processes that produce 3D objects through deposition of one layer at a time (Boland et al., 2007; Dimitrov, Schreve, & Beer, 2006).

The medical manufacturing industry has strict regulations on the sterility of manufactured goods. This is critical because the presence of microbial pathogens and other contaminants could negatively impact human life through tissue inflammation, infection, or even death (FDA, 2008). Traditionally, a wide variety of sterilization methods have been applied to medical devices, such as the application of dry or moist heat, application of ethylene oxide gas, gamma radiation, or chemical agents, in addition to a number of other non-conventional approaches (FDA, 2008). This variety of techniques allows for application-specific sterilization to ensure efficacy of the process and reduce unintended side effects on the device.

When addressing plastic manufacturing, it has been important to consider the effects of the sterilization procedure on the material properties of the product. High-temperature sterilization methods may result in material damage due to the inherent thermal sensitivity of most plastics, and as such, should be avoided (Rutala & Weber, 2008). Numerous low-temperature sterilization techniques exist, but each contains drawbacks that may negatively impact the performance of the material, or harm the patient when used *in vivo* (Gorna & Gogolewski, 2003b; Peniston & Choi, 2007; Woodruff & Hutmacher, 2010). Due to the difficulties that are involved with identifying material specific sterilization techniques, the research literature has identified that the medical device manufacturing industry is in need of evaluation guidelines for the effects of sterilization on material performance (Brown, Merritt, Woods, McNamee, & Hitchins, 2002). The lack of general guidelines for sterilization compatibility in conventional medical device manufacturing is an issue that extends into the 3D printing community. Material extrusion-based printing processes require elevated temperatures for material deposition dur-

ing printing, often these temperatures are high enough to sterilize the material during the manufacturing process (Boland et al., 2007). However, the research literature has shown that this is not always sufficient, creating a need for post-print sterilization of these medical devices (Kondor et al., 2013; Rankin et al., 2014).

1.2 Scope and Objectives

The scope of this thesis focuses on the effects that hydrogen peroxide vapour sterilization has on the physical and mechanical properties of medical-grade 3D printed plastics: polylactic acid, polycaprolactone, and polycarbonate. This technique of sterilization is a low-temperature method that sees widespread use (Johnston, Lawson, & Otter, 2005). The three plastics studied are all commonly used thermoplastics in 3D printing, and were selected due to their biocompatibility and thus their suitability for use in medical applications.

As discussed, the research literature has identified a need for sterilization compatibility guidelines for 3D printed devices. As such, the objectives of this study are to identify changes to the physical and mechanical properties of the plastics as a result of sterilization. Specifically, this study will identify if hydrogen peroxide sterilization causes:

1) Physical changes in appearance, dimensions, and mass of the 3D printed samples.
2) Mechanical changes in elasticity, ultimate tensile strength, and strain at ultimate tensile strength of the 3D printed samples.

The hypothesis of this research is that physical and mechanical changes will occur as a result of sterilization, but can be accommodated for during the design process.

1.3 Thesis Organization

This thesis has been broken into several thematic chapters typical in the reporting of experiments. This introductory chapter outlines the context of the research, gives an initial description of the research performed and the structure of the thesis document. Finally this chapter provides technical background on 3D printing, its use in medicine and biocompatibility.

Chapter 2 reviews the research literature pertaining to 3D printing, biocompatible plastics, and sterilization. Specifically, the chapter introduces and describes the properties of the biocompatible polymers studied in this thesis. Lastly, the chapter discusses the low-temperature sterilization of plastic, and emphasizes the lack of specific guidelines for sterilizing plastic medical devices produced through 3D printing.

Chapter 3 discusses the materials and experimental methods applied to execute this thesis research. The chapter specifically describes: the production of tensile test specimens; their sterilization; their pre-test conditioning; and the collection of physical and mechanical property data.

Chapter 4 presents the results of the thesis research. The chapter begins by identifying physical changes in sample appearance, thickness, width, and mass. It concludes with details of the changes in sample Young's modulus, ultimate tensile strength, and strain at ultimate tensile strength comparing sterilized and non-sterilized samples.

In Chapter 5, discusses the causes for the observed changes in physical and mechanical performance of the materials. Additionally, a series of predictive mathematical models are presented that will allow medical device designers to accommodate for some dimensional changes due to sterilization.

Lastly, the conclusion summarizes the results, discusses the implications of the presented research, and comments on related future research.

1.4 Technical Background

This section provides a general background to 3D printing in medicine. A general description of the 3D printing process is provided, followed by an overview of documented applications of the technology in medicine. Lastly, some sufficient conditions of material biocompatibility are discussed.

1.4.1 3D Printing Technology

Three-dimensional (3D) printing, as referred to throughout this thesis, is a collection of manufacturing technologies that produce physical objects layer-by-layer through computer-guided material deposition. Several approaches to material deposition exist, with the most common being: stereolithography (SLA), selective laser sintering (SLS), and fused deposition modelling (FDM) (Dimitrov et al., 2006).

Upcraft and Fletcher (2003) explain that SLA utilizes a movable horizontal platform in a container of liquefied plastic resin, and a laser that can solidify the resin. The platform is raised until a thin layer of liquefied plastic has pooled on top of it, after which the laser outlines and fills-in a thin layer of the object that is being printed. Once the layer is complete, the platform lowers, and the printing process repeats until all layers have been produced. The completed product is a physical object, made entirely of the resin solidified together within the pool.

SLS operates in a similar fashion to SLA, except that it uses powdered materials instead of liquid resins (Upcraft & Fletcher, 2003). With this technology, an arm slides

across a material powder bed, spreading a thin layer of material over a build platform. An overhead laser then 'sinters' (i.e., partially melts) the powdered particles together to form the shape and fill in a layer of the object that is being printed. With each successive layer, the build platform is lowered until the object is finished. SLS is a versatile technology that can be used with both plastic materials or metals (Upcraft & Fletcher, 2003).

FDM technology differs from SLA and SLS, in that material is extruded into the build area from an external source, as opposed to the build area being immersed in raw material (Masood, 1996). With FDM, plastic or composite filament is fed from a spool to an extruder, where the material is heated close to or past its melting point and pushed through a nozzle. Material is deposited onto a tray for each layer, after which the tray is lowered in preparation for the next layer and the process repeats until the object is completed (Bagsik & Schöoppner, 2011; Masood, 1996). In order to ensure adhesion of the object to the build area, some manufacturers utilize disposable trays (Hiemenz, 2011). Reusable build trays are also common, but may require the use of an adhesive to adhere the printed object to the tray (Fonda, 2013, p. 52).

For each of these three approaches to 3D printing, the thickness of each layer is dependent upon the ability of the printer to resolve material. For SLA and SLS, layer thickness is determined by the size and power of the laser used to fuse material, and varies from machine to machine (Upcraft & Fletcher, 2003). With FDM, layer thickness is determined by the size of the filament extrusion nozzle, which also varies between machines (Ahn, Montero, Odell, Roundy, & Wright, 2002). In some instances, extrusion nozzle size can be adjusted (Agarwala et al., 1996).

Prior to printing, a 3D model of the object is produced and exported as a stereolithographic (.stl) file. This file converts the model into a series of triangles and 3D coordinates for positioning model features in space (Wong & Hernandez, 2012). The resultant model can be scaled to a desired size, oriented to different axes, duplicated, and positioned in space, before finally being sliced into layers (Masood, 1996). During slicing, a laser or filament extruder movement path, or toolpath, is generated for the production of each layer. These layer-specific toolpaths typically first outline the layer before filling it in. This layer filling process is known as a raster fill (Agarwala et al., 1996), and an example is given in Figure 1. On many printers, the raster fill pattern and space between deposited material can be customized (Agarwala et al., 1996; Bagsik & Schöoppner, 2011). After computing the path for the extruder, commonly referred to as the toolpath, the printer references the position of the model in virtual space with locations on a build tray and can begin the printing process.

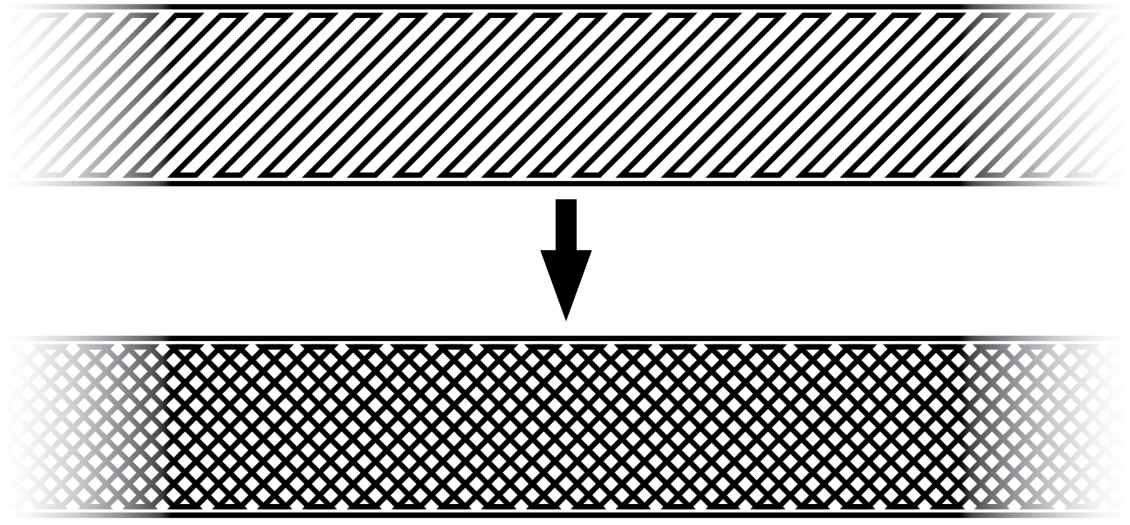

Figure 1. FDM printers frequently begin by outlining objects, before filling them in with material. This example of a common raster fill is extruded in a back-and-forth pattern at a 45º angle (top), and is reversed for the following layer, producing an internal lattice structure within the object (bottom). Adapted from Agarwala et al. (1996).

Upcraft and Fletcher (2003) discuss that each approach to 3D printing has advantages and disadvantages. Objects with complex geometries that are produced through SLA often require the use of structures to support components that are suspended in space. Additionally, the resins used in the SLA printing process are toxic and require special storage and handling processes, thus making the technology impractical for many applications (Upcraft & Fletcher, 2003). SLS benefits from having an abundance of rigid materials to print from, such as ceramics and metals, and does not rely on the use of support structures or secondary support materials to the same degree as SLA. However, SLS printers are typically large, expensive, and the technology produces products that are porous, with rough surface finishes (Upcraft & Fletcher, 2003).

Upcraft and Fletcher (2003) identify FDM as being the most attainable 3D printing technology. The authors found that FDM machines are typically compact and inexpensive, and have a wide variety of available materials to print with. Furthermore, FDM printing processes do not require the use of toxic resins, making them suitable for use in most workplaces (Upcraft & Fletcher, 2003). However, FDM has been criticized for its susceptibility to internal defects from excess material dropping between layers, over- or under-extrusion (Bellini & Guceri, 2003), rough surface finishes, the need for support structures (Groth, Kravitz, Jones, Graham, & Redmond, 2014), void production and air entrapment during the layer filling process (Agarwala et al., 1996). Additionally, a study carried out by Kim, Shin, and Ahn (2016) found that FDM-manufactured products are susceptible to water absorption through diffusion. The authors identified that FDM-produced products can absorb on 17 to 23 times more water than their injection-moulded counterparts due to the prevalence of voids within the samples. Despite these shortcom-

ings, FDM has become a popular method of 3D printing because of the low risk, low cost, and overall accessibility of the technology (Groth et al., 2014).

1.4.2 Applications of 3D Printing in Medicine

3D printing technology has found numerous applications in the medical manufacturing sector. Both Dimitrov et al. (2006) and Ventola (2014) discuss that the technology has been applied in the design of surgical aids to increase the speed and accuracy of surgical procedures. The authors explained that patient models could be acquired through medical imaging, and then quickly and inexpensively printed to scale. The use of 3D printing allows printed models to be used as visual aids in surgical procedure planning, fracture fixation device preparation, or the test fitting of orthopaedic implants. This technology is valuable in providing aid in the operating theatre, but it also shows promise in both the large- and small-scale medical manufacturing industries.

Medical Devices

The engineering design process is a cycle of information gathering, problem definition, production, and evaluation, until a satisfactory solution to the problem can be selected. The process is inherently iterative, in that it relies on the development of models and prototypes to evaluate a proposed design (Pahl & Beitz, 2013 p. 17). As discussed previously, 3D printing has proven itself as a valuable tool in the development of models, from which parallels can be drawn with product prototyping.

Within manufacturing industries, the use of 3D printing in the design process continues to be referred to as rapid prototyping, and has been used in medical device manufacturing (Ventola, 2014; Webb, 2000). Chua, Leong, and Lim (2010, p. 423-4) discuss a case study, where Baxter Healthcare utilized the technology in the development of biopsy

needle housings. The company integrated 3D printing into their product development process by printing different production mould designs for the housings, allowing for comparative testing before investing in a design and advancing further along the design process. Baxter Healthcare benefitted from this by being able to quickly implement design changes, reducing the amount of time between iterations and ultimately streamlining the design process.

The benefits of this technology have also expanded into rapid production of custom medical devices. A case study by Rankin et al. (2014) explores the successful use of rapid prototyping of custom surgical tools. The authors develop and used FDM to print a single-use surgical retractor, which is a common tool used in tissue retraction after incisions are made, and explore its suitability in an operating theatre. The custom tool was ready for use in only 90 minutes, and was found to be strong enough to withstand prolonged use during surgery.

Implants and Prosthetics

The orthopaedic and dental industries have similarly applied 3D printing technology in the production of custom internal implants and external prosthetics. A study conducted by Singare et al. (2009) applies 3D printing in the production of a custom jaw implant for a patient who had survived oral cancer. Similar to the design and production of custom surgical models, the authors used computed tomography (CT) to acquire anatomical patient models, after which a mould for a custom fit jaw implant was printed in titanium. The authors discuss that the process of designing the model allows for surgical planning and simulation. Furthermore, installation of the implant is similar to a bone segment fixation procedure due to the high quality of fit achieved with the custom implant. These

findings are echoed by Banks (2013), who explores the application of direct 3D printing of patient-specific hip replacements and cranial plates. The author explains that the technology is versatile enough to create porous microstructures on the implant fixation points, allowing for osseo-integration once implanted. Other documented applications of the technology with the production of internal implants include the repair of femoral bone, hip and knee joints, and even cartilage (Harrysson, Hosni, & Nayfeh, 2007; Jiankang, Dichen, Bingheng, Zhen, & Tao, 2006; Webb, 2000). Specific applications in tissue engineering are discussed in the following subsection.

In the design of external prosthetics, 3D printing has proven itself to be a valuable technology. Webb (2000) discusses early use of the technology in the production of prosthetic ears from silicone rubber. In this case study, a model was acquired through CT imaging and electronically sliced into 22 pieces. Each piece was machined, glued together, and hand finished to form a prosthetic for the patient. The technology has advanced significantly since the ear was produced, as models for an external prosthetic can now be acquired through 3D laser scanning (Shuxian, Wanhua, & Bingheng, 2005) that are then available to be printed into casting moulds.

Tissue Engineering

Regenerative medicine faces a number of problems pertaining to the availability of tissues that could be used for transplantation. A large, aging population, coupled with low donor availability causes difficulties for those requiring organ transplants (Fedorovich, Alblas, Hennink, Öner, & Dhert, 2011; Ventola, 2014). Additionally, there exist numerous risks associated with organ transplants, ranging from infection to complete organ rejection (Hutmacher, 2000). The field of tissue engineering remains dedicated to resolv-

ing a number of these issues, through the development and production of artificial tissues and organs (Sachlos & Czernuszka, 2003). 3D printing now sees use in this capacity, through the production of tissue scaffolds needed for artificial organ production and the direct printing of organic tissues (Hutmacher, 2000).

Organic tissues cannot grow into complex three-dimensional shapes without a porous substructure, or scaffold, to support them (Sachlos & Czernuszka, 2003). 3D printers can be used to produce scaffolds of complex geometries, allowing for cell proliferation into shapes resembling organs of interest. Additionally, production of these scaffolds can be done with biodegradable materials that slowly break down once the tissue or organ has formed (Hutmacher, 2000). To complement 3D printable scaffold production, the direct printing of cellular tissues has recently become feasible. Ventola (2014) discusses the production of a heart valve, articular cartilage, as well as an artificial liver through the printing of stem cells. While the application of this technology is still in its infancy, it has shown great promise.

Drug Delivery Devices

3D printing technology also presents a number of capabilities not seen in conventional manufacturing, such as the ability to control material composition on a layer-by-layer basis. This level of material control has been of interest to the pharmaceutical manufacturing industry, as it has been applied in the production of printable, biodegradable drug-infused plastic tablets (Sharke, 2001). Such an association allows versatility in drug delivery, enabling controlled, uniform distribution of a drug throughout a tablet, or a concentration gradient that can control drug elution over time (Dimitrov et al., 2006; Nagarajan & Reddy, 2009). This technology is expected to lead to tablets with personal-

ized doses, long-term drug delivery, and even combinations of multiple medications into a single tablet (Ventola, 2014).

1.4.3 Material Biocompatibility

Biocompatibility is defined by Williams (2003) as "the ability for a material to perform with an appropriate host response in a specific application." For a material to comply with this definition, it must remain inert when interacting with the human body, *in vivo*. Woodruff and Hutmacher (2010) explain that an immune response could be triggered if a material were to release low molecular weight particles through degradation or elute impurities during biodegradation. A study by Woodward et al. (1985) found that the resultant shortened molecular chains of *in vivo* degraded poly(ε-caprolactone) are consumed by white blood cell macrophages, further broken down through intracellular processes, and are eventually eliminated from the host. The foreign-body responses seen in that study only occur once the material byproducts degrade to between 10 to 80 μm in size, allowing for consumption by macrophages. Additionally, the rate of intracellular breakdown is rapid, resulting in a transient immune response (Woodward et al., 1985). Woodruff and Hutmacher (2010) explain that this intracellular processing rate can be influenced by blood vessel access or metabolic activity of surrounding tissues. Regions that are highly vascular and offer good metabolic activity can process byproduct breakdown at a faster rate, indicating that response and processing rates vary throughout the body. As such, the biocompatible designation for a material is dependent on its ability to produce little to no inflammation due to immune responses at multiple sites within the body (Pulkkinen et al., 2009). In order to decrease the likelihood of an acute *in vivo* immune response, the vas-

cular anatomy where the component would interact is considered along with the selection of chemically inert materials (Shastri, 2003; Woodruff & Hutmacher, 2010).

Biocompatibility is not always material-dependent, primarily due to physiological and hence biochemical variations between individuals. In many instances, material-independent factors such as age, gender, level of overall health, lifestyle, or even the process of medical device implantation play a role in the chemical inertness of implantable devices (D. F. Williams, 2008). For the purposes of this thesis, biocompatibility is addressed from a purely materials standpoint, regardless of influences due to other physiological and sociological factors.

2 Literature Review

The literature reviewed in this thesis pertains to the mechanical and chemical properties of polylactic acid, polycaprolactone, and polycarbonate (the chemical structures of these materials can be seen in Figures 3, 4, and 5 respectively), and their compatibility with common sterilization techniques. Additionally, the need for adequate sterility guidelines in medical 3D printing is discussed.

2.1 Mechanical Strength of Plastics

Plastic strength is dependent on several internal and external factors. Plastics are composed of repeating molecular structures that differ in chemical properties such as molecular weight, composition, structure, and chain orientation. These intrinsic chemical properties can also be influenced externally, through ambient temperature, pressure, material age, and exposure to moisture, which can contribute to differences in performance of otherwise identical materials (Landel & Nielsen, 1993).

2.1.1 Mechanical Properties

Material tensile testing is a commonly used to evaluate the mechanical response/performance of plastics (Brown et al., 2002; Gorna & Gogolewski, 2003b; Szelest-Lewandowska, Masiulanis, Szymonowicz, Pielka, & Paluch, 2007). In these tests, a force is exerted uniaxially along the length of the sample and material displacement in this direction is recorded. This force and displacement data is used as the basis of calculating material stress and strain. Young and Budynas (2002) define stress as the "internal force per unit area exerted on a specified surface." To calculate stress, the force, F, is divided by the cross-sectional unit area of the sample, A. With this definition,

the engineering stress, σ, is found if the initial cross-sectional area measurement, A_0, is used for all stress calculations, as can be seen in Equation (1) (Beer & Johnston, 1985, p. 37). Some ductile materials may change in cross-sectional area during loading; with these materials, true stress, σ_τ, can be found. True stress differs from engineering stress in that it considers a dynamically changing cross-sectional area, A_τ, in the calculation, as seen in Equation (2) (Beer & Johnston, 1985, p. 37).

$$\sigma = \frac{F}{A_0} \tag{1}$$

$$\sigma_\tau = \frac{F}{A_\tau} \tag{2}$$

When stress is exerted along the axis of an object, the object undergoes axial loading (Beer & Johnston, 1985, p. 4). If an axial load pulls away from the surface of an object, then the object is in tension. On the contrary, if the load pushes towards the surface, the object is in compression. The stresses associated with axial tensile and compressive loading are therefore designated tensile and compressive stresses (Young & Budynas, 2002, p. 824).

Strain is a measure of the change in sample dimensions due to stress. Engineering strain, ε, is measured as the ratio of total material displacement, δ, to the initial length of the sample, L_0, as seen in Equation (3) (Beer & Johnston, 1985, p. 38). True strain, ε_τ, differs from engineering strain in that it considers all successive changes seen in sample length with each measurement. The incremental changes in sample length at each measurement are divided by total sample length, L, and are integrated over the total change in length, as seen in Equation (4).

$$\varepsilon = \frac{\delta}{L_0} \tag{3}$$

$$\varepsilon_\tau = \int_{L_0}^{L} \frac{dL}{L} = \ln \frac{L}{L_0} \tag{4}$$

While true stress and true strain provide more accurate representations of the stresses and strains seen in a material, they require precise measurements of cross-sectional areas and length that are continuously recorded the duration of the test. Beer and Johnston (1985, p. 38) explain that engineering stress and strain are commonly used, because the collection of initial cross-sectional area, A_0, and initial length, L_0, is straight-forward.

The relationship between stress and strain is unique in every material, and can be graphed in what is known as a stress-strain curve. Stress-strain curves allow for other material properties to be found, as seen in Figure 2. Many materials exhibit some degree of elasticity, which is a property that describes the ability of the material to resist permanent physical deformation when stressed (Beer & Johnston, 1985, pp. 38-9). The maximum stress and strain that a material can withstand while still remaining elastic is known as its proportional limit, after which the material yields plastically. Up until the proportional limit, the ratio of stress and strain that a material exhibits when deforming elastically is known as the Young's modulus, *E* (Young & Budynas, 2002, p. 819). The yield point is the portion of a stress-strain curve where stress and strain no longer increase linearly and permanent physical deformation begins to occur (Young & Budynas, 2002, p. 826). As additional stress is applied past this point, the material continues to deform through the stretching, movement, and change in orientation of its internal molecular

structures, creating irreversible (i.e., plastic) changes to the molecular structure of the material. With additional stress/strain, plastic flow occurs in the material, and the strength of the material begins to decrease with increasing strain (Bartczak, 2005). The maximum engineering stress that the material can sustain before complete material failure is known as the ultimate tensile strength, σ_{UTS} (Young & Budynas, 2002, p. 825); the strain measured at ultimate tensile strength is denoted as ε_{UTS}, after which material hardening cannot occur with added strain (Nikbin, 2009, p. 128). The location of these values on a stress-strain curve can be found in Figure 2.

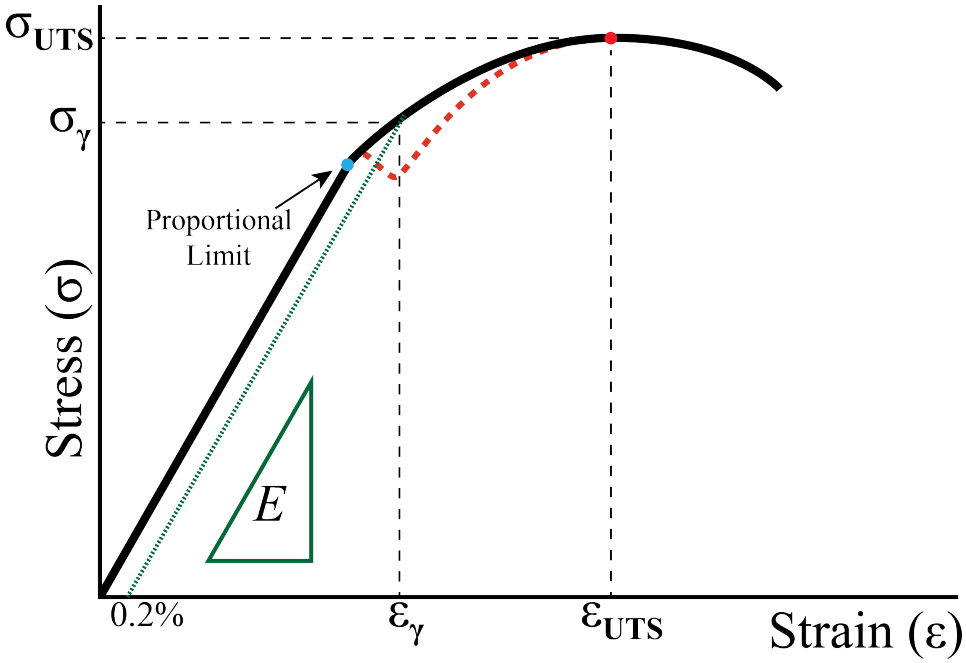

Figure 2. Engineering stress-strain curve. The Young's Modulus, *E*, is shown as the slope of the elastic portion of the curve. The proportional limit, in blue, is the point at which the material is no longer elastic, and the material reaches its yield point, $\boldsymbol{\sigma_\gamma}$, and $\boldsymbol{\varepsilon_\gamma}$; some materials display a clearly-defined yield point, as seen from the red dotted portion of the curve. If yield must be calculated using the offset yield method, a line is drawn parallel to the elastic portion of the curve, offset by a chosen percentage of strain (often 0.2%), as shown by the green dotted line. The point ultimate tensile strength, $\boldsymbol{\sigma_{UTS}}$, in red, is the point of maximum engineering stress before material failure. Strain at ultimate tensile strength, $\boldsymbol{\varepsilon_{UTS}}$, is the measurement of strain at the point of ultimate tensile strength. Adapted from ASM International (2002).

Some materials transition smoothly from elastic to plastic deformation, without a clearly identified yield point. In these cases, yield can be found through the offset yield method. In this method, *E* is linearly regressed from an offset location on the x-axis, often 0.2%, and the point where the regressed line intersects with the stress-strain curve is deemed the yield point, as seen in Figure 2 (Beer & Johnston, 1985, p. 36). This method is of significant use when measuring the mechanical properties of ductile materials, such as many metals (Brinson & Brinson, 2008, p. 24; Eshraghi & Das, 2010), but material property comparisons of plastics can be difficult due to a wide range of offset recommendations; the research literature has identified offsets ranging from 0.2% to as high as 10% (Eshraghi & Das, 2010; Fernández, Larrañaga, Etxeberria, Wang, & Sarasua, 2014; Hutmacher et al., 2001; Kurtz et al., 1998).

2.1.2 Effects of Chemical Structure

Plastics are classified as polymers, which differ from metals and ceramics due to their long-chained macromolecular structures. At the molecular level, polymers consist of repeating chemical subunits that are covalently bonded together, forming long molecular chains. The length of these chains dictate molecular weight, which in turn influences properties such as strength, and thermal stability (Meijer & Govaert, 2005). These properties are also influenced by the degree of crystallinity, or organization of the chains within the polymer matrix. Plastics that are highly amorphous exhibit little order in chain positioning, whereas crystalline plastics are highly organized (Brinson & Brinson, 2008, p.16). Furthermore, external treatments to many plastics, such as sterilization or coating, can result in moisture uptake or changes to their molecular structures. Such treatments can potentially lead to hydrolysis, the generation of radicals, or crosslinking.

The thermal stability of a plastic is determined by its glass transition and melting temperatures (Brinson & Brinson, 2008, p. 80). The glass transition temperature (T_g) is the temperature at which the amorphous polymer chains become mobile within the polymer matrix (Ravve, 2012, pp. 22-3). At this temperature, thermal expansion of the material results in an increase in space for molecular vibrations, leading to mobility (Brinson & Brinson, 2008, pp. 81-2). Physically, a plastic is hard and brittle below T_g, and becomes soft and ductile above T_g. Brinson and Brinson (2008, p. 80-2) explain that the melting temperature (T_m) is higher than T_g. At this temperature, the bonds responsible for retaining order in the crystalline polymeric structures are broken. As a result, the crystalline structures become amorphous, and the material enters a fluid-like state. The T_g and T_m of a plastic can be affected by molecular chain length (Meijer & Govaert, 2005) or by the presence of plasticizers, which are additives that can increase chain mobility through direct chain interaction (Brinson & Brinson, 2008, p. 59; Massey, 2005, pp. 394-5).

Water is a known plasticizer in many polymers (Levine & Slade, 1988, pp. 79-80). With increasing moisture content, chain mobility increases in the amorphous regions of some polymers (Levine & Slade, 1988, p. 91), leading to a decrease in T_g and E (M. Chanda and S. Roy & Raton, 2007, p. 104). Additionally, some plastics are susceptible to swelling in response to moisture absorption (Sharp, Forrest, & Jones, 2001). Moisture can also lead to material degradation through hydrolysis. Hydrolysis is a process where water reacts with polymer chains and through scission, produces shortened molecular chains (Woodruff & Hutmacher, 2010). Similarly, some treatments can create radicals in the backbone of a polymer chain by knocking valence electrons out of the outer shells of the affected atom (International Union of Pure and Applied Chemisty, 2014; Tamboli,

Mhaske, & Kale, 2004). This can generate highly reactive chemical structures that are susceptible to further polymerization. In some instances, radical generation can lead to chain scission, or bonding between adjacent polymer chains. This bonding can form highly intertwined networks of branched polymers, in a process known as crosslinking. Crosslinking produces physical resistances between intertwined molecular chains when in tension, through a combination of chain bonding, branching and entanglement (Tamboli et al., 2004). It also prevents chain reptation, which is a snake-like sliding movement that linear chain components could experience within the polymeric matrix (de Gennes, 1971). When a material consists of shorter, unbranched molecular chains, it is less likely to experience entanglement, and is therefore more prone to reptation and permanent material deformation (de Gennes, 1971; Meijer & Govaert, 2005; Narkis, Raiter, Shkolnik, Siegmannz, & Eyerer, 1987). To quantify the performance of polymers with different chemical structures, the field of materials science evaluates mechanical properties, such as stress, strain, and elasticity.

2.2 Printable Plastics

Plastics are classified as either thermoplastics or thermosets, depending on the amount of crosslinking that exists in the material (Brinson & Brinson, 2008, p. 55; Rauwendaal, 2014, p. 1). Thermoplastics are typically ductile because they contain little molecular crosslinking, while thermosets are hard and brittle due to high crosslinking into complex networks. Thermoplastics by definition melt when heated, and can be reformed to take different shapes without chemical change. Thermosets will not melt when heated (Dodiuk & Goodman, 2013, p. 1), but may instead break down due to chemical change (Brinson & Brinson, 2008, p. 240). As discussed in Section 1.4.1, the basic principle be-

hind 3D printing with FDM is to heat a plastic to fluid-like state, use pressure to extrude it onto a surface and enable it to fuse with the materials around it as it cools to solid state again. In order for material extrusion with FDM to be possible, thermoplastics must be used for printing (Rauwendaal, 2014, p. 1). Common non-biodegradable thermoplastics that are used for medical device manufacturing include polycarbonate (PC), polyethylene, polymethylmethacrylate, polypropylene, and polytetrafluoroethylene (Schohn, Jahn, Eber, & Hauptmann, 1986; Shastri, 2003). Numerous biocompatible, biodegradable thermoplastics exist, but polylactic acid (PLA), and polycaprolactone (PCL) are two of the most commonly used in medical applications (Armentano, Dottori, Fortunati, Mattioli, & Kenny, 2010; Nair & Laurencin, 2007). This research focuses on the use of PLA, PCL, and PC in 3D printing, because they range of strengths and eleasticities, while being biocompatible and readily available to the 3D printing industry.

2.2.1 Polylactic Acid

PLA is a naturally derived polyester that is both biocompatible and biodegradable (Drumright, Gruber, & Henton, 2000). The *in vivo* degradation process of PLA breaks the material into oligomers through hydrolytic breakdown of the ester bonds present in its chemical structure, as seen in Figure 3. The process is influenced by temperature, moisture content, and pH of the surrounding fluids (Drumright et al., 2000; Weir, Buchanan, Orr, Farrar, & Boyd, 2004). The biodegradability of this material has proven useful in the design of medical devices that may otherwise require surgical retrieval, such as sutures, tissue scaffolds, and fracture fixation devices (Kontakis, Pagkalos, Tosounidis, Melissas, & Katonis, 2015; Weir et al., 2004). PLA melts at a temperature of approximately 180 ºC, which decreases if defects or other compounds are present in the material

(Drumright et al., 2000; Garlotta, 2002). The article by Drumright et al. (2000) details an examination of PLA's mechanical properties. The authors identify that the material lacks ductility and has both a high Young's modulus (E) and ultimate strength of 3,500 MPa and 53 MPa, respectively. A study by Engelberg and Kohn (1991) found that E varies with weight-average molecular weight (M_w), ranging from 1,200 to 3,000 MPa for samples with M_w 50,000 to 300,000. The authors found that tensile strength increases from 28 to 50 MPa between M_w 50,000 and 100,000, but does not increase in E from M_w 100,000 to 300,000; these results are indicative of a strong correlation between molecular chain length and tensile strength in PLA.

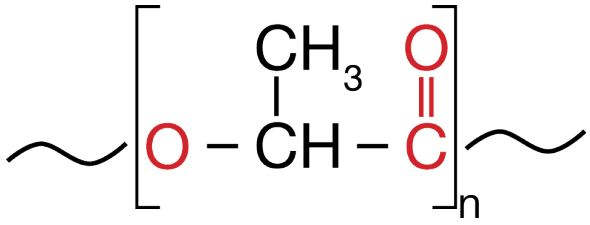

Figure 3. The chemical structure of PLA. The ester group (red) is responsible for PLA's susceptibility to hydrolysis. Adapted from Engelberg and Kohn (1991).

2.2.2 Polycaprolactone

PCL is a biocompatible and biodegradable polyester, with a wide range of applications in the medical manufacturing industry. This plastic is unique in that it has low T_g and T_m of -60 ºC and 59 to 64 ºC respectively, and is highly reformable due to its semi-crystalline structure (Woodruff & Hutmacher, 2010). These properties result in PCL's use in both tissue engineering and drug delivery systems. Specifically, the low T_g and T_m allow the material to remain highly ductile at internal body temperatures, making it ideal in the design of soft tissue scaffolds (Ulery, Nair, & Laurencin, 2011). The ductility seen in PCL is indicative of a low E, which Engelberg and Kohn (1991) note as only being 400 MPa.

PCL is useful in flexible applications, and limited in load-bearing applications due to its low tensile strength and high fracture strain (Gorna & Gogolewski, 2003a).

PCL breaks down through hydrolytic chain scission through ester cleavage, forming shorter oligomers and monomers. When the degradation of PCL takes place *in vivo*, the shortened chains are further processed and excreted through enzymatic pathways, as shown in Figure 4 (Woodruff & Hutmacher, 2010). Additionally, PCL degrades very slowly, which has been exploited in the design of long-term drug delivery systems that may need to remain functional *in vivo* for upwards of one year (Middleton & Tipton, 2000; Woodruff & Hutmacher, 2010). These properties are useful in the design of medical devices where time-dependent material degradation is desired, such as flexible sutures, fracture fixation devices, dental grafts, and contraceptive devices (Cottam, Hukins, Lee, Hewitt, & Jenkins, 2009; Woodruff & Hutmacher, 2010).

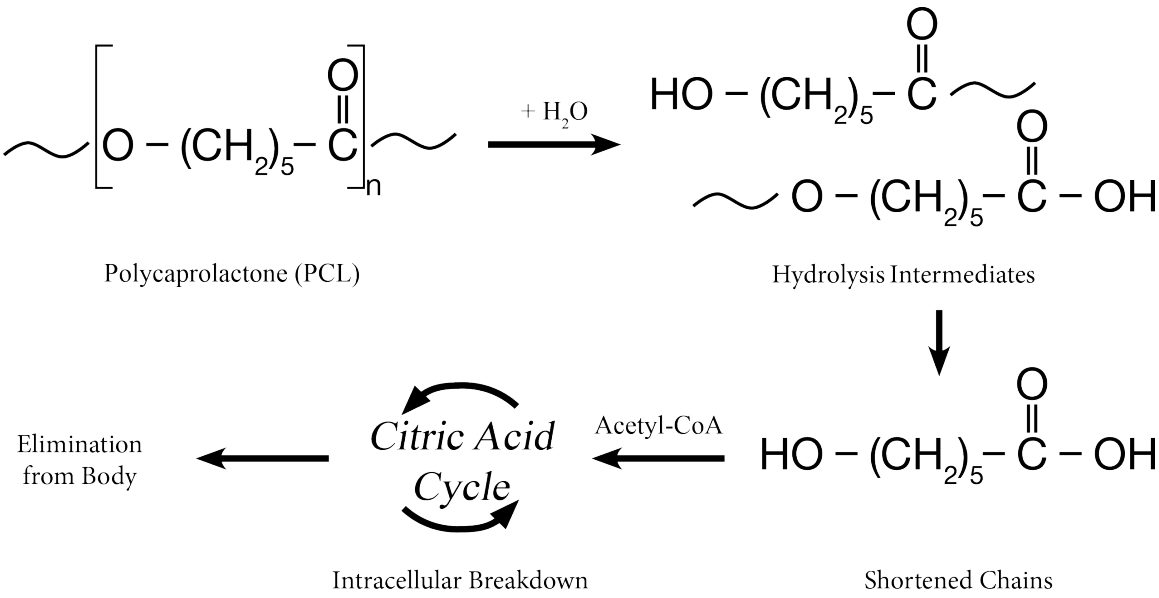

Figure 4. The process of hydrolytic breakdown in PCL. In the presence of water, PCL degrades into low molecular weight chains. When *in vivo*, sufficiently shortened chains are consumed by macrophages, within which they are further broken down by acetyl coenzyme A. The molecular remnants are then eliminated from the body. Adapted from Woodruff and Hutmacher (2010).

2.2.3 Polycarbonate

PC is a thermoplastic that is used in the design of medical devices (Sastri, 2010, p. 129), and is characterized by its high T_m range of 220 to 260 ºC (Martienssen & Warlimont, 2005, p. 504). The carbonate groups present in the chemical structure of PC make the polymer susceptible to hydrolytic breakdown in the presence of moisture (Senden, Engels, Söntjens, & Govaert, 2012). Ulery et al. (2011) discuss that variants of PC suitable for *in vivo* medical device design are derived from tyrosine. Tyrosine-derived PCs release biocompatible byproducts during material degradation, which are similar to those found in amino acids. Despite the susceptibility of PC to degradation, this material exhibits better resistance to hydrolysis than most biodegradable plastics due to the stability of carbonyl and geminal ether groups (see Figure 5) present in its chemical structure (Ulery et al., 2011).

PC has been praised for its excellent mechanical properties, thermal stability, biocompatibility, and ability to adsorb fluids; some hydrophilic variants of the material have been designed specifically to adsorb blood, plasma, and other bodily fluids (Dempsey et al., 2014; Szelest-Lewandowska et al., 2007). A study carried out by Engelberg and Kohn (1991) found that tyrosine-derived PC is fairly rigid, exhibiting an E of 1,630 MPa, and tensile strength of 40 MPa. With these properties, PC sees use in the design of a wide range of medical devices, including tissue scaffolds (Helsen & Missirlis, 2010, pp. 272-3), prosthetics (Webb, 2000), dialysis filters (Sastri, 2010, p. 129), and infusion equipment (Massey, 2005, p. 81).

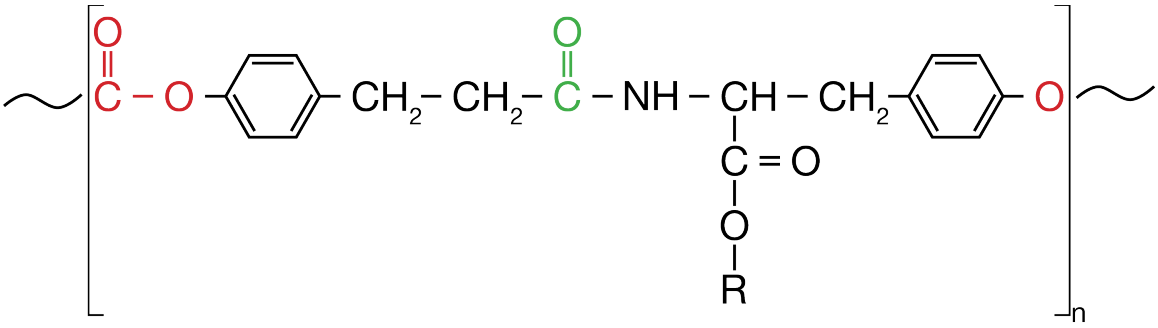

Figure 5. The chemical structure of tyrosine-derived polycarbonate. The carbon-oxygen double bonds provide resistance to hydrolysis; components of the carbonate group, including the geminal ether groups (-O-), are identified in red, while the carbonyl group is identified in green. Adapted from Hooper, Cox, and Kohn (1997).

2.3 Sterilization in Medical 3D Printing

Medical devices must be sterilized, because the presence of microbial pathogens and pathogenic byproducts can lead to tissue inflammation, infection, or even death (Rutala & Weber, 2008). Regulatory bodies of the medical manufacturing industry have imposed numerous guidelines and regulations to ensure that manufactured goods remain sterile (FDA, 2008). As such, these guidelines are relied on heavily in the reprocessing of reusable devices, in addition to new and single-use devices (Greene, 1986). Common regulatory body-approved sterilization methods include exposure to steam or dry heat, gamma irradiation, ethylene oxide (EO) gas, and hydrogen peroxide (H_2O_2) (FDA, 2008; Moisan et al., 2001). Each method aims to achieve terminal sterility in the object, despite interacting with the materials in different ways. However, the research literature identifies that these guidelines lack adequate evaluations on the effects of sterilization on material performance, specifically with devices manufactured through 3D printing (Brown et al., 2002).

Rankin et al. (2014) hypothesized that the high material extrusion temperatures are sufficient to produce sterile, pathogen-free surgical tools, but reported evidence against

such a hypothesis. Device sterility was tested in accordance with Food and Drug Administration (FDA) protocols, identifying that only 92% of the printed devices were free of microbial activity. This implies that sterility was not achieved in the remaining 8% of the 3D printed devices, and suggests the need for post-print sterilization to ensure device sterility. However, some properties of these products that are not typically associated with conventional manufacturing practices introduce a number of other complications.

When addressing sterility in plastic products, the selection of an appropriate sterilization technique is important, as some materials are less thermally stable than others and can be physically deformed when sterilized (Rutala & Weber, 2008). A guideline document produced for the Centre for Disease Control (CDC) suggests that dry heat sterilization be carried out at 170 ºC for 60 minutes to ensure medical device sterility (Rutala & Weber, 2008). While the melt temperatures (T_m) for printing PLA and PC are typically higher than this, these materials are only at this temperature for a brief period of time, and would therefore not meet CDC sterility guidelines (Ho, Cheung, & Gibson, 2002; Nair & Laurencin, 2007). Furthermore, the T_m for PCL is less than 60 ºC, suggesting that the process of printing with these materials would not meet sterility regulations (Nair & Laurencin, 2007).

Defects associated with 3D printing (see Section 1.4.1) could result in unintended subsurface sterilant penetration from surface-limited chemical sterilization techniques (Lee et al., 2008; Lucas et al., 2003). Additionally, a rough surface finish presents a larger surface area exposed to sterilant, potentially leading to an increased rate of material degradation (Lam, Savalani, Teoh, & Hutmacher, 2008). With 3D printing gaining popularity in the medical manufacturing sector, products that undergo sterilization could be

more susceptible to changes in material strength than those produced through conventional means. As such, the following sections introduce a number of common sterilization techniques, and review the literature pertaining to their suitability with PLA, PCL, and PC.

2.3.1 Hydrogen Peroxide

H_2O_2 is a chemical sterilant that is capable of breaking down into water and oxygen (French et al., 2004). H_2O_2 sterilization operates in a low temperature range of 25 to 45 ºC (Chung, Kern, Koukol, Barengoltz, & Cash, 2008; Feldman & Hui, 1997); H_2O_2 is not gaseous at room temperature, and instead functions as an effective sterilant in either plasma or vapour form (Bathina et al., 1998; Hultman, Hill, & McDonnell, 2007). Objects that undergo H_2O_2 plasma sterilization are packed in a flexible bag that is permeable to the sterilant, then placed in a sealed chamber (Feldman & Hui, 1997). As explained by Feldman and Hui (1997), the chamber undergoes gaseous evacuation in order to remove moisture, typically down to approximately 0.04 kPa, after which a small amount of liquid H_2O_2 is introduced. The chamber is then heated up to between 40 and 45 ºC while the pressure is decreased, allowing the liquid H_2O_2 to evaporate. The sterilant is given enough time to diffuse throughout the chamber, ensuring that all contents come into contact with the vapour. Lastly, radio-frequency energy is released from an electrode into the chamber, exciting the vapourized H_2O_2 into a plasma state (Feldman & Hui, 1997). This energy ionizes the H_2O_2, creating radicals within the chamber that kill living cells by reacting with their metabolic contents (Bathina et al., 1998; Feldman & Hui, 1997).

H_2O_2 is also inherently antiseptic when kept in liquid form or as a high-concentration gas. As such, H_2O_2 vapour sterilization systems operate on the principal of

sterilizing through direct exposure to a high-concentration H_2O_2 (Klapes & Vesley, 1990). Hultman et al. (2007) explain that a mixture of high-concentration H_2O_2 and water, often up to 52%, is added to a flash vapourizer, where a heating surface rapidly heats the mixture to the point of simultaneous evaporation of both liquids. Through rapid heating, the resultant gas vapour is maintained at a concentration approximate to the initial liquid concentration of H_2O_2. As with plasma sterilization, the gas vapour is then injected into a low-pressure sealed chamber, maintained between 25 to 45 ºC (Chung et al., 2008). The vapour cycles within the chamber, sterilizing all surfaces through direct contact, before finally being evacuated from the chamber (Hultman et al., 2007). Hultman et al. (2007) make note that a complication with this process is that gaseous H_2O_2 is unstable and decomposes into oxygen and water over time. This breakdown causes a gradual decrease in concentration, and therefore sterilization efficacy. To address this, H_2O_2 vapour sterilizers are designed to perform several cycles of flash vaporization and injection, as seen in Figure 6. This ensures that the H_2O_2 concentration remains relatively constant. H_2O_2 vapour sterilization offers the benefits of high efficacy and use of a sterilant that is safer than other chemical sterilants (French et al., 2004), so it has become a common technique in medical equipment decontamination (Johnston et al., 2005).

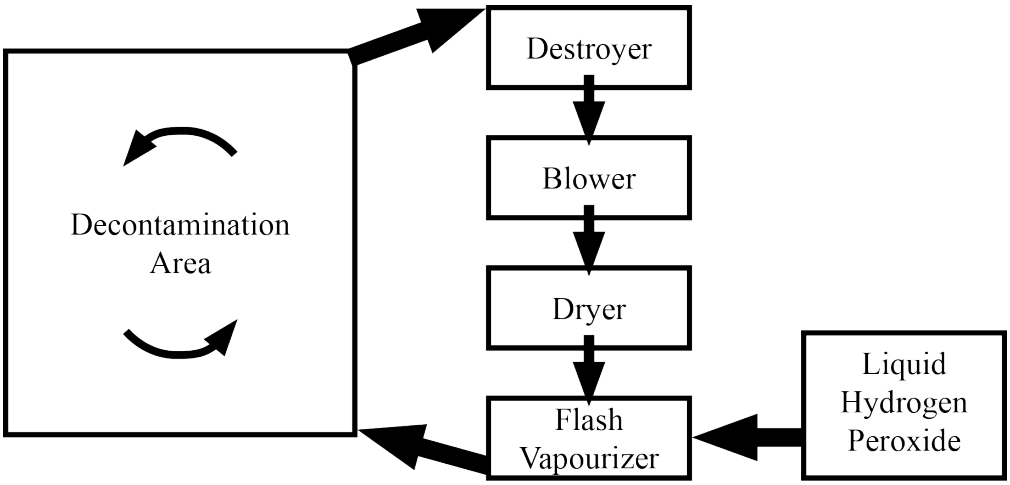

Figure 6. H_2O_2 vapour sterilization cycle. These systems require multiple cycles of liquid H_2O_2 injection, to ensure that sterilant concentration remains sufficient within the decontamination chamber. Adapted from Hultman et al. (2007).

A long-term study conducted by Peniston and Choi (2007) found that exposure of H_2O_2 plasma to PLA causes a slight increase in its molecular weight. This change suggests that cross-linking of the polymeric chains occurs as a result of plasma-phase H_2O_2 free radicals bombarding the surface of the material, which generates free radicals from the polymer chains. The authors also found that the samples undergo a slight increase in T_g and decrease in elongation to break, which can be attributed to physical aging due to the long-term duration of the study. Gorna and Gogolewski (2003a) examined the effects of H_2O_2 plasma on several PCL variants, identifying changes in tensile strength, E, and material strain. The authors' findings are varied, including a decrease in tensile strength and E of one variant by 7.5% and 11% respectively, and an increase in another variant by 2% and 30% respectively. Lastly, a study by Feldman & Hui (1997) found that PC has good compatibility with H_2O_2 plasma as a result of short-term exposure.

2.3.2 Ethylene Oxide Gas

Ethylene oxide (EO) gas sterilization is the most prevalent low-temperature sterilization method, with sterilizers of this type comprising approximately half of the industrial sterilization market (Lambert, Mendelson, & Craven, 2011). EO sterilization is antimicrobial, antifungal, and antiviral, as it reacts with the proteins, DNA and RNA within microorganisms (Kubyshkina et al., 2011). EO is flammable, toxic, and has a boiling point of 11 ºC, enabling sterilization at an operating temperature of 40 to 50 ºC. Objects intended for EO sterilization are packed into a container that is permeable to EO gas, which is then placed into a sealed sterilization chamber. Here, steam is added until a relative humidity (RH) of 60% to 80% is reached. EO gas is then introduced into the chamber, where the EO-steam mixture is kept for a period of time sufficient to sterilize the contents of the chamber. The gas is then evacuated out of the chamber, and its contents are aerated within the chamber (Anderson et al., 2008, p.757). Adequate post-sterilization aeration is of importance with this technique, as carcinogenic EO residues can be difficult to remove from porous materials (Lucas et al., 2003; Middleton & Tipton, 2000). Additionally, EO sterilization cycles can often take several days, and the costs associated with equipment procurement, maintenance, consumables, and personnel training are higher than with other sterilization methods (Adler, Scherrer, & Daschner, 1998).

Researchers have reported different results on the effects of EO exposure on PLA, PCL, and PC. A study carried out by Hooper et al. (1997) found that EO exposure has no noticeable effects on the chemical, physical, or mechanical properties of PLA. To contrast this, a study by Weir, Buchanan, Orr, Farrar, and Boyd (2004) found that PLA increases in T_g. A study exposing PCL to EO gas found that the temperature of the process

is high enough to result in material softening and plastic flow of PCL samples, despite EO being classified as a low-temperature sterilization method (Woodruff & Hutmacher, 2010). Hooper et al. (1997) also explored the effects of EO gas sterilization on different variants of PC, and found that the materials do not change significantly in physical appearance, molecular weight, or strength. However, it was noted that one variant containing an octyl functional group in its molecular structure saw a slight increase in material degradation over time.

2.3.3 Radiation

Exposure to gamma rays or accelerated electrons are basis of popular radiation based sterilization methods (Lambert et al., 2011). These low-temperature methods rely on ionizing radiation to penetrate through the surfaces of materials, breaking organic chemical bonds found within pathogens that may be on either the surface or the interior of the material. This ultimately results in both internal and external sterility. However, this process can generate radicals, as discussed in Section 2.1.2, which react with some polymers and result in chain scission, crosslinking, subsurface oxidation and a change in material strength (Gorna & Gogolewski, 2003b).

When exposed to electron-beam radiation, PLA decreases in water permeability and average molecular weight, and increases in T_g (Nugroho, Mitomo, Yoshii, & Kume, 2001; Park, 2011). Gamma irradiation produces similar results, wherein PLA decreases in molecular weight with increasing radiation dose, and decreases in both E and maximum strain at catastrophic failure (Hooper et al., 1997). For PCL, both Filipczak et al. (2006) and Cottam et al. (2009) found that gamma irradiation decreases the average molecular weight, and increases its compressive E and yield stress. Similarly, both

Middleton and Tipton (2000) and Weber, Vecchio, and Suarez (2010) found that irradiating PC results in chain scission, causing a decrease the average molecular weight of the material and increase in brittleness.

2.3.4 Steam Sterilization

Steam sterilization is the most widespread sterilization method in medical device reprocessing (Agalloco, Akers, & Madsen, 2004). This method achieves terminal sterility by exposing objects to high temperature steam, often between 121 to 132 ºC, for a prolonged period of time (Rutala & Weber, 2008). This method is popular in medical settings because it is effective, non-toxic, and easy to control, but cannot be applied to every material (Rutala & Weber, 2008). Rutala and Weber (2008) discuss that the moisture involved in the sterilization process may cause corrosion or rust in devices containing untreated or low-carbon steel. Additionally, the high temperature of sterilization may result in physical deformation or chemical change, such as thermosetting, in devices containing plastics (Brown et al., 2002; Rutala & Weber, 2008).

Despite PLA having a print temperature well above the temperature at which steam sterilization is carried out at, previous research has found that the material decreases in strength as a result of hydrolysis from this method (Rozema et al., 1991). Other studies determined that PCL should not be steam sterilized, as its inherently low melting point would result in severe material deformation (Armentano et al., 2010; Woodruff & Hutmacher, 2010). Similar to PLA, PC has a T_g and T_m that are high enough to resist physical deformation due to material melting when steam sterilized (Senden et al., 2012). However long-term or cyclic exposure to this method causes embrittlement in PC due to

hydrolysis of the carbonate groups in the chemical structure of the material (Pryde & Hellman, 1980; Schilling, Ringo, Sloane, & Bovey, 1981; Senden et al., 2012).

3 Materials and Methods

In this section of the thesis, an introduction to the specific materials used in the experiment is presented, followed by descriptions of test specimen production, preparation, and testing. All production, preparation, and testing was done in accordance with ASTM standards D638 (Standard Test Methods for Tensile Properties of Plastics) and D618 (Standard Practice for Conditioning Plastics for Testing).

3.1 Sample Preparation

To test the mechanical properties of materials, tensile samples needed to be produced. This subsection describes the specific details of the 3D printed plastics studied in this thesis, as well as the printers used to produce samples. Additionally, the specific processes of sample production, sterilization, and sample conditioning are explained.

3.1.1 Printing Equipment and Materials

The materials examined in this experiment were PLA, PCL, and PC. The PCL and PLA were experimental, research-grade materials, each containing 1% gentamicin antibiotic by weight, with filament diameter of 1.3 mm (Petrak & Rodgers, 2015). These two materials were used with a *Stratasys® Mojo™* 3D printer, which has a 5 in x 5 in x 5 in build envelope. The PC was a generic consumer-grade material (trade name of PC-ISO) with filament diameter of 1.75 mm. PC was used with a *Stratasys® Fortus™ 400mc* printer, which has a 16 in x 14 in x 16 in build envelope. To ensure parity of all samples, 0.178 mm diameter extrusion nozzles were used with both machines. Each material used new nozzles to prevent material contamination.

The PLA and PCL samples produced on the *Mojo*™, were printed directly onto a smooth Garolite build sheet, purchased from McMaster-Carr® Supply Company. This sheet was affixed to a standard *Mojo*™ build tray using J-B Weld® polyurethane epoxy. To ensure adhesion to the sheet, a thin layer of Elmer's® Glue-All™ was uniformly applied to the Garolite. The PC samples produced on the *Fortus*™ *400mc* were printed to an acrylic sheet, and required the use of *Stratasys® SR-30* support material to adhere.

Prior to printing, all material was stored in sealable polypropylene bags with silica gel desiccant in them, to limit environmental degradation effects on the materials. Additionally, the print material was handled with powder-free nitrile disposable gloves when being transported outside of their containment bags, loaded into the printers, and fed to the material extruders.

3.1.2 Test Specimens

The design and fabrication of the tensile samples followed ASTM standard D638 as closely as possible (ASTM, 2013). As discussed in Section 2.2.2, PCL has a low Young's modulus (E) and is therefore classified as a semirigid plastic, whereas PLA and PC are both considered rigid (ASTM, 2012). Standard D638 requires that dimensions for a Type IV (Figure 7) sample must be used when comparing materials that differ in rigidity classification. A model matching this sample type was produced in *Dassault Systèmes SOLIDWORKS® 2015* and exported to a .stl (stereolithography) file. This file was scaled, oriented in space, duplicated and sliced in *Stratasys® Insight™ 10.1* and *Control Center™ 10.1*. Additionally, files destined for print on the *Mojo*™ were modified to ensure that no support material would be used.

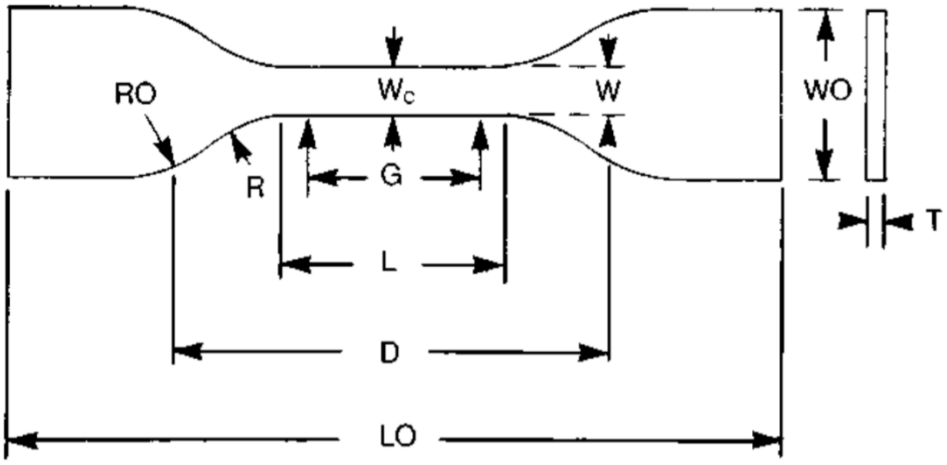

Figure 7. An ASTM D638-Type IV tensile test sample. Key dimensions include gage width, W_C = 6 ± 0.05 mm, length of narrow section, L = 33 ± 0.5 mm, gage length, G = 25 ± 1.3 mm, overall width, WO = 19 + 6.4 mm, overall length, LO = minimum 115 mm, and thickness, T = 3.2 ± 0.4 mm (ASTM, 2013).

To meet the replicate requirements of ASTM D638, twenty samples of each type were produced, with half destined for sterilization. Due to the size constraints of the build envelope of the *Mojo*™, only four samples could be produced per print cycle, as seen in Figure 8; printing was completed through five cycles. The *Fortus*™ *400mc* was able to produce all twenty samples at once.

The *Mojo*™ required that the extrusion and build chamber temperatures be defined for the PLA and PCL materials prior to print. Through the recommendations of a Stratasys® technician, twenty PCL samples were printed first, extruded at 80 ºC, with a build chamber temperature of 30 ºC, followed by twenty PLA samples, which were extruded at 190 ºC, with a chamber temperature of 40 ºC. The *Fortus*™ *400mc* was limited in its software adjustability and information display, so the extrusion and build chamber temperatures used to print the PC samples are not known and unconfigurable.

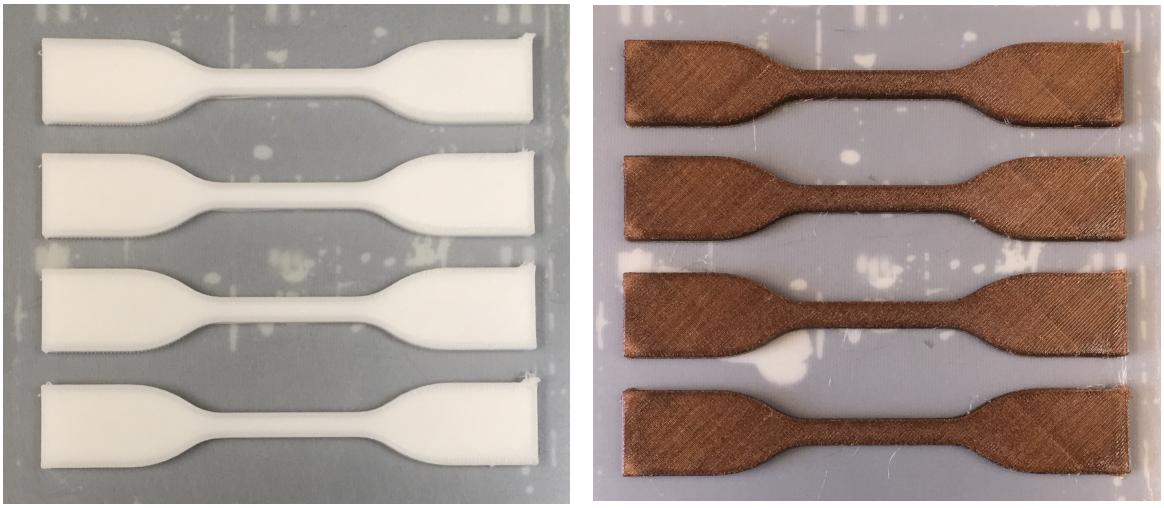

Figure 8. PCL (left) and PLA (right) samples were printed on a *Stratasys® Mojo*™ 3D printer in batches of four samples at a time on Garolite, due to size limitations of the printer.

Once printed, all samples were photographed, separated from their build trays, and had any adhesive removed from their undersides as applicable. Post-print sample photographs can be seen in Appendix B. The PLA and PCL samples had excess material built up at the location where extrusion for each layer began and ended, which resembled material flashing from an injection moulding process. This 'start and stop' point was located at a corner of one of the sample grip sections, and was consistent throughout each sample. This excess material was trimmed away with a razor, as it was deemed to be in a location that would not have any impact on the results of a tensile test.

The samples were all numbered at the ends of the grip sections with a black marker to indicate sample number, and batch number, if applicable. They were then weighed, and measured in accordance with ASTM D638; the thickness width was measured along the gage section at three separate locations. These measurements were averaged to produce single thickness and width measurements that would then be used for all subsequent

calculations. Once measured, all samples were in new cardboard boxes, which were labeled for their respective material.

3.1.3 Bulk Sterilization

Half of the samples of each material were selected at random for sterilization. For PLA and PCL, this was done by randomly selecting half the samples for each batch. The samples destined for sterilization were placed in a stainless steel basket, separated based on material, and samples within each material were arranged randomly; care was taken to ensure that adjacent samples were spaced sufficiently to avoid contact. Both the basket and samples were handled using powder-free nitrile gloves, to prevent potential contamination.

Once arranged in the basket, the samples were then loaded into a *STERIS® Amsco® V-PRO® maX* H_2O_2 vapour sterilizer, loaded with a new, unused cup of 52% concentration sterilant (STERIS Corporation, 2011). The sterilizer was set to 'lumen cycle', which exposed the samples to four cycles 0.13 kPa of pressure, at approximately 50 ºC over 28 minutes. Specifics of the sterilization cycle can be seen in Table 29 of Appendix A, and referred to in the *STERIS® Amsco® V-PRO® maX* operator manual (STERIS Corporation, 2011).

Upon completion of the sterilization cycle, the basket was removed from the chamber, and the samples were given an opportunity to cool to room temperature. Once cooled, the sterilized samples were weighed, and measured for gage thickness and width, as per ASTM D638, before being stored in unused cardboard boxes, separate from their unsterilized control counterparts.

3.1.4 Sample Conditioning

Prior to tensile testing, the tensile samples were conditioned on a material-by-material basis in accordance with ASTM D618, specifying sample exposure at 23 ± 2 ºC and 50 ± 10% RH, for 40 hours. The samples were conditioned in a Pyrex® 10.5L non-vacuum conditioning chamber, containing a saturated calcium nitrate tetrahydrate constant humidity solution, which exposed the samples to 52% RH at 22 ºC (Wexler, 2016, p. 33). An *Onset® HOBO® U12-011* data logger monitored temperature and RH in the conditioning chamber, to ensure that the conditions would remain within the tolerances specified by ASTM D618. This logger recorded that conditioning temperature was within a range of 22.27 to 23.33 ºC and conditioning RH was within a range of 57.25% to 58.46%. These values are within the specified tolerances of ASTM D618.

Sterilized and unsterilized control samples were conditioned at the same time, but were kept separated within the conditioning chamber. The samples were retained by a 3D printed polycarbonate comb, which allowed the grip sections of each sample to sit between the teeth. This comb kept the samples separated and standing upright along their long edges, maximizing the sample surface area exposed to the conditions within the conditioning chamber. Once conditioned, the samples were weighed, measured for thickness and width at three different points along the gage section, placed back in their respective boxes, and transported for testing.

3.2 Image Processing

Sample photographs collected immediately after printing were imported into *Fiji* (Schindelin et al., 2012), which is a software tool used for image processing and analysis, and commonly sees use in scientific publications. A number of photos were taken at an

angled perspective, preventing the collection of accurate dimensional measurements. Each sample underwent a Hough transform, which identified straight lines within the image, which were then straightened through a perspective correction transformation, using the *interactive perspective* plugin in *Fiji* (Jagannathan & Jawahar, 2005). To retain proportionality, the images were scaled using known measurements of the imaged samples. From this transformation, accurate horizontal and vertical measurements could be acquired from the photos that were originally taken at an angle, as can be seen in Figure 9. After this, each image was sharpened, to aid in edge selection for sample measurement, and total sample length and gage length were measured.

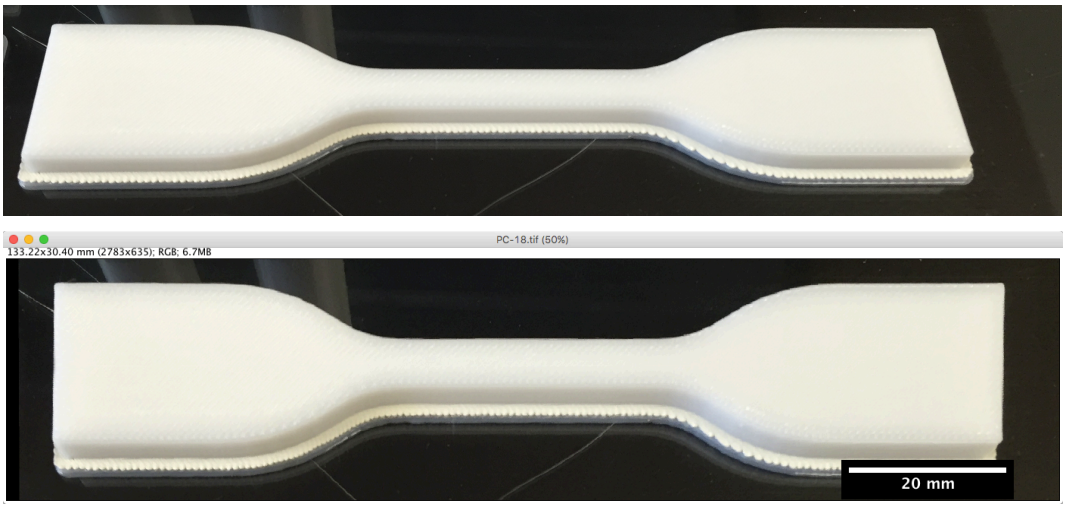

Figure 9. Top, Initial photograph of a PC sample; bottom, PC sample photograph, after perspective correction and sharpening transformations in ImageJ. This correction was carried out for the purposes of measurement collection.

3.3 Mechanical Properties of Samples

Once conditioned, the tensile samples were tested using an *Instron*® *ElectroPuls*™ *E10000* load frame, on a material-by-material basis. To ensure test parity, there was no differentiation between the sterilized and unsterilized control samples, and test order was randomized.

Each sample was fixed in position by a pair of ASTM D638-compliant jaws at the grip section of the samples, with a grip pressure of 5 bar. Once gripped, the samples were checked to ensure that they were positioned vertically, and the load frame was tared. Tensile loading was carried out at a rate of 5 mm/min. In the case of PLA and PC, testing was completed once the samples broke along the gage region, and with PCL, testing ended once the load frame reached its maximum displacement, as those samples did not break. During the course of testing, force and displacement data was recorded through the load frame control software, called *Instron® WaveMatrix™*, at a sampling frequency of 100 Hz.

Upon completion of each test, the broken halves of the samples were kept together, placed within the box from which they were retrieved, and the load frame was brought back to its starting position.

4 Results

This section of the thesis pertains to the changes observed in the physical and mechanical properties of PLA, PCL, and PC, as a result of exposure to H_2O_2 vapour sterilization and sample conditioning. Specifically, changes to the physical appearance and dimensions of the samples are presented, in addition to observed changes in E, σ_{UTS}, and ε_{UTS}.

4.1 Physical Appearance

Tensile samples printed in PLA and PCL that were exposed to a cycle of H_2O_2 vapour sterilization exhibited changes in both physical appearance and size, when compared to their unsterilized control counterparts. The colour of the PLA print filament was initially golden-brown in colour, and once printed, the tensile samples were significantly darker. Once exposed to a cycle of sterilization, the samples were bleached in colour, as can be seen in Figure 10, left. Changes in sample colour were limited to PLA, as neither the PCL or PC materials displayed any noticeable pigmentation. While they did not change in colour, the PCL samples did exhibit noticeable physical changes to their surfaces. Every PCL sample experienced some degree of melting and bubbling in both the grip and gage sections, as can be seen in Figure 10, right.

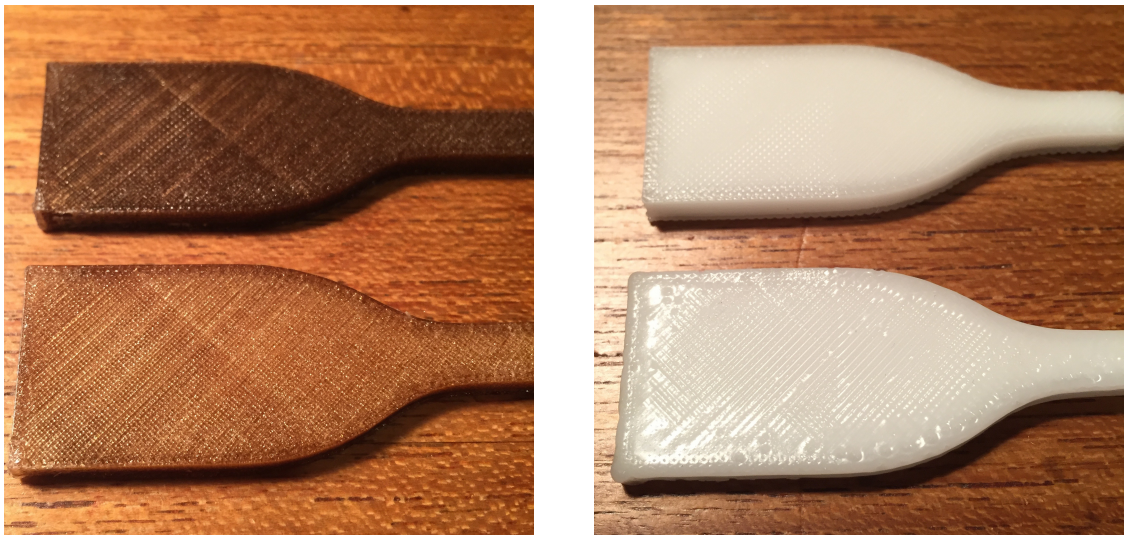

Figure 10. Left, colour difference between PLA samples that were unsterilized control (top), and sterilized (bottom); right, PCL material deformation occurred in the sterilized samples (bottom), which was not present in the control samples (top).

4.2 Dimensions and Mass

The thickness, width, and mass measurements of all samples that were recorded throughout the experiment were compared through paired t-tests. This comparative analysis was carried out in *Minitab® 17*, to identify if dimensional changes took place as a result of sterilization or conditioning. These tests functioned to test hypotheses by comparing group means; if the further the group means fall from one another, there is less likelihood that the differences could have occurred solely by chance. The output from this method of analysis was a level of statistical significance (i.e., p-value), between 0 and 1; values closer to 0 indicate higher levels of statistical significance. In this experiment, the p-value was compared to a significance level of 0.05, corresponding to a confidence level of 95%. Statistical significance was identified if the p-value fell below 0.05.

4.2.1 Sample Thickness

Measurements collected before and after sterilization, as per 3.1.2, revealed a statistically significant increase for PCL and PC sample thickness. On average, the PCL samples increased by 1.60%, while the PC samples increased by 0.21%, as seen in Table 1.

Before tensile testing, the sterilized and unsterilized control samples where conditioned for 40 hours in a 23 ºC environment of 52% RH (see Section 3.1.4 for details). Of the three sterilized materials, PC saw a statistically significant increase of 0.20% in response to conditioning, as seen in Table 2.

Conditioning of the unsterilized control samples showed a decrease in PLA sample thickness. These samples decreased, on average, by 1.16%, as seen in Table 3.

Individual sample measurements for each material at all stages of measurement can be found in Tables 17 through 25 in Appendix A.

Table 1. Average thickness of n=10 PLA, PCL, and PC sterilized samples prior to sterilization and prior to conditioning. Standard deviations are reported in parentheses. Comparisons were performed through paired t-tests; bolding indicates statistical significance at the 95% confidence level.

	Thickness (mm)		
	PLA	PCL	PC
Pre-Sterilization	4.20 (0.0418)	**4.16 (0.0188)**	**3.87 (6.99×10^{-3})**
Pre-Conditioning	4.20 (0.0418)	**4.23 (0.0410)**	**3.88 (0.0129)**
Difference	-3.30×10^{-4} (0.0284)	**0.0663 (0.0407)**	**8.00×10^{-3} (0.0106)**

Table 2. Average thickness of n=10 PLA, PCL, and PC sterilized samples prior to conditioning and prior to testing. Standard deviations are reported in parentheses. Comparisons were performed through paired t-tests; bolding indicates statistical significance at the 95% confidence level.

	Thickness (mm)		
	PLA	PCL	PC
Pre-Conditioning	4.20 (0.0418)	4.23 (0.0410)	**3.88 (0.0129)**
Pre-Testing	4.21 (0.0309)	4.22 (0.0348)	**3.87 (0.0126)**
Difference	7.00×10^{-3} (0.0191)	-1.00×10^{-3} (0.0217)	**-7.67×10^{-3} (5.89×10^{-3})**

Table 3. Average thickness of n=10 PLA, PCL, and PC unsterilized control samples prior to conditioning and prior to testing. Standard deviations are reported in parentheses. Comparisons were performed through paired t-tests; bolding indicates statistical significance at the 95% confidence level.

	Thickness (mm)		
	PLA	PCL	PC
Pre-Conditioning	**4.22 (0.0190)**	4.16 (0.0635)	3.87 (0.0159)
Pre-Testing	**4.17 (0.0253)**	4.17 (0.0683)	3.87 (0.0159)
Difference	**-0.0490 (0.0196)**	6.33×10^{-3} (0.0140)	-5.67×10^{-3} (8.17×10^{-3})

The observed changes in thickness as a result of conditioning in the unsterilized control samples, and as a result of sterilization and conditioning in the sterilized samples are illustrated on a material basis for PLA, PCL, and PC in Figures 11, 12, and 13 respectively.

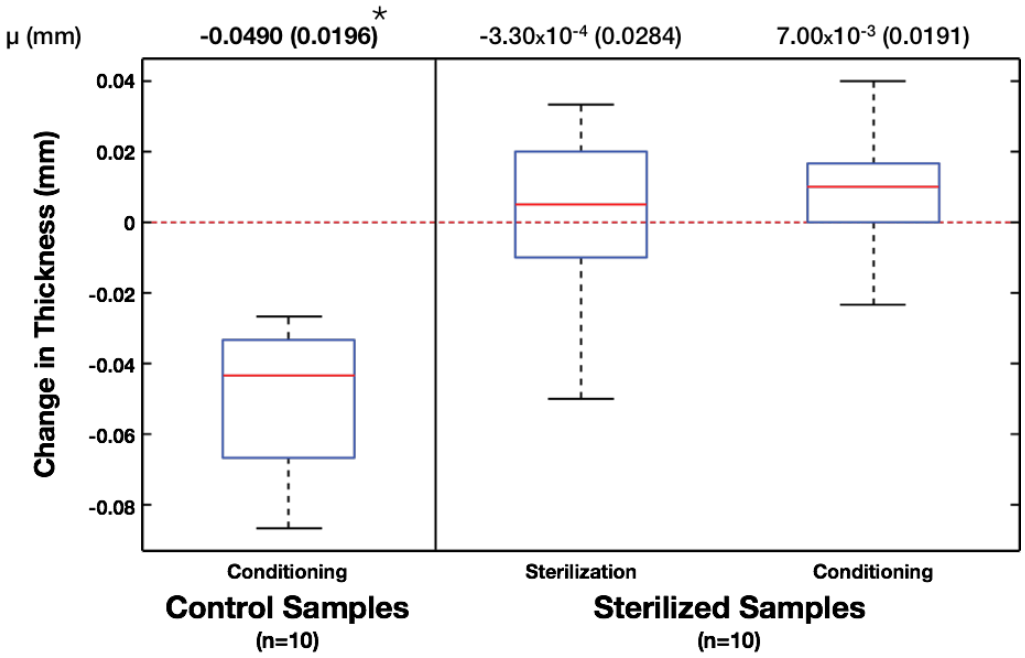

Figure 11. Changes in PLA sample thickness at each stage of measurement, for the un-sterilized control and sterilized samples. Average change is above each boxplot, with standard deviation reported in parentheses. Comparisons were performed through paired t-tests; an asterisk indicates statistical significance at the 95% confidence level.

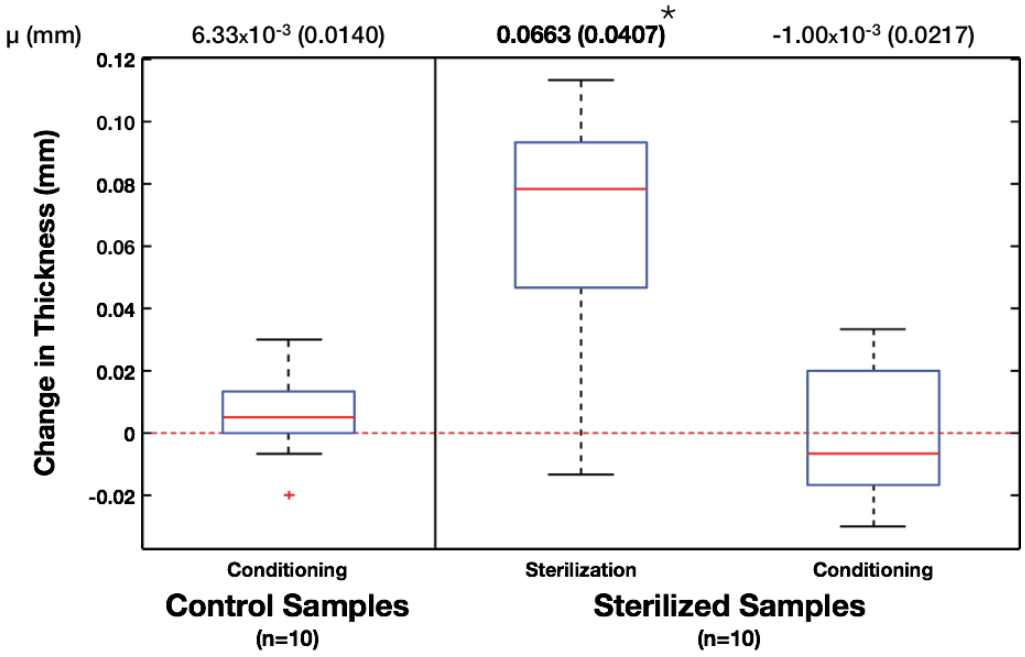

Figure 12. Changes in PCL sample thickness at each stage of measurement, for the un-sterilized control and sterilized samples. Average change is above each boxplot, with standard deviation reported in parentheses. Comparisons were performed through paired t-tests; an asterisk indicates statistical significance at the 95% confidence level.

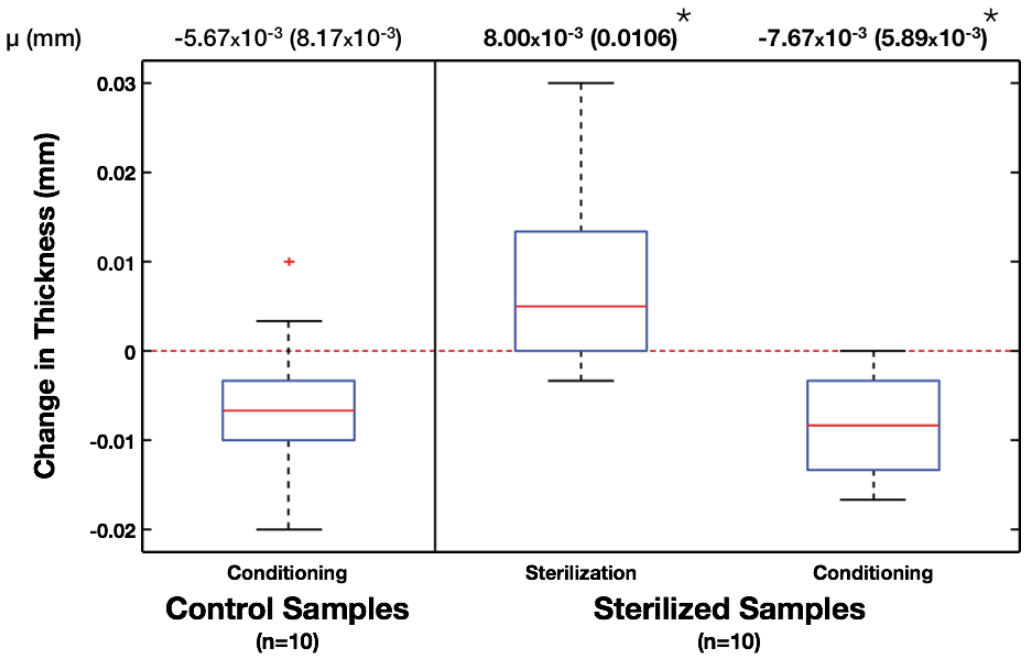

Figure 13. Changes in PC sample thickness at each stage of measurement, for the unsterilized control and sterilized samples. Average change is above each boxplot, with standard deviation reported in parentheses. Comparisons were performed through paired t-tests; an asterisk indicates statistical significance at the 95% confidence level.

4.2.2 Sample Width

Of the three materials, PC sample width changed with statistical significance. On average, PC sample width increased by 0.18%, as can be seen in Table 4.

Conditioning presented no significant change in the average widths of any of the sterilized samples, as seen in Table 5.

Only the unsterilized control PC samples saw a statistically significant in width. These samples decreased on average by 0.08%, as seen in Table 6.

Individual sample measurements for each material at all stages of measurement can be found in Tables 17 through 25 in Appendix A.

Table 4. Average width of n=10 PLA, PCL, and PC sterilized samples prior to sterilization and prior to conditioning. Standard deviations are reported in parentheses. Comparisons were performed through paired t-tests; bolding indicates statistical significance at the 95% confidence level.

	Width (mm)		
	PLA	PCL	PC
Pre-Sterilization	5.99 (0.0155)	5.99 (0.0148)	**6.00 (9.20×10^{-3})**
Pre-Conditioning	5.99 (0.0130)	6.01 (0.0158)	**6.01 (0.0155)**
Difference	-5.00×10^{-3} (0.0123)	0.0123 (0.0187)	**0.0107 (9.27×10^{-3})**

Table 5. Average width of n=10 PLA, PCL, and PC sterilized samples prior to conditioning and prior to testing. Standard deviations are reported in parentheses. Comparisons were performed through paired t-tests; bolding indicates statistical significance at the 95% confidence level.

	Width (mm)		
	PLA	PCL	PC
Pre-Conditioning	5.99 (0.0130)	6.01 (0.0158)	6.01 (0.0155)
Pre-Testing	5.99 (7.41×10^{-3})	6.00 (0.0183)	6.00 (0.0127)
Difference	6.70×10^{-4} (9.79×10^{-3})	-3.30×10^{-4} (9.22×10^{-3})	-3.67×10^{-3} (7.28×10^{-3})

Table 6. Average width of n=10 PLA, PCL, and PC unsterilized control samples prior to conditioning and prior to testing. Standard deviations are reported in parentheses. Comparisons were performed through paired t-tests; bolding indicates statistical significance at the 95% confidence level.

	Width (mm)		
	PLA	PCL	PC
Pre-Conditioning	5.99 (0.0102)	5.98 (8.20×10^{-3})	**6.00 (0.0105)**
Pre-Testing	5.99 (4.73×10^{-3})	5.98 (0.0103)	**6.00 (0.0128)**
Difference	6.70×10^{-4} (0.0113)	6.70×10^{-4} (0.0164)	**-4.67×10^{-3} (5.92×10^{-3})**

The observed changes in width as a result of conditioning in the unsterilized control samples, and as a result of sterilization and conditioning in the sterilized samples are illustrated on a material basis for PLA, PCL, and PC in Figures 14, 15, and 16 respectively.

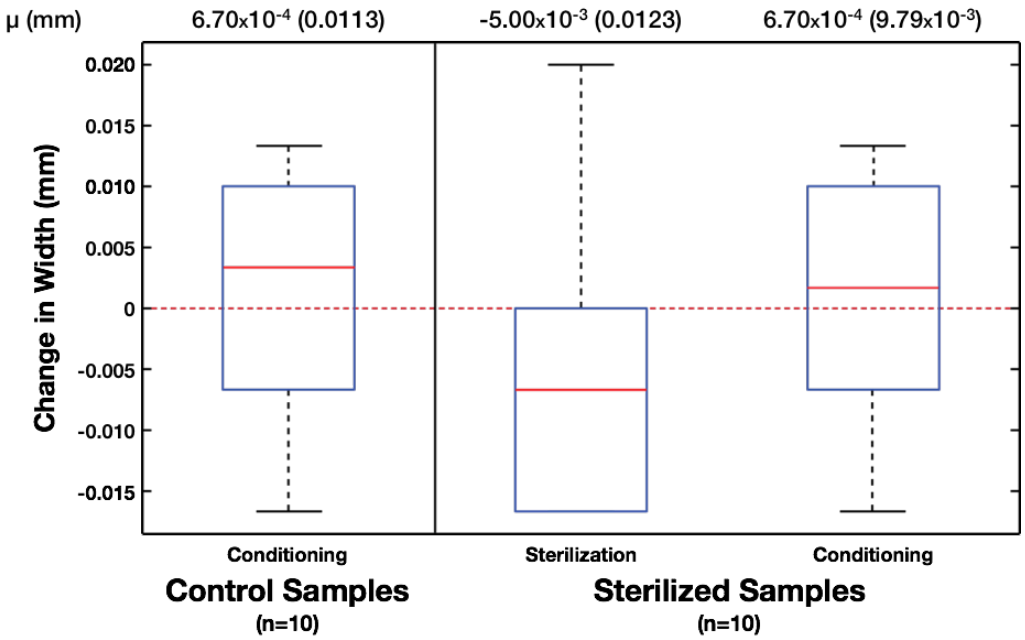

Figure 14. Changes in PLA sample width at each stage of measurement, for the unsterilized control and sterilized samples. Average change is above each boxplot, with standard deviation reported in parentheses. Comparisons were performed through paired t-tests; an asterisk indicates statistical significance at the 95% confidence level.

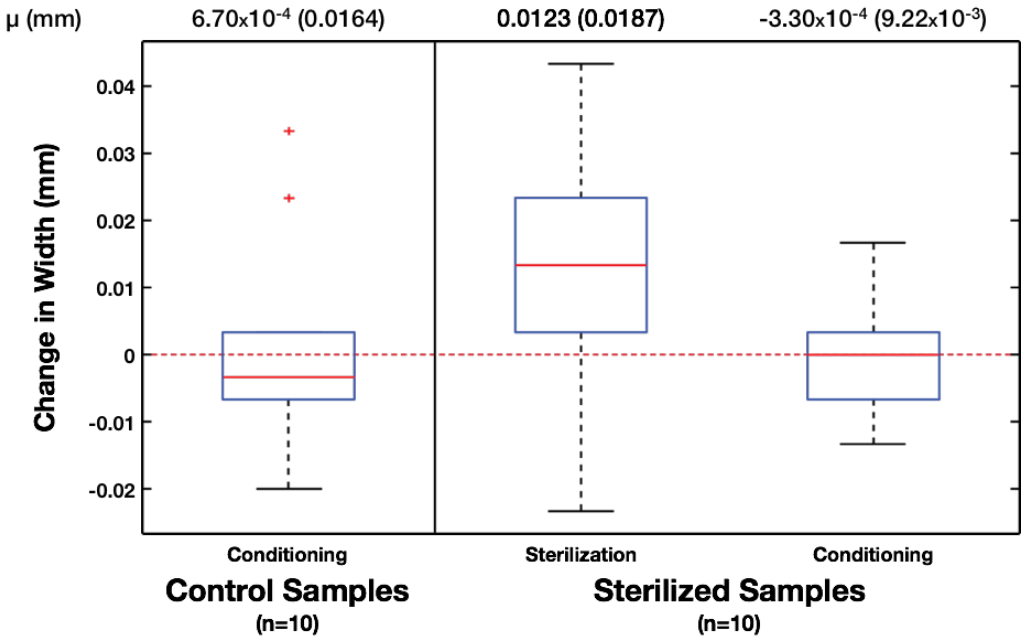

Figure 15. Changes in PCL sample width at each stage of measurement, for the unsterilized control and sterilized samples. Average change is above each boxplot, with standard deviation reported in parentheses. Comparisons were performed through paired t-tests; an asterisk indicates statistical significance at the 95% confidence level.

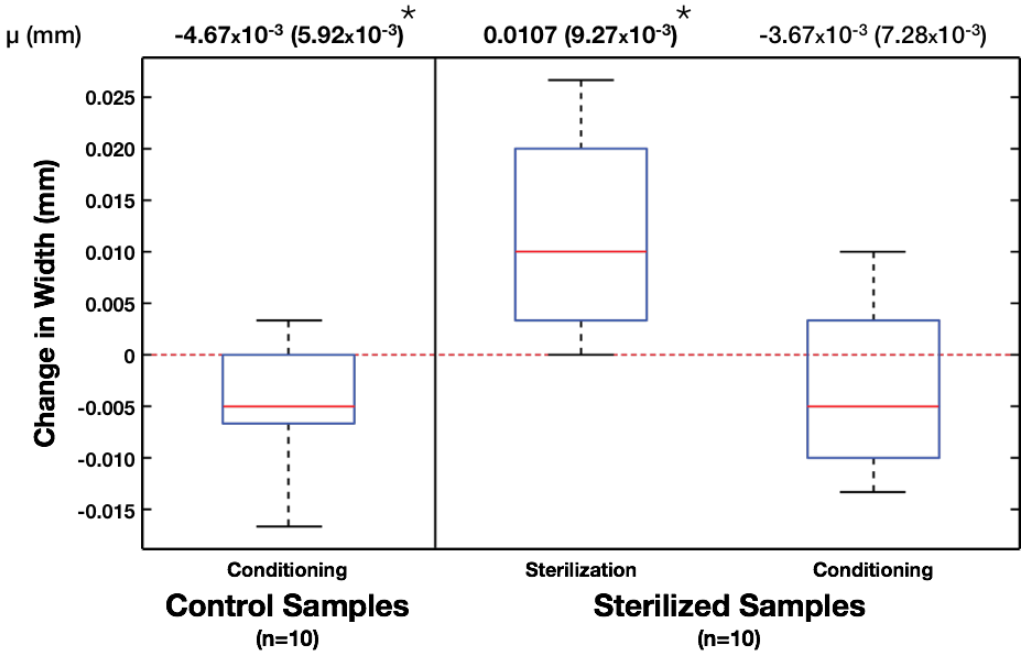

Figure 16. Changes in PC sample width at each stage of measurement, for the unsterilized control and sterilized samples. Average change is above each boxplot, with standard deviation reported in parentheses. Comparisons were performed through paired t-tests; an asterisk indicates statistical significance at the 95% confidence level.

4.2.3 Sample Mass

Sample mass increased in all materials as a result of sterilization. For PLA, PCL, and PC, average mass increased, respectively, by 0.24%, 0.36%, and 0.06%. These results can be seen below, in Table 7.

Post-sterilization conditioning also affected the masses of all materials. PLA and PC increased 0.08% and 0.08% respectively, while PCL decreased by 0.17%. These results can be seen in Table 8.

Conditioning increased mass in all control materials. For PLA, PCL, and PC, average mass increased by 0.14%, 0.13%, and 0.15%, respectively. These results can be seen in Table 9.

Individual sample measurements for each material at all stages of measurement can be found in Tables 17 through 25 in Appendix A.

Table 7. Average mass of n=10 PLA, PCL, and PC sterilized samples prior to sterilization and prior to conditioning. Standard deviations are reported in parentheses. Comparisons were performed through paired t-tests; bolding indicates statistical significance at the 95% confidence level.

	Mass (g)		
	PLA	PCL	PC
Pre-Sterilization	**7.45 (0.0146)**	**6.44 (0.0720)**	**6.58 (9.85×10^{-3})**
Pre-Conditioning	**7.46 (0.0148)**	**6.46 (0.0737)**	**6.59 (0.0110)**
Difference	**0.0180 (2.37×10^{-3})**	**0.0230 (3.00×10^{-3})**	**3.82×10^{-3} (1.66×10^{-3})**

Table 8. Average mass of n=10 PLA, PCL, and PC sterilized samples prior to conditioning and prior to testing. Standard deviations are reported in parentheses. Comparisons were performed through paired t-tests; bolding indicates statistical significance at the 95% confidence level.

	Mass (g)		
	PLA	PCL	PC
Pre-Conditioning	**7.46 (0.0148)**	**6.46 (0.0737)**	**6.59 (0.0110)**
Pre-Testing	**7.47 (0.0142)**	**6.45 (0.0725)**	**6.59 (0.0117)**
Difference	**6.07×10^{-3} (2.44×10^{-3})**	**-0.0112 (2.42×10^{-3})**	**5.21×10^{-3} (3.14×10^{-3})**

Table 9. Average mass of n=10 PLA, PCL, and PC unsterilized control samples prior to conditioning and prior to testing. Standard deviations are reported in parentheses. Comparisons were performed through paired t-tests; bolding indicates statistical significance at the 95% confidence level.

	Mass (g)		
	PLA	PCL	PC
Pre-Conditioning	**7.46 (0.0126)**	**6.42 (0.0817)**	**6.60 (9.77×10^{-3})**
Pre-Testing	**7.47 (0.0127)**	**6.43 (0.0824)**	**6.61 (0.0105)**
Difference	**0.0105 (7.02×10^{-4})**	**8.06×10^{-3} (1.33×10^{-3})**	**0.0102 (4.96×10^{-3})**

The observed changes in mass as a result of conditioning in the unsterilized control samples, and as a result of sterilization and conditioning in the sterilized samples are illustrated on a material basis for PLA, PCL, and PC in Figures 17, 18, and 19 respectively.

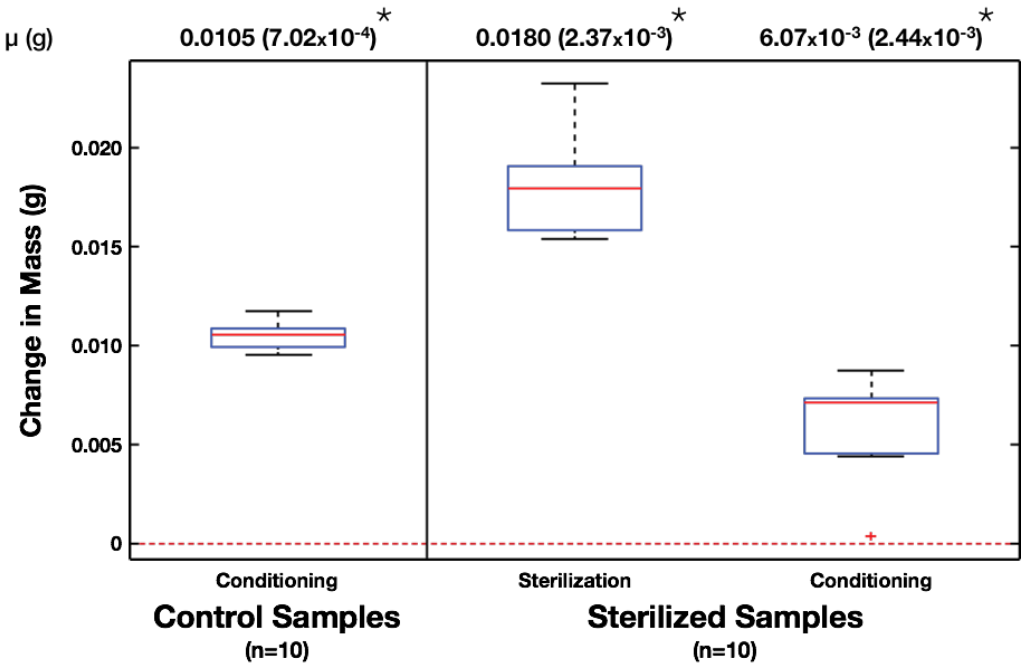

Figure 17. Changes in PLA sample mass at each stage of measurement, for the unsterilized control and sterilized samples. Average change is above each boxplot, with standard deviation reported in parentheses. Comparisons were performed through paired t-tests; an asterisk indicates statistical significance at the 95% confidence level.

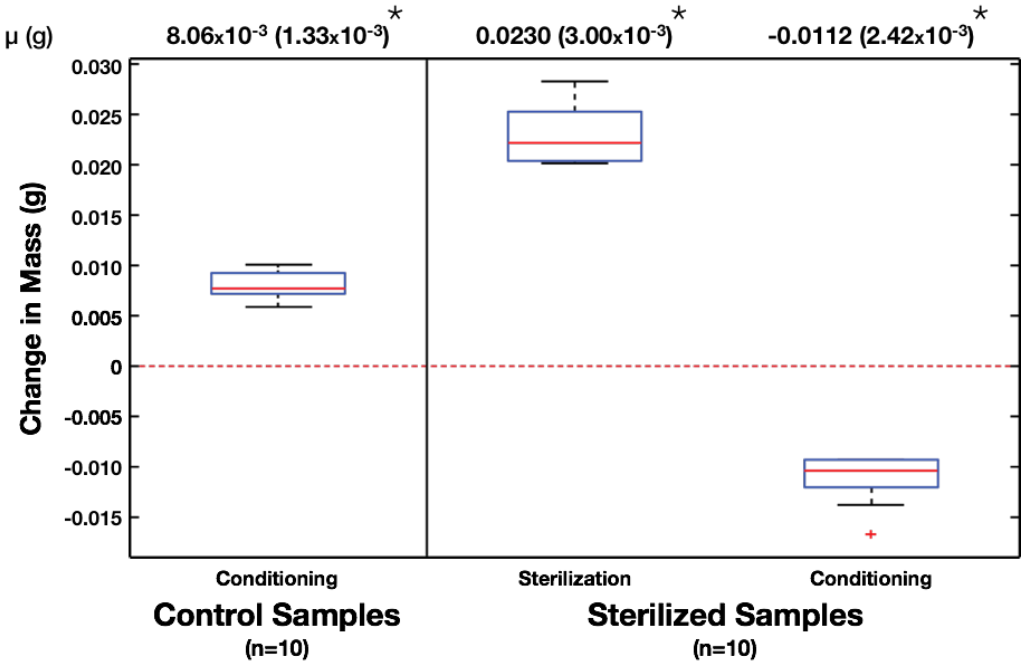

Figure 18. Changes in PCL sample mass at each stage of measurement, for the unsterilized control and sterilized samples. Average change is above each boxplot, with standard deviation reported in parentheses. Comparisons were performed through paired t-tests; an asterisk indicates statistical significance at the 95% confidence level.

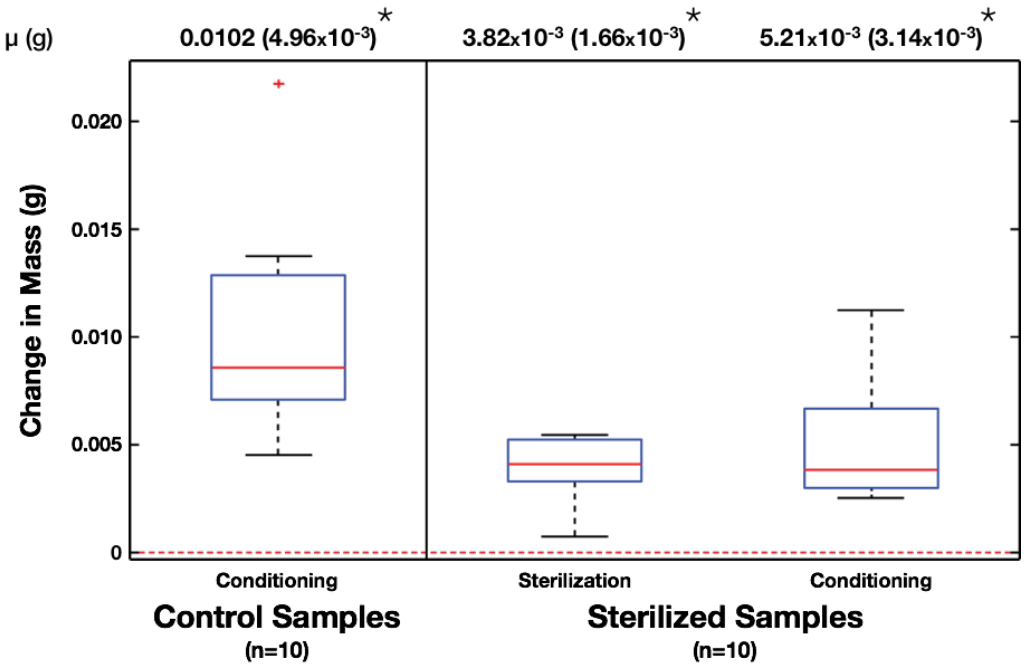

Figure 19. Changes in PC sample width at each stage of measurement, for the unsterilized control and sterilized samples. Average change is above each boxplot, with standard deviation reported in parentheses. Comparisons were performed through paired t-tests; an asterisk indicates statistical significance at the 95% confidence level.

4.3 Changes in Mechanical Properties

Using the raw data collected in *WaveMatrix*, stress and strain data was calculated using the pre-testing cross-sectional area measurements. The cross-sectional area was determined from the average thickness and average width measurements recorded prior to testing, and were used to calculate stress over the duration of the tests. Strain was calculated as the displacement over the duration of the test, relative to the original specified gage length of 25 mm. The stress and strain data was then plotted on a graph, to produce stress-strain curves for each sample.

E, σ_{UTS}, and ε_{UTS} were determined through analysis in *Mathworks® MATLAB® R2013a*. E was computed from each curve by determining the slope of the linear portion in the elastic region. In PC and PLA, the linear region was identified between the 5th and

15th percentiles of ε_{max}, as seen in Equations (5) and (6). The locations of ε_1 and ε_2 are visualized in Figure 20.

$$\varepsilon_1 = 0.05(\varepsilon_{\max}) \quad (5)$$

$$\varepsilon_2 = 0.15(\varepsilon_{\max}) \quad (6)$$

PCL had a significantly larger post-elastic region than PLA and PC, so the linear region was identified between the 1st and 5th percentiles of ε_{max}, as seen in Equations (7) and (8). The locations of ε_1 and ε_2 are visualized in Figure 20.

$$\varepsilon_1 = 0.01(\varepsilon_{\max}) \quad (7)$$

$$\varepsilon_2 = 0.05(\varepsilon_{\max}) \quad (8)$$

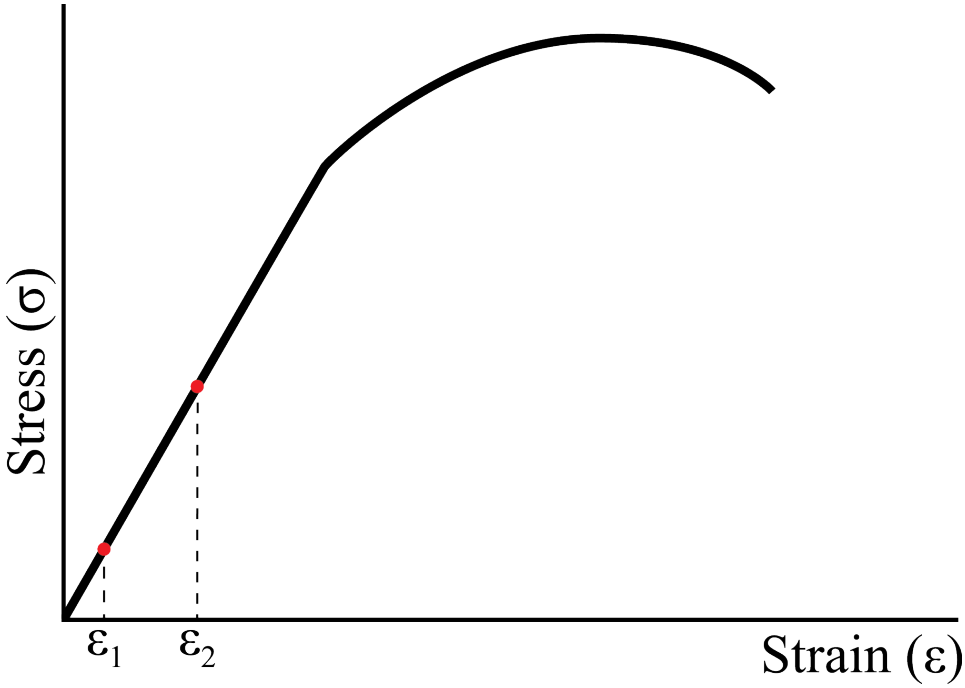

Figure 20. Engineering stress-strain curve, identifying the positions of $\boldsymbol{\varepsilon_1}$ and $\boldsymbol{\varepsilon_2}$ that define the linear region used to calculate Young's modulus (*E*).

σ_{UTS} is the maximum value for stress over the duration of each test; ε_{UTS} is the strain corresponding to σ_{UTS}. As discussed in Section 2.1.1, the identification of yield in plastics through the offset yield method can be difficult, due to the variability in recommended strain offsets in the research literature (Eshraghi & Das, 2010; Fernández et al., 2014; Hutmacher et al., 2001; Kurtz et al., 1998). As such, yield was not computed in this study.

The sterilized and unsterilized control E, σ_{UTS}, and ε_{UTS} of each material were compared through a one-way analysis of variance, or ANOVA, in *MATLAB*®. ANOVA was applied to identify a statistically significant change between the sterilized and unsterilized control test samples. This method of analysis compares groups of like data from differing treatments, and calculates a mean from each group. The mean of the entirety of all treatments was found, known as the grand mean, and was used as a point of comparison for each treatment to determine between-group variance. Like the paired t-test, the output from this method of analysis is also a p-value. In this method, the p-value was compared to a significance level of 0.05, corresponding to a confidence level of 95%; if the p-value fell below 0.05, the resulting variance between treatments would be statistically significant.

A comparison of E between the control and sterilized samples revealed a statistically significant decrease in all three materials as a result of sterilization; the E of PLA, PCL, and PC decreased by an average of 2.15%, 4.13%, and 1.85%. σ_{UTS} saw a statistically significant change in PC, where it decreased by 1.52%. The average ε_{UTS} only saw a statistically significant change in PLA, where it increased by 13.5%. These results are summarized in Table 10.

Individual sample measurements of E, σ_{UTS}, and ε_{UTS} for each material can be found in Tables 26 through 28 in Appendix A.

Table 10. Average of n=10 samples for Young's modulus (E), ultimate tensile strength ($\boldsymbol{\sigma_{UTS}}$), and strain at the point of ultimate tensile strength ($\boldsymbol{\varepsilon_{UTS}}$) in PLA, PCL, and PC. Statistically significant values from an ANOVA at a 95% confidence are bolded.

		PLA	PCL	PC
E (MPa)	Control	**979 (20.4)**	**121 (4.72)**	**595 (8.18)**
	Sterilized	**958 (22.0)**	**116 (4.14)**	**584 (6.50)**
σ_{UTS} (MPa)	Control	38.8 (0.732)	12.8 (0.496)	**42.4 (0.688)**
	Sterilized	38.9 (1.31)	12.6 (0.342)	**41.8 (0.528)**
ε_{UTS} ($^{mm}/_{mm}$)	Control	0.0586 (3.15 x10^{-3})	**0.333 (0.0154)**	0.108 (1.06 x10^{-3})
	Sterilized	0.0587 (2.63 x10^{-3})	**0.378 (0.0193)**	0.108 (1.53 x10^{-3})

5 Discussion

The discussion in this thesis pertains to the physical and mechanical changes observed in the results. Specifically, the changes observed were attributable to flaws introduced to the samples through the 3D printing process, in combination with the heat, moisture and vacuum associated with sterilization and conditioning. Furthermore, this section presents a series of predictive models that can be used to accommodate for dimensional changes in 3D printed PLA, PCL, and PC objects that would be sterilized by H_2O_2 vapour.

5.1 Physical Changes

The results have shown that H_2O_2 vapour sterilization affected the dimensional properties of PCL and PC, as well as the mass of all three materials. As discussed in Sections 2.3.1 and 3.1.3, the sterilization cycle relied on heat, moisture, and vacuum to operate. Despite the sterilization method being low-temperature, the ten PCL samples that underwent sterilization, had permanent physical deformation due to plastic flow on the sample surfaces due to the treatment. This resulted in samples with a glossy and smooth finish when compared to the unsterilized control samples. Additionally, the FDM printing process is capable of creating internal material defects, as discussed in Section 1.4.1. Agarwala et al. (1996) found that voids are formed during printing at locations where the external layer outline intersects with the raster fill. The presence of these voids was confirmed in the appearance of the PCL samples that underwent sterilization, which appears to be due to a combination of elevated temperatures and low pressures associated with the sterilization process. The samples bubbled around their peripheral edges, indicating that air was either entrapped and escaped in response to the elevated chamber temperatures

and low pressures, or a chemical reaction occurred; this deformation was responsible for the measured increase in PCL sample thickness.

The sterilization process also resulted in an increase in sample mass of all three materials. The mechanisms of H_2O_2 vapour sterilization were described in Section 2.3.1, where it was explained that this technique relies on the use of water to diffuse and condense sterilant on all surfaces within the chamber. As such, the sterilization cycle exposed the PLA, PCL, and PC samples to moisture. It was noted in Section 1.4.1 that FDM printed products are highly susceptible to moisture absorption (Kim et al., 2016). This susceptibility can be observed in the results of this experiment, where mass increased in all of the samples of PLA, PCL, and PC exposed to sterilization. A possible explanation for the increases in thickness and width observed in the PC samples is that some thermoplastics can swell in response to moisture absorption (Sharp et al., 2001); see Section 2.1.2 for relevant discussion.

As discussed in Section 1.4.1, 3D printing with FDM relies on the deposition of material at each layer in long, continuous deposits. In this process, each subsequent layer is bonded to the layer below it through the heat of the material that is extruded. This results in anisotropy of FDM-produced products. That is, they are strongest in tension in the direction axial to the fibres, and weakest in the direction that is transverse (Ahn et al., 2002; Bellini & Guceri, 2003). This weakness to transversely applied tensile loads may explain the susceptibility to changes in sample thickness, rather than width, as was seen in the PC samples in response to sterilization and conditioning, and the control PLA and PC samples in response to conditioning. The increase in PC sample thickness after steri-

lization is likely attributable to a combination of moisture uptake and low chamber pressures 'pulling' upwards the samples.

Furthermore, sample mass changed significantly in PLA, PCL, and PC, as a result of conditioning. The humid environment within the conditioning chamber caused additional increases in mass from their post-sterilization states in the PLA and PC samples, but a decrease in mass in the PCL samples. Additionally, all of the control samples of PLA, PCL, and PC increased in mass during conditioning. Similarly to what was observed during sterilization, increases in mass were likely the result of moisture uptake by the samples, due to the susceptibility of FDM-printed products to absorb moisture (Kim et al., 2016).

The decrease in mass in response to conditioning seen in the sterilized PCL samples indicates that the physical deformations that were incurred during sterilization possibly impacted the ability of the samples to absorb moisture. The peripheral bubbling on the sample surfaces appears to be the result of air entrapment within internal voids created by the FDM manufacturing process (Agarwala et al., 1996), which then escaped during the sterilization process. The observed bubbling in PCL may have resulted in elimination of the voids from the sample, thus decreasing the ability of the material to absorb moisture. This would therefore explain the inability of the sterilized PCL samples to gain additional mass due to moisture uptake, unlike their control counterparts. The extent of this is unknown and outside the scope of this study.

The decreases in thickness observed in the sterilized PC, control PLA, and control PC samples in response to conditioning could be attributed to the weakness in transverse loading inherent to FDM-produced products, in combination with the presence of mois-

ture within the samples. In Section 1.4.1, moisture was identified as a plasticizer capable of decreasing mechanical strength of FDM-produced plastic products (Kim et al., 2016), and can increase material plasticity, stress relaxation, and creep (Allen & Bauer, 1988, pp. 762-3). While these bulk effects may have played a role in decreasing sample thickness, further studies are required to determine the impact that they may have had on decreasing sample thickness.

The research literature makes note that PLA is typically translucent or opaque in appearance, whereas the material used in this experiment was brown in colour (Weir et al., 2004). The source of the colour exhibited in the PLA is likely the low concentration of gentamicin antibiotic in the material that was discussed in Section 3.1.2.

During H_2O_2 vapour sterilization, the samples became noticeably lighter in colour; this effect could be attributed to several causes. First, hydrogen peroxide is a known bleaching agent, used to decolourize products in several industries, and likely contributed to the removal of pigmentation from the sterilized samples (Jones & Clark, 1999). Second, gentamicin is "freely soluble in water" (O'Neil, Heckelman, Koch, & Roman, 2006, p. 757). Since water is a component in the H_2O_2 vapour sterilization process, sterilization may have caused dissolution of the antibiotic from the plastic, causing loss of color and enlargement of voids within the samples. Further exploration of this hypothesis could be carried out in future work by evaluating the antimicrobial effectiveness of H_2O_2 vapour sterilized antibiotic eluting plastics.

5.2 Decreases in Mechanical Strength

H_2O_2 vapour sterilization had statistically significant effects on the material properties of PLA, PCL, and PC; each of the three materials decreased in Young's Modulus (E), while only PC saw a decrease in σ_{UTS} (see Figure 21), and only PCL saw an increase in ε_{UTS}.

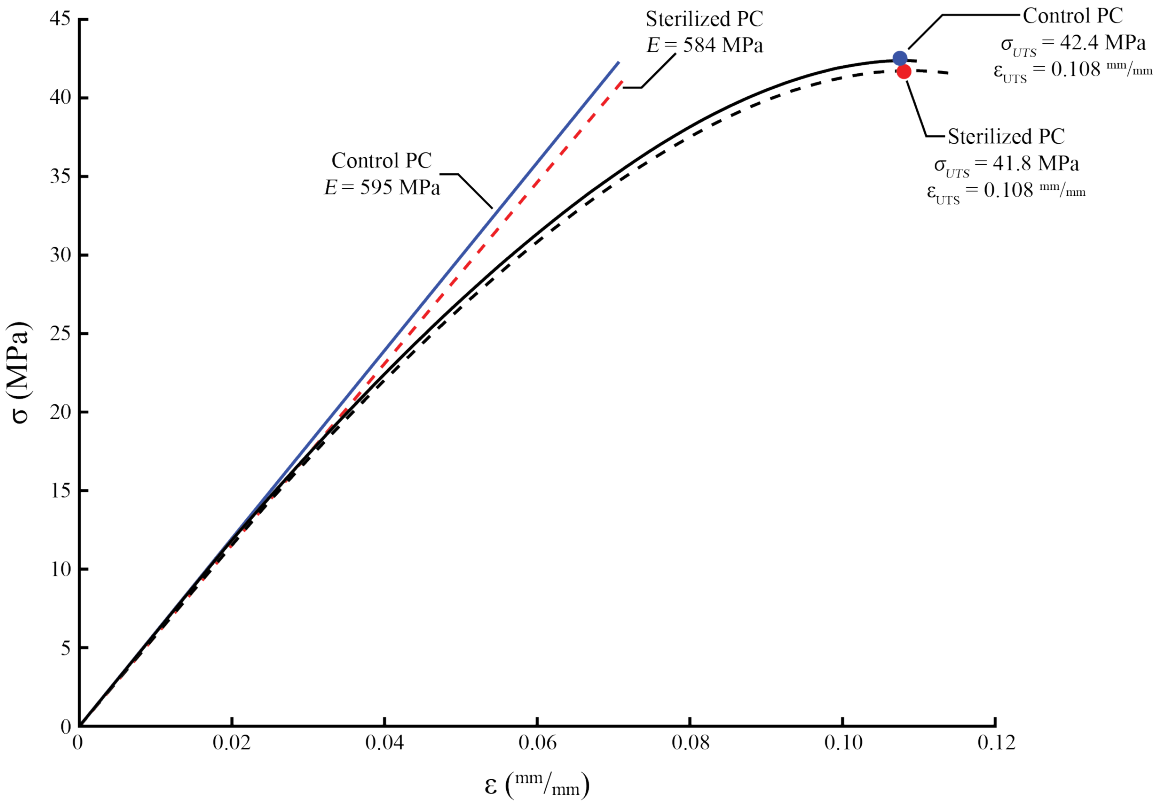

Figure 21. Average stress-strain curves of n=10 unsterilized control and sterilized PC samples. The control curve is a solid line, while the sterilized curve is dashed. E is linearly regressed for the unsterilized control (blue), and sterilized (red, dashed) samples. Coloured dots represent the point of UTS for the unsterilized control (blue) and sterilized (red) stress-strain curves.

Of the three materials, PCL was the only material with visible deformation resulting from sterilization, which contributed to decreased material performance. As observed in Section 4.1, the PCL samples bubbled along their peripheral edges, including the gage regions. Young and Budynas (2002) explain that fibrous materials experience decreased

properties when loaded in directions off-axis to their fibres, with more than half of the elasticity of the fibre lost at a loading angle of 15º. The composition of each 3D printed sample layer was made up of an outline oriented in the direction of sample loading and raster fill oriented at 45º from loading. With this material structure, the outline material in the gage sections provided the samples with a majority of their tensile strength, with the infill acting as a secondary support; the bubbling observed on the PCL samples caused localized disruptions to the axial orientation of the plastic fibres limiting their response to an axial load. Re-orientation of the fibres would not have occurred until sufficient sample elongation would 'pull' them straight, by which point mechanical failure in the samples would have already occurred elsewhere; these phenomena likely explain the decrease in E and significant increase in ε_{UTS} observed in PCL.

Analysis using gel permeation chromatography (GPC) was performed to identify if hydrolysis had taken place in any of the materials. This analysis was done using an *Agilent Technologies 1100 Series* high-performance liquid chromatography (HPLC) system. Unsterilized control and sterilized samples (n=5) of PLA, PCL, and PC were analyzed using HPLC-grade tetrahydrofuran and chloroform solvents, through an *Agilent Technologies PLgel 5 μm Guard* column. The GPC results were inconclusive, as the differences in retention times between the control and sterilized samples were indistinguishable. We believe that other factors are responsible for the decrease in E of PLA and PC, and decrease in σ_{UTS} of PC.

It is possible that the low pressures within the sterilization chamber caused the change in mechanical performance of the PLA and PC samples, albeit on a smaller scale than the effects seen in PCL. The research literature has shown that both PLA and PC

have high glass transition temperatures (T_g) of 60 to 65 ºC (Armentano et al., 2010) and 150 ºC (Martienssen & Warlimont, 2005, p. 504) respectively, when compared to that of PCL which is -60 ºC (Woodruff & Hutmacher, 2010). These temperatures indicate that PLA and PC would resist plastic flow when sterilized at 50 ºC. Instead, the low pressures of the sterilization chamber may have caused expansion of any entrapped air, causing internal material deformation before the air could escape. Additionally, Kim et al. (2016) identified that the presence of moisture within FDM-produced products significantly decreased their mechanical strength, due to water acting as a plasticizer in polymers (Levine & Slade, 1988, pp. 79-80). Regions within the sample that had previously contained entrapped air, or even washed-out gentamicin in the PLA samples, may instead absorb moisture and further impacting material performance. Further work to determine the extent of the effect of low pressure without heat or chemical involvement on 3D printed material water absorptivity and mechanical performance is currently underway in Dr. Morrison's lab.

5.3 Designing for Sterilization

The results presented in this study indicate that physical changes occurred in the PLA, PCL, and PC samples, as a result of H_2O_2 vapour sterilization. However, it can be difficult to provide an absolute answer as to whether or not the materials are 'compatible' with H_2O_2 vapour sterilization. Accounting for a decrease in material performance can be as simple as changing the value of a variable in an equation, but forecasting changes to the physical dimensions of a product destined for sterilization can be difficult. To address this, predictive statistics, such as stepwise linear regression, can be applied to develop models for forecasting the physical changes that could occur in 3D printed PLA,

PCL, and PC medical devices that will undergo H_2O_2 vapour sterilization. As such, the gage section thickness and width measurements acquired in this study can be analyzed through this predictive technique.

Stepwise linear regression systematically adds and removes variables from a linear model, in order to retain the variables that best described changes observed in the data; variables that did not describe changes were not retained in the final model, as they were deemed insignificant. For the purposes of this experiment, the pre-sterilization and pre-conditioning thickness and width measurements for each sterilized sample were analyzed using the *LinearModel.stepwise* function in *MATLAB*®, in which models were output that could mathematically predict the effects of sterilization on the samples.

This method of analysis considered the sterilized sample measurements immediately after they were printed and immediately after they underwent sterilization, and formed quadratic predictive models for the thickness and width for each material. For PLA, stepwise linear regression yielded the results found in Table 11, and the linear regression models for thickness and width in Equations (9) and (10) respectively.

Table 11. Regression results for n=10 PLA sample thickness and width measurements. Standard errors are reported in parentheses; *, ** indicate statistical significance at the 95% and 99% confidence levels, respectively.

	Regression Coefficient Estimates	
	Thickness	Width
Constant	0.762 (0.572)	1.99 * (0.855)
Stage of Measurement	0.819 ** (0.136)	0.668 ** (0.143)
R-Squared	0.669	0.549

$$T_{pred} = 0.762 + (0.819 * T_0) \quad (9)$$

$$W_{pred} = 1.99 + (0.668 * W_0) \quad (10)$$

In these models, T_{pred} and W_{pred} are the predicted thickness and width, respectively, and T_0 and W_0 are the initial thickness and width of the sample, respectively. Regression yielded no coefficients for whether or not the samples underwent sterilization.

For PCL, stepwise linear regression yielded the results found in Table 12, and the linear regression models for thickness and width in Equations (11) and (12) respectively.

Table 12. Regression results for n=10 PCL sample thickness and width measurements. Standard errors are reported in parentheses; *, ** indicate statistical significance at the 95% and 99% confidence levels, respectively.

	Regression Coefficient Estimates	
	Thickness	Width
Constant	0.156 (0.620)	3.31 * (1.38)
Sterilization	0.0662 ** (0.0132)	0.0203 ** (0.00621)
Stage of Measurement	0.962 ** (0.149)	0.446 (0.231)
R-Squared	0.790	0.634

$$T_{pred} = 0.156 + (0.0662 * S) + (0.962 * T_0) \quad (11)$$

$$W_{pred} = 3.31 + (0.0203 * S) + (0.446 * W_0) \quad (12)$$

In both of these models, T_{pred} and W_{pred} are the expected thickness and width, respectively, S is 1 if the sample was sterilized and 0 if it was not sterilized, and T_0 and W_0 are the initial thickness and width of the sample, respectively.

Stepwise linear regression for PC yielded the results found in Table 13, and the linear regression models for thickness and width in Equations (13) and (14) respectively.

Table 13. Regression results for n=10 PC sample thickness and width measurements. Standard errors are reported in parentheses; *, ** indicate statistical significance at the 95% and 99% confidence levels, respectively.

	Regression Coefficient Estimates	
	Thickness	Width
Constant	-0.0352 (0.572)	-1.07 (0.934)
Sterilization	0.00803 * (0.00348)	0.0119 ** (0.00309)
Stage of Measurement	1.01 ** (0.148)	1.18 ** (0.156)
R-Squared	0.740	0.777

$$T_{pred} = -0.0352 + (0.00803 * S) + (1.01 * T_0) \quad (13)$$

$$W_{pred} = -1.07 + (0.0119 * S) + (1.18 * W_0) \quad (14)$$

In both of these models, T_{pred} and W_{pred} are the expected thickness and width, respectively, S is 1 if the sample was sterilized and 0 if it was not sterilized, and T_0 and W_0 are the initial thickness and width of the sample, respectively.

6 Conclusions and Recommendations

The work presented in this study aimed to identify the suitability of hydrogen peroxide vapour sterilization on the physical and mechanical properties of medical-grade 3D printed PLA, PCL, and PC. It was determined that PLA increased in elasticity, which was likely attributable to a combination of moisture uptake and the low pressures involved with the sterilization process. The heat and low pressures of sterilization caused PCL to undergo permanent physical deformations, resulting in an increase in thickness, an increase in elasticity, and an increase in strain at ultimate tensile strength. Lastly, PC experienced a statistically significant increase in thickness and width as a result of sterilization, likely attributable to the uptake of moisture and exposure to low pressures, which contributed to an increase in elasticity and ultimate tensile strength.

The implications of this work are directed at benefitting the medical device manufacturing industry. With the advent of applying 3D printing technology in the medical manufacturing sector, a need has been identified for sterile medical manufacturing guidelines, that can provide insight as to the effects of sterilization on material performance (Brown et al., 2002). Sterile device design and production should be of utmost importance to this sector, as post-print microbial activity could compromise the well-being of patients who may one day rely on *in vivo* medical devices manufactured with this technology. This study explored how several common, biocompatible, printable plastics respond to exposure to a single sterilization technology. Additionally, it presented rudimentary predictive models that can guide medical device designers in accommodating for some dimensional changes that may occur in response to H_2O_2 vapour sterilization. The-

se findings can function as a building block for future work on other materials and sterilization technologies.

Further work is required to determine the extent of the moisture- and vacuum-induced changes in sample thickness, and whether or not printer-specific phenomena occurred in this study. Additionally, many other biocompatible and printable materials exist on the market that can be evaluated for the application of other sterilization methods. Lastly, due to the antibiotic-eluting properties of the PLA and PCL materials used in this experiment, work could be done to determine the efficacy of the antibiotic post-sterilization.

References

Adler, S., Scherrer, M., & Daschner, F. D. (1998). Costs of low-temperature plasma sterilization compared with other sterilization methods. *Journal of Hospital Infection*, *40*(2), 125–134. http://doi.org/10.1016/S0195-6701(98)90091-3

Agalloco, J., Akers, J., & Madsen, R. (2004). Aseptic processing: A review of current industry practice. *Pharmaceutical Technology*, *28*(10), 126.

Agarwala, M. K., Jamalabad, V. R., Langrana, N. A., Safari, A., Whalen, P. J., & Danforth, S. C. (1996). Structural quality of parts processed by fused deposition. *Rapid Prototyping Journal*, *2*(4), 4–19. http://doi.org/10.1108/13552549610732034

Ahn, S.-H., Montero, M., Odell, D., Roundy, S., & Wright, P. K. (2002). Anisotropic material properties of fused deposition modeling ABS. *Rapid Prototyping Journal*, *8*(4), 248–257. http://doi.org/10.1108/13552540210441166

Allen, R. C., & Bauer, R. S. (1988). Moisture-Related Failure. In *Engineered Materials Handbook Volume 2: Engineering Plastics* (pp. 761–769). Metals Park, OH: ASM International.

Anderson, J. M., Brown, S. A., Hoffman, A. S., Kowalski, J. B., Merritt, K., Morrissey, R. F., Ratner, B. D., & Schoen, F. J. (2008). Implants, Devices, and Biomaterials: Issues Unique to this Field. In *Biomaterials Science: An Introduction to Materials in Medicine* (pp. 752–766).

Armentano, I., Dottori, M., Fortunati, E., Mattioli, S., & Kenny, J. M. (2010). Biodegradable polymer matrix nanocomposites for tissue engineering: A review. *Polymer Degradation and Stability*, *95*(11), 2126–2146. http://doi.org/10.1016/j.polymdegradstab.2010.06.007

ASM International. (2002). *Atlas of Stress-Strain Curves* (2nd ed.).

ASTM. (2012). *D883-12 Standard Terminology Relating to Plastics*.

ASTM. (2013). *D638-03 Standard Test Method for Tensile Properties of Plastics*.

Bagsik, A., & Schöoppner, V. (2011). Mechanical Properties of Fused Deposition Modeling Parts Manufactured with ULTEM 9085. *Proceedings of ANTEC (Vol.*

2011), 1294–1298.

Banks, J. (2013). Adding Value in Additive Manufacturing. *IEEE Pulse*, *4*(6), 22–26. http://doi.org/10.1109/mpul.2013.2279617

Bartczak, Z. (2005). Effect of Chain Entanglements on Plastic Deformation Behavior of Linear Polyethylene. *Macromolecules*, *38*(18), 7702–7713. http://doi.org/10.1021/ma050815y

Bathina, M. N., Mickelsen, S., Brooks, C., Jaramillo, J., Hepton, T., & Kusumoto, F. M. (1998). Safety and efficacy of hydrogen peroxide plasma sterilization for repeated use of electrophysiology catheters. *Journal of the American College of Cardiology*, *32*(5), 1384–1388. http://doi.org/10.1016/S0735-1097(98)00401-X

Beer, F. P., & Johnston, E. R. J. (1985). *Mechanics of Materials*. Toronto: McGraw-Hill Ryerson Ltd.

Bellini, A., & Guceri, S. (2003). Mechanical characterization of parts fabricated using fused deposition modeling. *Rapid Prototyping Journal*, *9*(4), 252–264. http://doi.org/Doi 10.1108/13552540310489631

Boland, T., Ovslanikov, A., Chickov, B. N., Doraiswamy, A., Narayan, R. J., Yeong, W. Y., Leong, K. F., & Chua, C. K. (2007). Rapid Prototyping of Artificial Tissues and Medical Devices. *Advanced Materials & Processes*, *165*(4), 51–53.

Brinson, H. F., & Brinson, L. C. (2008). *Polymer Engineering Science and Viscoelasticity: An Introduction*. Boston, MA: Springer US. http://doi.org/10.1007/978-0-387-73861-1

Brown, S. A., Merritt, K., Woods, T. O., McNamee, S. G., & Hitchins, V. M. (2002). Effects of Different Disinfection and Sterilization Methods on Tensile Strength of Materials Used for Single-Use Devices. *Biomedical Instrumentation & Technology*, *36*(1), 23–27. http://doi.org/10.2345/0899-8205(2002)36[23:EODDAS]2.0.CO;2

Chua, C. K., Leong, K. F., & Lim, C. S. (2010). *Rapid Prototyping: Principles and Applications (3rd Edition)*. Singapore: World Scientific Publishing Co. Pte. Ltd.

Chung, S., Kern, R., Koukol, R., Barengoltz, J., & Cash, H. (2008). Vapor hydrogen

peroxide as alternative to dry heat microbial reduction. *Advances in Space Research*, *42*(6), 1150–1160. http://doi.org/10.1016/j.asr.2008.01.005

Cottam, E., Hukins, D. W. L., Lee, K., Hewitt, C., & Jenkins, M. J. (2009). Effect of sterilisation by gamma irradiation on the ability of polycaprolactone (PCL) to act as a scaffold material. *Medical Engineering and Physics*, *31*(2), 221–226. http://doi.org/10.1016/j.medengphy.2008.07.005

de Gennes, P. G. (1971). Reptation of a Polymer Chain in the Presence of Fixed Obstacles. *The Journal of Chemical Physics*, *55*(2), 572. http://doi.org/10.1063/1.1675789

Dempsey, D. K., Carranza, C., Chawla, C. P., Gray, P., Eoh, J. H., Cereceres, S., & Cosgriff-Hernandez, E. M. (2014). Comparative analysis of in vitro oxidative degradation of poly(carbonate urethanes) for biostability screening. *Journal of Biomedical Materials Research - Part A*, *102*(10), 3649–3665. http://doi.org/10.1002/jbm.a.35037

Dimitrov, D., Schreve, K., & Beer, N. De. (2006). Advances in three dimensional printing - state of the art and future perspectives. *Rapid Prototyping Journal*, *12*(3), 136–147. http://doi.org/10.1108/13552540610670717

Dodiuk, H., & Goodman, S. H. (2013). *Handbook of thermoset plastics*. USA: William Andrew.

Drumright, R. E., Gruber, P. R., & Henton, D. E. (2000). Polylactic acid technology. *Advanced Materials*, *12*(23), 1841–1846. http://doi.org/10.1002/1521-4095(200012)12:23<1841::AID-ADMA1841>3.0.CO;2-E

Engelberg, I., & Kohn, J. (1991). Physico-mechanical properties of degradable polymers used in medical applications: A comparative study. *Biomaterials*, *12*(3), 292–304. http://doi.org/10.1016/0142-9612(91)90037-B

Eshraghi, S., & Das, S. (2010). Mechanical and microstructural properties of polycaprolactone scaffolds with one-dimensional, two-dimensional, and three-dimensional orthogonally oriented porous architectures produced by selective laser sintering. *Acta Biomaterialia*, *6*(7), 2467–2476.

http://doi.org/10.1016/j.actbio.2010.02.002

FDA. (2008). Updated 510(k) Sterility Review Guidance K90-1 ; Guidance for Industry and FDA, *510*.

Fedorovich, N. E., Alblas, J., Hennink, W. E., Öner, F. C., & Dhert, W. J. A. (2011). Organ printing: The future of bone regeneration? *Trends in Biotechnology*, *29*(12), 601–606. http://doi.org/10.1016/j.tibtech.2011.07.001

Feldman, L. A., & Hui, H. K. (1997). Compatibility of Medical Devices and Materials with Low-Temperature Hydrogen Peroxide Gas Plasma. *Medical Device and Diagnostic Industry*, *19*, 57–63.

Fernández, J., Larrañaga, A., Etxeberria, A., Wang, W., & Sarasua, J. R. (2014). A new generation of poly(lactide/ε-caprolactone) polymeric biomaterials for application in the medical field. *Journal of Biomedical Materials Research Part A*, *102*(10), 3573–3584. http://doi.org/10.1002/jbm.a.35036

Filipczak, K., Wozniak, M., Ulanski, P., Olah, L., Przybytniak, G., Olkowski, R. M., Lewandowska-Szumiel, M., & Rosiak, J. M. (2006). Poly(ε-caprolactone) biomaterial sterilized by E-beam irradiation. *Macromolecular Bioscience*, *6*(4), 261–273. http://doi.org/10.1002/mabi.200500215

Fonda, C. (2013). A Practical Guide to Your First 3D Print. In *Low-Cost 3D Printing for Science, Education and Sustainable Development* (pp. 25–60). ICTP—The Abdus Salam International Centre for Theoretical Physics. Retrieved from http://sdu.ictp.it/3D/

French, G. L., Otter, J. A., Shannon, K. P., Adams, N. M. T., Watling, D., & Parks, M. J. (2004). Tackling contamination of the hospital environment by methicillin-resistant Staphylococcus aureus (MRSA): A comparison between conventional terminal cleaning and hydrogen peroxide vapour decontamination. *Journal of Hospital Infection*, *57*(1), 31–37. http://doi.org/10.1016/j.jhin.2004.03.006

Garlotta, D. (2002). A Literature Review of Poly (Lactic Acid). *Journal of Polymers and the Environment*, *9*(2), 63–84. http://doi.org/10.1023/A:1020200822435

Gorna, K., & Gogolewski, S. (2003a). Molecular stability, mechanical properties, surface

characteristics and sterility of biodegradable polyurethanes treated with low-temperature plasma. *Polymer Degradation and Stability*, *79*(3), 475–485. http://doi.org/10.1016/S0141-3910(02)00363-4

Gorna, K., & Gogolewski, S. (2003b). The effect of gamma radiation on molecular stability and mechanical properties of biodegradable polyurethanes for medical applications. *Polymer Degradation and Stability*, *79*(3), 465–474. http://doi.org/10.1016/S0141-3910(02)00362-2

Greene, V. W. (1986). Reuse of disposable medical devices: historical and current aspects. *Infection Control : IC*, *7*(10), 508–513.

Groth, C., Kravitz, N. D., Jones, P. E., Graham, J. W., & Redmond, W. R. (2014). Three-dimensional printing technology. *Journal of Clinical Orthodontics*, *48*(8), 475–85. Retrieved from http://www.ncbi.nlm.nih.gov/pubmed/25226040

Harrysson, O. L. A., Hosni, Y. A., & Nayfeh, J. F. (2007). Custom-designed orthopedic implants evaluated using finite element analysis of patient-specific computed tomography data: femoral-component case study. *BMC Musculoskeletal Disorders*, *8*(4), 91. http://doi.org/10.1186/1471-2474-8-91

Helsen, J. A., & Missirlis, Y. (2010). *Biomaterials: a Tantalus experience*. Springer Science & Business Media.

Hiemenz, B. J. (2011). 3D Printing with FDM: How it Works. Eden Prairie, MN: Stratasys Inc.

Ho, H. C. H., Cheung, W. L., & Gibson, L. (2002). Effects of graphite powder on the laser sintering behaviour of polycarbonate. *Rapid Prototyping Journal*, *8*(4), 233–242. http://doi.org/Doi 10.1108/13552540210441148

Hooper, K. A., Cox, J. D., & Kohn, J. (1997). Comparison of the effect of ethylene oxide and γ-irradiation on selected tyrosine-derived polycarbonates and poly(L-lactic acid). *Journal of Applied Polymer Science*, *63*(11), 1499–1510. http://doi.org/10.1002/(SICI)1097-4628(19970314)63:11<1499::AID-APP12>3.0.CO;2-Y

Hultman, C., Hill, A., & McDonnell, G. (2007). The physical chemistry of

decontamination with gaseous hydrogen peroxide. *Pharmaceutical Engineering*, *27*(1), 22–32.

Hutmacher, D. W. (2000). Scaffolds in tissue engineering bone and cartilage. *Biomaterials*, *21*(24), 2529–2543. http://doi.org/10.1016/S0142-9612(00)00121-6

Hutmacher, D. W., Schantz, T., Zein, I., Ng, K. W., Teoh, S. H., & Tan, K. C. (2001). Mechanical properties and cell cultural response of polycaprolactone scaffolds designed and fabricated via fused deposition modeling. *Journal of Biomedical Materials Research*, *55*(2), 203–216. http://doi.org/10.1002/1097-4636(200105)55:2<203::AID-JBM1007>3.0.CO;2-7

International Union of Pure and Applied Chemisty. (2014). radical (free radical). In *IUPAC Compendium of Chemical Terminology* (p. 1662). Research Triagle Park, NC: IUPAC. http://doi.org/10.1351/goldbook.R05066

Jagannathan, L., & Jawahar, C. (2005). Perspective Correction Methods for Camera Based Document Analysis. In *Proc. First Int. Workshop on Camera-based Document Analysis and Recognition* (pp. 148–154). Retrieved from http://imlab.jp/cbdar2005/proceedings/papers/P6.pdf

Jiankang, H., Dichen, L., Bingheng, L., Zhen, W., & Tao, Z. (2006). Custom fabrication of composite tibial hemi-knee joint combining CAD/CAE/CAM techniques. *Proceedings of the Institution of Mechanical Engineers, Part H: Journal of Engineering in Medicine*, *220*(8), 823–830. http://doi.org/10.1243/09544119JEIM207

Johnston, M. D., Lawson, S., & Otter, J. A. (2005). Evaluation of hydrogen peroxide vapour as a method for the decontamination of surfaces contaminated with Clostridium botulinum spores. *Journal of Microbiological Methods*, *60*(3), 403–411. http://doi.org/10.1016/j.mimet.2004.10.021

Jones, C. W., & Clark, J. H. (1999). *Applications of Hydrogen Peroxide and Derivatives*. *Journal of Chemical Information and Modeling* (Vol. 53). http://doi.org/10.1017/CBO9781107415324.004

Kim, E., Shin, Y.-J., & Ahn, S.-H. (2016). The effects of moisture and temperature on the

mechanical properties of additive manufacturing components: fused deposition modeling. *Rapid Prototyping Journal*, *22*(6), 887–894. http://doi.org/10.1108/RPJ-08-2015-0095

Klapes, N. A., & Vesley, D. (1990). Vapour-phase hydrogen-peroxide as a surface decontaminant and sterilant. *Applied and Environmental Microbiology*, *56*(2), 503–506.

Kondor, S., Grant, G., Liacouras, P., Schmid, J. R., Parsons, M., Rastogi, V. K., Smith, L. S., Macy, B., Sabart, B., & Macedonia, C. (2013). On Demand Additive Manufacturing of a Basic Surgical Kit. *Journal of Medical Devices*, *7*(September 2013), 30916–1. http://doi.org/10.1115/1.4024490

Kontakis, G. M., Pagkalos, J. E., Tosounidis, T. I., Melissas, J., & Katonis, P. (2015). Bioabsorbable materials in orthopaedics, *73*(2), 159–169.

Kubyshkina, G., Zupančič, B., Štukelj, M., Grošelj, D., Marion, L., & Emri, I. (2011). The influence of different sterilization techniques on the time-dependent behavior of polyamides.". *Journal of Biomaterials and Nanobiotechnology*, *2*(4), 361–368. http://doi.org/10.4236/jbnb.2011.24045

Kurtz, S. M., Pruitt, L., Jewett, C. W., Crawford, R. P., Crane, D. J., & Edidin, A. A. (1998). The yielding, plastic flow, and fracture behavior of ultra-high molecular weight polyethylene used in total joint replacements. *Biomaterials*, *19*(21), 1989–2003. http://doi.org/10.1016/S0142-9612(98)00112-4

Lam, C. X., Savalani, M. M., Teoh, S. H., & Hutmacher, D. W. (2008). Dynamics of in vitro polymer degradation of polycaprolactone-based scaffolds: accelerated versus simulated physiological conditions. *Biomed Mater*, *3*(3), 34108. http://doi.org/S1748-6041(08)69192-5 [pii]\r10.1088/1748-6041/3/3/034108

Lambert, B. J., Mendelson, T. A., & Craven, M. D. (2011). Radiation and ethylene oxide terminal sterilization experiences with drug eluting stent products. *AAPS PharmSciTech*, *12*(4), 1116–26. http://doi.org/10.1208/s12249-011-9644-8

Landel, R. F., & Nielsen, L. E. (1993). *Mechanical properties of polymers and composites*. CRC Press.

Langer, R., & Tirrell, D. A. (2004). Designing materials for biology and medicine. *Nature*, *428*(6982), 487–492. http://doi.org/10.1038/nature02388

Lee, M. H., Kim, H. L., Kim, C. H., Lee, S. H., Kim, J. K., Lee, S. J., & Park, J. C. (2008). Effects of low temperature hydrogen peroxide gas on sterilization and cytocompatibility of porous poly(d,l-lactic-co-glycolic acid) scaffolds. *Surface and Coatings Technology*, *202*(22–23), 5762–5767. http://doi.org/10.1016/j.surfcoat.2008.06.114

Levine, H., & Slade, L. (1988). Water as a plasticizer: physio-chemical aspects of low-moisture polymeric systems. In F. Franks (Ed.), *Water Science Reviews 3: Water Dynamics* (pp. 79–185). Cambridge, UK: Cambridge University Press.

Lucas, A. D., Merritt, K., Hitchins, V. M., Woods, T. O., McNamee, S. G., Lyle, D. B., & Brown, S. A. (2003). Residual ethylene oxide in medical devices and device material. *Journal of Biomedical Materials Research. Part B, Applied Biomaterials*, *66*(2), 548–552. http://doi.org/10.1002/jbm.b.10036

M. Chanda and S. Roy, & Raton, B. (2007). *Plastics technology handbook*. *CRC Press/Taylor & Francis Group* (Vol. 8). http://doi.org/10.1007/SpringerReference_22934

Martienssen, W., & Warlimont, H. (2005). *Springer Handbook of Condensed Matter and Materials Data*. (W. Martienssen & H. Warlimont, Eds.) (Vol. 1). Berlin: Springer Berlin Heidelberg. http://doi.org/10.1007/3-540-30437-1

Masood, S. H. (1996). Intelligent rapid prototyping with fused deposition modelling. *Rapid Prototyping Journal*, *2*(1), 24–33. http://doi.org/10.1108/13552549610109054

Massey, L. K. (2005). *The Effects of Sterilization Methods on Plastics and Elastomers*. *Thermoplastics*. Retrieved from http://link.springer.com/content/pdf/10.1007/978-94-009-1531-2_30.pdf

Meijer, H. E. H., & Govaert, L. E. (2005). Mechanical performance of polymer systems: The relation between structure and properties. *Progress in Polymer Science*, *30*(8–9), 915–938. http://doi.org/10.1016/j.progpolymsci.2005.06.009

Middleton, J. C., & Tipton, A. J. (2000). Synthetic biodegradable polymers as orthopedic

devices. *Biomaterials*, *21*(23), 2335–2346. http://doi.org/10.1016/S0142-9612(00)00101-0

Moisan, M., Barbeau, J., Moreau, S., Pelletier, J., Tabrizian, M., & Yahia, L. (2001). Low-temperature sterilization using gas plasmas: a review of the experiments and an analysis of the inactivation mechanisms. *International Journal of Pharmaceutics*, *226*(1–2), 1–21. http://doi.org/10.1016/S0378-5173(01)00752-9

Nagarajan, S., & Reddy, B. S. R. (2009). Bio-absorbable polymers in implantation-an overview. *Journal of Scientific and Industrial Research*, *68*(12), 993–1009.

Nair, L. S., & Laurencin, C. T. (2007). Biodegradable polymers as biomaterials. *Progress in Polymer Science*, *32*(8–9), 762–798. http://doi.org/10.1016/j.progpolymsci.2007.05.017

Narkis, M., Raiter, I., Shkolnik, S., Siegmannz, A., & Eyerer, P. (1987). Structure and tensile behavior of irradiation-and peroxide-crosslinked polyethylenes. *Journal of Macromolecular Science, Part B*, *26*(1), 37–58. http://doi.org/10.1080/00222348708248057

Nikbin, K. M. (2009). Predicting Creep and Creep/Fatigue Crack Initiation and Growth for Virtual Testing and Life Assessment of Components. In *Virtual Testing and Predictive Modeling* (pp. 105–136). Boston, MA: Springer US. http://doi.org/10.1007/978-0-387-95924-5_5

Nugroho, P., Mitomo, H., Yoshii, F., & Kume, T. (2001). Degradation of poly(L-lactic acid) by γ-irradiation. *Polymer Degradation and Stability*, *72*(2), 337–343. http://doi.org/10.1016/S0141-3910(01)00030-1

O'Neil, M. J., Heckelman, P. E., Koch, C. B., & Roman, K. J. (Eds.). (2006). *The Merck Index - An Encyclopedia of Chemicals, Drugs, and Biologicals*. *Merck Research Laboratories* (14th ed.). Whitehouse Station, NJ.

Pahl, G., & Beitz, W. (2013). *Engineering design: a systematic approach*. Springer Science & Business Media.

Park, E. (2011). Effects of Electron Beam Irradiation on Properties of. *Iranian Polymer Jornal*, *20*(11), 873–885.

Peniston, S. J., & Choi, S. J. (2007). Effect of sterilization on the physicochemical properties of molded poly(L-lactic acid). *Journal of Biomedical Materials Research Part B: Applied Biomaterials*, *80B*(1), 67–77. http://doi.org/10.1002/jbm.b.30570

Peppas, N. A., & Langer, R. (2014). New Challenges in Biomaterials, *263*(5154), 1715–1720.

Petrak, M., & Rodgers, L. M. B. (2015). Antimicrobial articles produced by additive manufacturing. United States: Google Patents. Retrieved from https://www.google.com/patents/US20150290280

Pryde, C. A., & Hellman, M. Y. (1980). Solid state hydrolysis of bisphenol-A polycarbonate. I. Effect of phenolic end groups. *Journal of Applied Polymer Science*, *25*(11), 2573–2587. http://doi.org/10.1002/app.1980.070251114

Pulkkinen, M., Malin, M., Böhm, J., Tarvainen, T., Wirth, T., Seppälä, J., & Järvinen, K. (2009). In vivo implantation of 2,2'-bis(oxazoline)-linked poly-ε-caprolactone: Proof for enzyme sensitive surface erosion and biocompatibility. *European Journal of Pharmaceutical Sciences*, *36*, 310–319. http://doi.org/10.1016/j.ejps.2008.10.011

Rankin, T. M., Giovinco, N. A., Cucher, D. J., Watts, G., Hurwitz, B., & Armstrong, D. G. (2014). Three-dimensional printing surgical instruments: Are we there yet? *Journal of Surgical Research*, *189*(2), 193–197. http://doi.org/10.1016/j.jss.2014.02.020

Rauwendaal, C. (2014). *Polymer Extrusion*. *Polymer Extrusion*. München: Carl Hanser Verlag GmbH & Co. KG. http://doi.org/10.3139/9781569905395

Ravve, A. (2012). *Principles of Polymer Chemistry*. *Journal of Chemical Information and Modeling* (3rd ed., Vol. 53). New York, NY: Springer New York. http://doi.org/10.1007/978-1-4614-2212-9

Rozema, F. R., Bos, R. R., Boering, G., van Asten, J. A., Nijenhuis, A. J., & Pennings, A. J. (1991). The effects of different steam-sterilization programs on material properties of poly(L-lactide). *Journal of Applied Biomaterials*, *2*(1), 23–28. http://doi.org/10.1002/jab.770020104

Rutala, W. A., & Weber, D. J. (2008). *Guideline for Disinfection and Sterilization in*

Healthcare Facilities , 2008. *Centers for Disease Control and Prevention*.

Sachlos, E., & Czernuszka, J. T. (2003). Making tissue engineering scaffolds work. Review on the application of solid freeform fabrication technology to the production of tissue engineering scaffolds. *European Cells and Materials*, *5*, 29–40.

Sastri, V. R. (2010). Engineering Thermoplastics. In *Plastics in Medical Devices* (pp. 121–174).

Schilling, F. C., Ringo, W. M., Sloane, N. J. A., & Bovey, F. A. (1981). 13C NMR study of the hydrolysis of bisphenol A polycarbonate. *Macromolecules*, *14*(18), 532–537.

Schindelin, J., Arganda-Carreras, I., Frise, E., Kaynig, V., Longair, M., Pietzsch, T., Preibisch, S., Rueden, C., Saalfeld, S., Schmid, B., Tinevez, J.-Y., White, D. J., Hartenstein, V., Eliceiri, K., Tomancak, P., & Cardona, A. (2012). Fiji: an open-source platform for biological-image analysis. *Nature Methods*, *9*(7), 676–682. http://doi.org/10.1038/nmeth.2019

Schohn, D. C., Jahn, H. A., Eber, M., & Hauptmann, G. (1986). Biocompatibility and Hemodynamic Studies during Polycarbonate versus Cuprophane Membrane Dialysis. *Blood Purification*, *4*(1–3), 102–111. Retrieved from http://www.karger.com/DOI/10.1159/000169433

Senden, D. J. A., Engels, T. A. P., Söntjens, S. H. M., & Govaert, L. E. (2012). The effect of physical aging on the embrittlement of steam-sterilized polycarbonate. *Journal of Materials Science*, *47*(16), 6043–6046. http://doi.org/10.1007/s10853-012-6512-1

Sharke, P. (2001). Rapid transit to manufacturing. *Mechanical Engineering*, *123*(3), 63–67.

Sharp, J. S., Forrest, J. A., & Jones, R. A. L. (2001). Swelling of Poly (DL-lactide) and Polylactide-co-glycolide in Humid Environments. *Macromolecules*, *34*(25), 8752–8760. http://doi.org/10.1021/ma011163q

Shastri, V. P. (2003). Non-degradable biocompatible polymers in medicine: past, present and future. *Current Pharmaceutical Biotechnology*, *4*(5), 331–337. http://doi.org/10.2174/1389201033489694

Shuxian, Z., Wanhua, Z., & Bingheng, L. (2005). 3D reconstruction of the structure of a residual limb for customising the design of a prosthetic socket. *Medical Engineering & Physics*, *27*(1), 67–74. http://doi.org/10.1016/j.medengphy.2004.08.015

Singare, S., Lian, Q., Wang, W. P., Wang, J., Liu, Y., Li, D., & Lu, B. (2009). Rapid prototyping assisted surgery planning and custom implant design. *Rapid Prototyping Journal*, *15*, 19–23. http://doi.org/10.1108/13552540910925027

STERIS Corporation. Amsco® V-PRO® maX Low Temperature Sterilization System Operator Manual (2011). P129385-447.

Szelest-Lewandowska, A., Masiulanis, B., Szymonowicz, M., Pielka, S., & Paluch, D. (2007). Modified polycarbonate urethane: Synthesis, properties and biological investigation in vitro. *Journal of Biomedical Materials Research*, *82*(2), 509–520. http://doi.org/10.1002/jbm.a

Tamboli, S. M., Mhaske, S. T., & Kale, D. D. (2004). Crosslinked polyethylene. *Indian Journal of Chemical Technology*, *11*, 853–864.

Ulery, B. D., Nair, L. S., & Laurencin, C. T. (2011). Biomedical applications of biodegradable polymers. *Journal of Polymer Science Part B: Polymer Physics*, *49*(12), 832–864. http://doi.org/10.1002/polb.22259

Upcraft, S., & Fletcher, R. (2003). The rapid prototyping technologies. *Assembly Automation*, *23*(4), 318–330. http://doi.org/10.1108/01445150310698634

Ventola, C. L. (2014). Medical Applications for 3D Printing: Current and Projected Uses. *Pharmacy and Therapeutics*, *39*(10), 704–11. http://doi.org/10.1016/j.infsof.2008.09.005

Webb, P. A. (2000). A review of rapid prototyping (RP) techniques in the medical and biomedical sector. *Journal of Medical Engineering & Technology*, *24*(4), 149–153. http://doi.org/10.1080/03091900050163427

Weber, R. P., Vecchio, K. S., & Suarez, J. C. M. (2010). Dynamic behavior of gamma-irradiated polycarbonate. *Revista Materia*, *15*(2), 223–230. http://doi.org/10.1016/j.polymertesting.2006.10.014

Weir, N. A., Buchanan, F. J., Orr, J. F., Farrar, D. F., & Boyd, A. (2004). Processing, annealing and sterilisation of poly-L-lactide. *Biomaterials*, *25*(18), 3939–3949. http://doi.org/10.1016/j.biomaterials.2003.10.076

Wexler, A. (2016). Constant Humidity Solutions. In *CRC Handbook of Chemistry and Physics* (97th ed., p. 33). Boca Raton, FL: CRC Press/Taylor & Francis.

Williams, D. (2003). Revisiting the definition of biocompatibility. *Medical Device Technology*, *14*(8), 10—13. Retrieved from http://europepmc.org/abstract/MED/14603712

Williams, D. F. (2008). On the mechanisms of biocompatibility. *Biomaterials*, *29*(20), 2941–2953. http://doi.org/10.1016/j.biomaterials.2008.04.023

Wong, K. V., & Hernandez, A. (2012). A Review of Additive Manufacturing. *ISRN Mechanical Engineering*, *2012*, 1–10. http://doi.org/10.5402/2012/208760

Woodruff, M. A., & Hutmacher, D. W. (2010). The return of a forgotten polymer—Polycaprolactone in the 21st century. *Progress in Polymer Science*, *35*(10), 1217–1256. http://doi.org/10.1016/j.progpolymsci.2010.04.002

Woodward, S. C., Brewer, P. S., Moatamed, F., Schindler, A., & Pitt, C. G. (1985). The intracellular degradation of poly(ε-caprolactone). *Journal of Biomedical Materials Research*, *19*(4), 437–444. http://doi.org/10.1002/jbm.820190408

Young, W. C., & Budynas, R. G. (2002). *Roark's Formulas for Stress and Strain* (8th ed.). New York: McGraw-Hill Professional. http://doi.org/10.1036/007072542X

Appendix A

Table 14. Initial dimensional measurements of PLA tensile samples, in accordance with **Figure 7**. Samples that were to be sterilized are identified in grey.

		Dimensional Measurements (mm)					
Batch	Sample	WO_{left}	WO_{right}	LO	L	Avg. W_c	Avg. T
1	1	20.01	20.00	119.99	33.04	5.99	4.20
	2	20.02	19.98	119.86	33.06	5.99	4.17
	3	19.99	19.99	120.20	33.05	5.99	4.20
	4	20.01	20.03	120.02	33.03	6.01	4.12
2	1	20.03	20.05	120.19	33.04	6.02	4.16
	2	19.97	19.95	120.04	33.07	5.97	4.18
	3	20.02	20.01	120.14	33.02	5.98	4.22
	4	19.97	20.01	120.25	33.08	5.99	4.21
3	1	20.01	20.02	120.02	33.05	6.01	4.22
	2	20.01	20.01	120.04	33.01	6.01	4.20
	3	20.01	20.00	120.11	33.02	6.00	4.22
	4	20.00	20.00	119.96	33.08	5.99	4.24
4	1	19.98	19.99	120.08	33.14	5.98	4.24
	2	20.01	20.00	120.01	32.92	5.99	4.20
	3	20.00	20.00	120.00	33.08	6.00	4.22
	4	19.98	20.01	120.01	33.11	5.99	4.26
5	1	19.96	19.98	120.00	33.00	5.98	4.24
	2	19.98	19.95	119.97	33.04	5.98	4.25
	3	19.98	19.99	120.03	33.19	5.98	4.21
	4	20.01	20.00	120.03	33.10	6.01	4.21

Table 15. Initial dimensional measurements of PCL tensile samples, in accordance with **Figure 7**. Samples that were to be sterilized are identified in grey.

		Dimensional Measurements (mm)					
Batch	Sample	WO_{left}	WO_{right}	LO	L	Avg. W_c	Avg. T
1	1	20.01	20.02	120.00	33.04	6.01	4.17
	2	19.96	19.98	120.62	32.92	5.97	4.20
	3	20.00	20.00	120.47	33.12	6.00	4.15
	4	19.99	19.99	120.50	33.10	5.97	4.21
2	1	19.97	19.96	120.08	33.05	5.97	4.18
	2	20.01	20.02	120.00	33.00	6.02	4.18
	3	20.00	20.00	120.49	33.07	5.98	4.17
	4	20.01	19.98	120.02	32.99	5.98	4.18
3	1	19.99	20.00	120.02	33.03	5.99	4.16
	2	20.01	20.00	120.07	33.04	5.98	4.22
	3	19.99	20.01	120.23	33.00	5.99	4.17
	4	20.01	19.99	120.46	33.09	5.98	4.20
4	1	20.01	20.01	120.33	33.11	5.99	4.15
	2	20.01	19.99	120.26	33.07	5.99	4.17
	3	19.97	19.98	120.03	32.95	5.97	4.17
	4	20.01	20.01	120.10	33.03	5.99	4.18
5	1	20.00	19.99	120.01	32.97	5.98	4.02
	2	20.00	20.00	120.12	33.03	5.99	4.12
	3	20.01	20.00	120.39	33.04	5.99	4.09
	4	19.99	19.98	120.08	33.03	5.98	4.14

Table 16. Initial dimensional measurements of PC tensile samples, in accordance with **Figure 7**. Samples that were to be sterilized are identified in grey.

	Dimensional Measurements (mm)					
Sample	WO_{left}	WO_{right}	LO	L	Avg. W_c	Avg. T
1	20.00	20.01	120.02	33.00	6.01	3.89
2	20.01	20.01	120.01	33.00	5.99	3.87
3	20.01	20.01	119.99	33.01	6.00	3.88
4	20.00	20.01	120.01	33.00	6.00	3.88
5	19.99	20.00	120.02	33.02	5.98	3.87
6	20.01	20.01	120.01	33.01	6.00	3.88
7	20.01	19.99	120.00	33.01	5.99	3.88
8	19.98	20.00	120.00	33.00	6.00	3.86
9	20.01	20.01	120.00	33.01	6.01	3.90
10	20.00	20.02	120.01	33.00	6.00	3.87
11	19.99	20.00	120.00	33.01	5.99	3.89
12	20.02	20.00	120.01	33.01	6.00	3.87
13	20.01	20.01	119.99	33.02	6.01	3.87
14	20.01	20.01	120.01	33.00	6.02	3.88
15	19.99	20.00	120.02	33.00	5.98	3.86
16	20.00	19.98	119.99	33.01	5.99	3.87
17	20.00	20.00	120.00	33.00	6.01	3.84
18	20.01	20.01	120.01	33.01	6.00	3.86
19	20.00	20.01	119.98	33.00	6.00	3.87
20	19.99	19.99	120.00	33.00	5.99	3.87

Table 17. Measured mass, thickness, and width of PLA samples, pre-sterilization. Samples that underwent sterilization are identified in grey.

Batch	Sample	Mass (g)	Thickness (mm)	Width (mm)
1	1	7.45282	4.203	5.987
	2	7.43343	4.173	5.987
	3	7.45004	4.203	5.990
	4	7.43830	4.123	6.007
2	1	7.44209	4.157	6.023
	2	7.43460	4.183	5.973
	3	7.45046	4.220	5.983
	4	7.43631	4.207	5.990
3	1	7.43000	4.220	6.007
	2	7.45053	4.200	6.010
	3	7.45447	4.217	5.997
	4	7.44331	4.237	5.990
4	1	7.45403	4.243	5.980
	2	7.46309	4.203	5.987
	3	7.44286	4.220	5.997
	4	7.46595	4.260	5.990
5	1	7.46133	4.237	5.977
	2	7.46056	4.253	5.983
	3	7.47760	4.213	5.980
	4	7.48339	4.210	6.007

Table 18. Measured mass, thickness, and width of PLA samples, pre-conditioning. Samples that underwent sterilization are identified in grey.

Batch	Sample	Mass (g)	Thickness (mm)	Width (mm)
1	1	7.45282	4.203	5.987
	2	7.45190	4.173	5.983
	3	7.45004	4.203	5.990
	4	7.45410	4.143	6.007
2	1	7.45863	4.157	6.010
	2	7.45366	4.197	5.993
	3	7.45046	4.220	5.983
	4	7.43631	4.207	5.990
3	1	7.44832	4.230	5.990
	2	7.45053	4.200	6.010
	3	7.45447	4.217	5.997
	4	7.46304	4.263	5.973
4	1	7.47158	4.233	5.973
	2	7.46309	4.203	5.987
	3	7.45825	4.253	5.980
	4	7.46595	4.260	5.990
5	1	7.46133	4.237	5.977
	2	7.48380	4.203	5.977
	3	7.49343	4.167	5.990
	4	7.48339	4.210	6.007

Table 19. Measured mass, thickness, and width of PLA samples, pre-testing. Samples that underwent sterilization are identified in grey.

Batch	Sample	Mass (g)	Thickness (mm)	Width (mm)
1	1	7.46351	4.173	5.983
	2	7.45782	4.190	5.987
	3	7.45958	4.117	6.000
	4	7.46208	4.160	6.003
2	1	7.46577	4.167	5.993
	2	7.45822	4.213	5.993
	3	7.46083	4.173	5.997
	4	7.44716	4.150	5.997
3	1	7.45541	4.230	5.980
	2	7.46094	4.163	5.993
	3	7.46440	4.150	5.990
	4	7.46745	4.240	5.980
4	1	7.47872	4.210	5.983
	2	7.47430	4.170	5.993
	3	7.46699	4.260	5.993
	4	7.47554	4.193	5.990
5	1	7.47307	4.210	5.990
	2	7.48416	4.213	5.987
	3	7.50077	4.207	5.983
	4	7.49426	4.170	5.990

Table 20. Measured mass, thickness, and width of PCL samples, pre-sterilization. Samples that underwent sterilization are identified in grey.

Batch	Sample	Mass (g)	Thickness (mm)	Width (mm)
1	1	6.35606	4.173	6.007
	2	6.34091	4.200	5.973
	3	6.37076	4.147	5.997
	4	6.36325	4.213	5.967
2	1	6.37198	4.177	5.970
	2	6.34830	4.180	6.023
	3	6.34535	4.170	5.977
	4	6.35180	4.177	5.977
3	1	6.50280	4.157	5.993
	2	6.52004	4.220	5.980
	3	6.48211	4.173	5.990
	4	6.51655	4.200	5.977
4	1	6.50184	4.153	5.993
	2	6.53902	4.167	5.987
	3	6.49308	4.173	5.970
	4	6.51244	4.177	5.993
5	1	6.35172	4.017	5.980
	2	6.40709	4.120	5.990
	3	6.36814	4.087	5.990
	4	6.47838	4.143	5.977

Table 21. Measured mass, thickness, and width of PCL samples, pre-conditioning. Samples that underwent sterilization are identified in grey.

Batch	Sample	Mass (g)	Thickness (mm)	Width (mm)
1	1	6.37874	4.160	5.983
	2	6.34091	4.200	5.973
	3	6.39330	4.213	6.010
	4	6.36325	4.213	5.967
2	1	6.39232	4.223	5.983
	2	6.36844	4.250	6.027
	3	6.34535	4.170	5.977
	4	6.35180	4.177	5.977
3	1	6.52380	4.270	5.987
	2	6.52004	4.220	5.980
	3	6.50248	4.260	6.020
	4	6.51655	4.200	5.977
4	1	6.52710	4.247	6.003
	2	6.56650	4.260	6.010
	3	6.49308	4.173	5.970
	4	6.51244	4.177	5.993
5	1	6.35172	4.017	5.980
	2	6.52889	4.217	6.007
	3	6.36814	4.087	5.990
	4	6.50665	4.153	6.020

Table 22. Measured mass, thickness, and width of PCL samples, pre-testing. Samples that underwent sterilization are identified in grey.

Batch	Sample	Mass (g)	Thickness (mm)	Width (mm)
1	1	6.36803	4.167	5.970
	2	6.34809	4.230	5.970
	3	6.38403	4.203	6.003
	4	6.37333	4.213	5.990
2	1	6.38304	4.250	5.987
	2	6.35809	4.233	6.030
	3	6.35123	4.173	5.973
	4	6.35966	4.190	5.980
3	1	6.51409	4.240	6.003
	2	6.52926	4.213	5.973
	3	6.49320	4.257	6.020
	4	6.52408	4.203	5.973
4	1	6.51508	4.227	5.993
	2	6.55273	4.280	6.020
	3	6.50234	4.193	6.003
	4	6.52172	4.190	5.973
5	1	6.35874	4.023	5.980
	2	6.41843	4.200	6.000
	3	6.37438	4.067	5.973
	4	6.48993	4.187	6.020

Table 23. Measured mass, thickness, and width of PC samples, pre-sterilization. Samples that underwent sterilization are identified in grey.

Sample	Mass (g)	Thickness (mm)	Width (mm)
1	6.60445	3.893	6.007
2	6.58451	3.867	5.990
3	6.59714	3.880	6.000
4	6.60452	3.877	6.003
5	6.56589	3.867	5.980
6	6.57967	3.877	6.000
7	6.58200	3.883	5.990
8	6.57286	3.863	5.997
9	6.59830	3.897	6.013
10	6.59633	3.870	6.003
11	6.60465	3.887	5.990
12	6.59092	3.867	5.997
13	6.58462	3.870	6.010
14	6.59339	3.877	6.017
15	6.57844	3.863	5.983
16	6.60412	3.873	5.990
17	6.58025	3.843	6.010
18	6.61796	3.860	6.003
19	6.60445	3.870	5.997
20	6.60570	3.867	5.987

Table 24. Measured mass, thickness, and width of PC samples, pre-conditioning. Samples that underwent sterilization are identified in grey.

Sample	Mass (g)	Thickness (mm)	Width (mm)
1	6.60445	3.893	6.007
2	6.58805	3.870	5.993
3	6.60114	3.900	6.027
4	6.60452	3.877	6.003
5	6.56722	3.880	5.980
6	6.58298	3.877	6.000
7	6.58695	3.893	6.003
8	6.57709	3.860	6.007
9	6.59830	3.897	6.013
10	6.60179	3.870	6.007
11	6.60465	3.887	5.990
12	6.59617	3.873	6.017
13	6.59003	3.870	6.030
14	6.59339	3.877	6.017
15	6.57919	3.893	5.993
16	6.60412	3.873	5.990
17	6.58025	3.843	6.010
18	6.61796	3.860	6.003
19	6.60445	3.870	5.997
20	6.60570	3.867	5.987

Table 25. Measured mass, thickness, and width of PC samples, pre-testing. Samples that underwent sterilization are identified in grey.

Sample	Mass (g)	Thickness (mm)	Width (mm)
1	6.61730	3.890	6.003
2	6.59473	3.867	5.997
3	6.61237	3.897	6.013
4	6.62627	3.857	5.997
5	6.57109	3.870	5.990
6	6.58679	3.860	6.003
7	6.58982	3.883	5.997
8	6.58084	3.860	5.997
9	6.60571	3.887	6.007
10	6.60480	3.863	6.000
11	6.61197	3.877	5.973
12	6.59870	3.873	6.013
13	6.59407	3.857	6.027
14	6.60713	3.870	6.010
15	6.58946	3.880	5.983
16	6.60865	3.870	5.980
17	6.59107	3.833	6.010
18	6.62772	3.870	6.003
19	6.61154	3.863	6.000
20	6.61272	3.870	5.987

Table 26. Young's modulus (E), ultimate tensile strength ($\boldsymbol{\sigma_{UTS}}$), and strain at the point of ultimate tensile strength ($\boldsymbol{\varepsilon_{UTS}}$) in PLA, as found through tensile testing. Samples that underwent sterilization are identified in grey. Average values for the control and sterilized samples are identified, with their corresponding p-values from an ANOVA.

Batch	Sample	E (MPa)	σ_{UTS} (MPa)	ε_{UTS} ($^{mm}/_{mm}$)
1	1	993	37.5	0.055
	2	989	39.8	0.057
	3	1,024	39.1	0.054
	4	984	40.5	0.057
2	1	971	39.7	0.058
	2	956	38.3	0.058
	3	967	38.3	0.057
	4	964	38.9	0.058
3	1	932	37.7	0.062
	2	981	39.1	0.058
	3	975	39.4	0.061
	4	962	39.1	0.060
4	1	941	36.6	0.055
	2	985	39.9	0.057
	3	922	37.5	0.060
	4	967	39.4	0.062
5	1	949	38.1	0.064
	2	950	39.5	0.064
	3	975	40.3	0.057
	4	985	38.4	0.060
Average Control		979	38.8	0.059
Average Sterilized		958	38.9	0.059
Significance		p = 0.043	p = 0.832	p = 0.932

Table 27. Young's modulus (E), ultimate tensile strength ($\boldsymbol{\sigma_{UTS}}$), and strain at the point of ultimate tensile strength ($\boldsymbol{\varepsilon_{UTS}}$) in PCL, as found through tensile testing. Samples that underwent sterilization are identified in grey. Average values for the control and sterilized samples are identified, with their corresponding p-values from an ANOVA.

Batch	Sample	E (MPa)	σ_{UTS} (MPa)	ε_{UTS} ($^{mm}/_{mm}$)
1	1	112	12.3	0.410
	2	114	12.1	0.344
	3	114	12.4	0.378
	4	117	12.2	0.337
2	1	110	11.9	0.386
	2	111	12.2	0.400
	3	120	12.7	0.336
	4	116	12.5	0.346
3	1	119	12.8	0.373
	2	124	13.0	0.308
	3	121	12.8	0.380
	4	121	12.9	0.338
4	1	122	13.0	0.343
	2	118	12.6	0.356
	3	129	13.2	0.321
	4	122	12.6	0.328
5	1	126	13.8	0.313
	2	116	12.6	0.377
	3	125	13.0	0.357
	4	119	12.8	0.376
Average Control		121	12.8	0.333
Average Sterilized		116	12.6	0.378
Significance		p = 0.019	p = 0.243	p < 0.001

Table 28. Young's modulus (E), ultimate tensile strength ($\boldsymbol{\sigma_{UTS}}$), and strain at the point of ultimate tensile strength ($\boldsymbol{\varepsilon_{UTS}}$) in PC, as found through tensile testing. Samples that underwent sterilization are identified in grey. Average values for the control and sterilized samples are identified, with their corresponding p-values from an ANOVA.

Sample	E (MPa)	σ_{UTS} (MPa)	ε_{UTS} ($^{mm}/_{mm}$)
1	589	41.9	0.107
2	590	42.1	0.107
3	595	42.5	0.108
4	601	42.7	0.107
5	587	42.4	0.109
6	572	40.7	0.107
7	579	41.8	0.111
8	579	41.4	0.109
9	585	41.9	0.109
10	587	42.0	0.109
11	600	43.3	0.110
12	584	41.5	0.106
13	584	41.6	0.109
14	591	42.0	0.109
15	582	41.7	0.106
16	596	42.4	0.108
17	609	43.2	0.108
18	590	41.9	0.108
19	588	41.5	0.107
20	605	43.4	0.108
Average Control	595	42.4	0.108
Average Sterilized	584	41.8	0.108
Significance	p = 0.003	p = 0.030	p = 0.715

Table 29. *STERIS® Amsco® V-Pro® maX* 'lumen cycle' chamber temperatures and pressures. The different stages of sterilization are separated by table shading.

Sterilization Phase	Elapsed Time (MM:SS)	Chamber Temperature (ºC)	Chamber Pressure (kPa)
Injection Prime	00:00	49.6	99.5
Conditioning Vacuum Hold	01:01	49.9	0.13
Conditioning Water Check	01:31	50.1	0.14
Injection Priming	01:33	50.1	0.13
Injection Cylinder Filling	01:50	50.2	0.13
H_2O_2 Injection	01:53	50.2	0.79
Sterilization Pulse 1	03:53	49.8	1.40
Post Transition Hold	04:19	49.7	66.9
Vacuum Pull	05:19	49.5	64.3
Injection Priming	06:28	49.7	0.13
Injection Cylinder Filling	06:46	49.8	0.14
H_2O_2 Injection	06:49	49.8	0.80
Sterilization Pulse 2	08:49	50.3	1.41
Post Transition Hold	09:15	50.2	67.0
Vacuum Pull	10:15	50.0	64.2
Injection Priming	11:29	49.4	0.13
Injection Cylinder Filling	11:47	49.4	0.14
H_2O_2 Injection	11:51	49.4	0.80
Sterilization Pulse 3	13:51	50.0	1.42
Post Transition Hold	14:16	50.2	67.0
Vacuum Pull	15:16	50.5	64.3
Injection Priming	16:33	50.2	0.13
Injection Cylinder Filling	16:52	50.0	0.14
H_2O_2 Injection	16:55	50.0	0.83
Sterilization Pulse 3	18:55	49.6	1.41
Post Transition Hold	19:21	49.7	67.0
Vacuum Pull	20:21	50.3	64.3
Aeration Vacuum Hold	21:39	50.3	0.13
Aeration Vacuum Hold	27:39	50.5	0.03
Chamber Vacuum Break	28:46	50.3	99.5

Appendix B

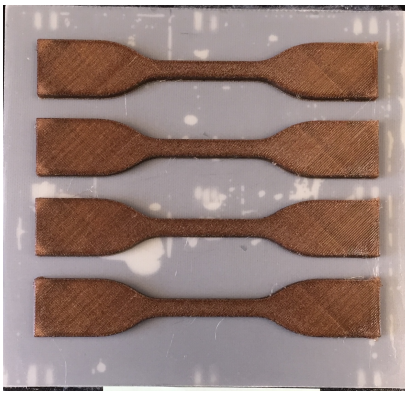

Figure 22. First PLA sample batch, printed Feb 5, 2016.

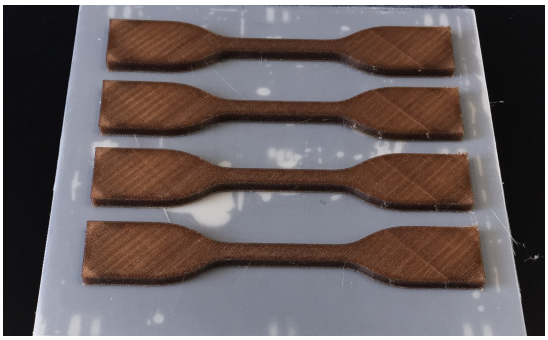

Figure 23. Second PLA sample batch, printed Feb 8, 2016.

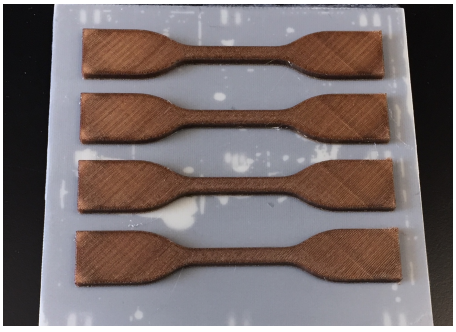

Figure 24. Third PLA sample batch, printed Feb 8, 2016.

Figure 25. Fourth PLA sample batch, printed Feb 8, 2016.

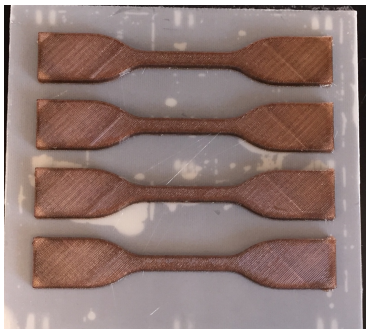

Figure 26. Fifth PLA sample batch, printed Feb 9, 2016.

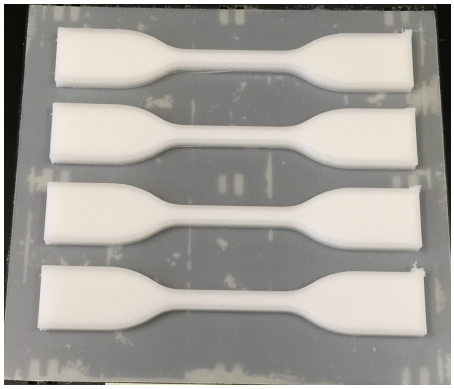

Figure 27. First PCL sample batch, printed Jan 10, 2016.

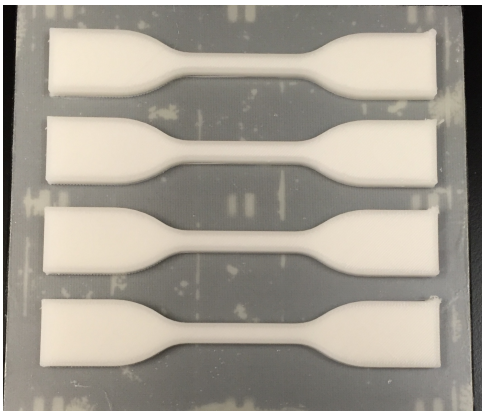

Figure 28. Second PCL sample batch, printed Jan 11, 2016.

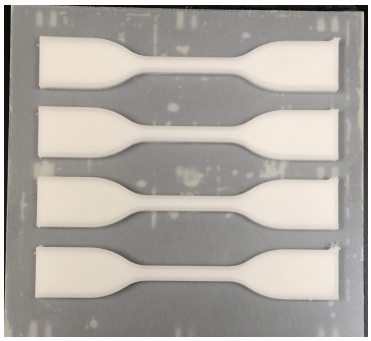

Figure 29. Third PCL sample batch, printed Jan 12, 2016.

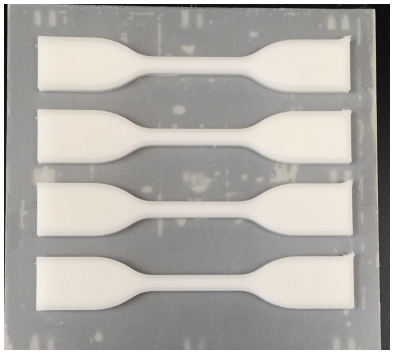

Figure 30. Fourth PCL sample batch, printed Jan 13, 2016.

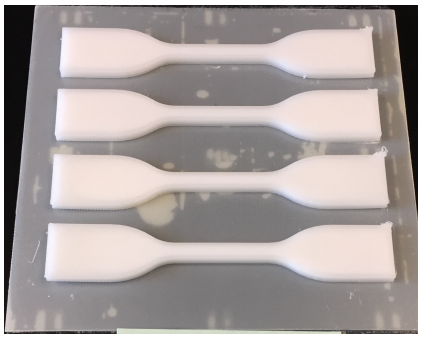

Figure 31. Fifth PCL sample batch, printed Feb 4, 2016.

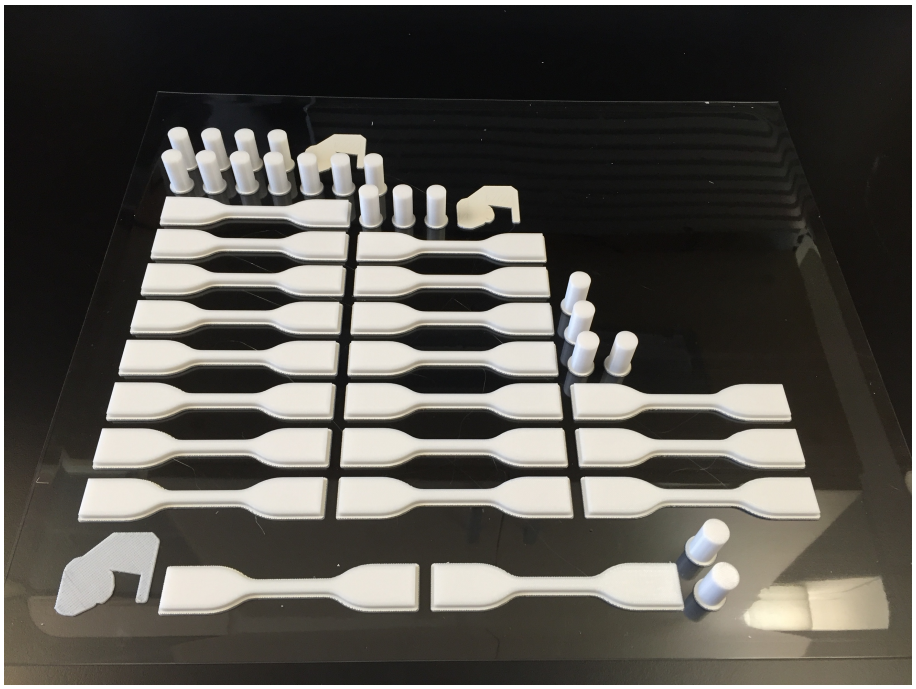

Figure 32. PC samples, printed Feb 25, 2016.

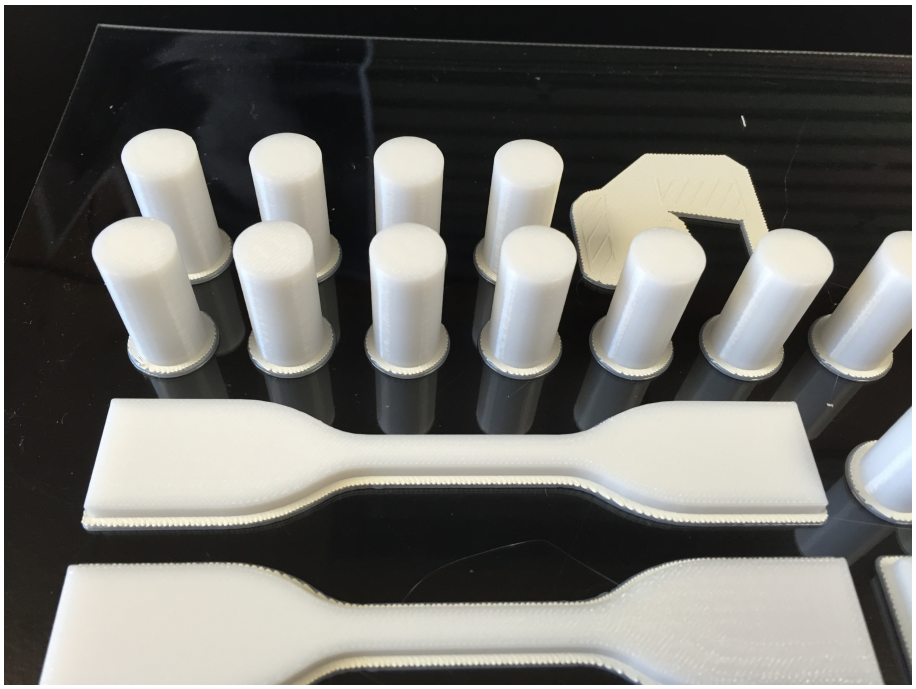

Figure 33. PC samples, printed Feb 25, 2016; close-up of sample 1.

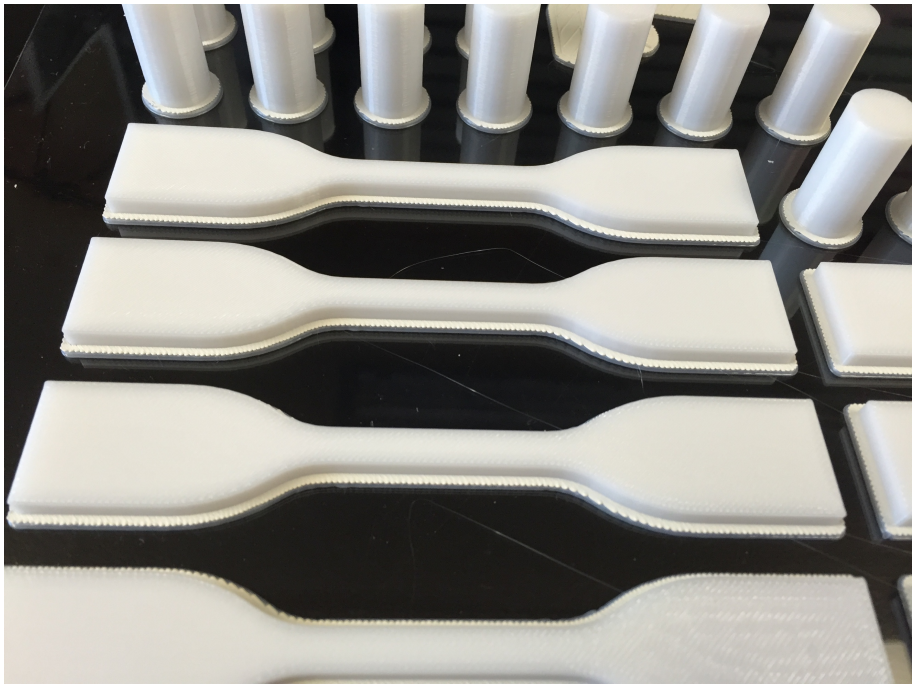

Figure 34. PC samples, printed Feb 25, 2016; close-up of samples 2 and 3.

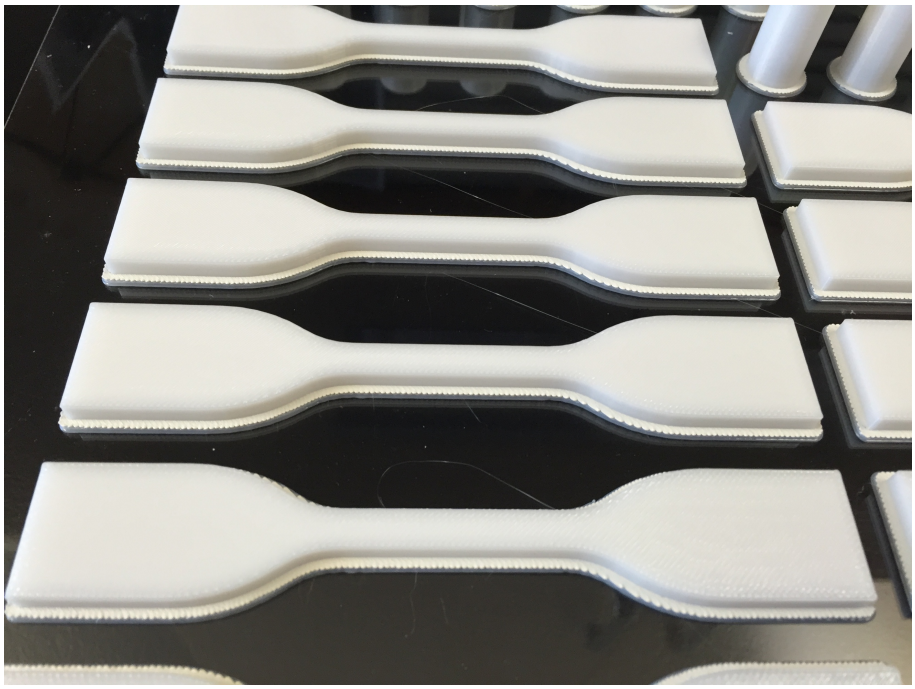

Figure 35. PC samples, printed Feb 25, 2016; close-up of samples 3, 4, and 5.

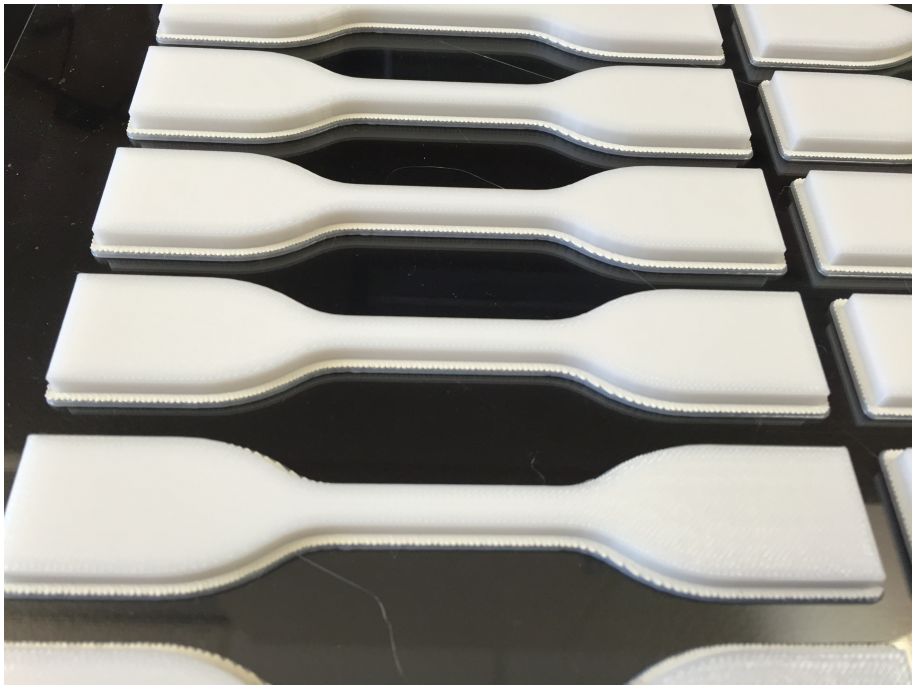

Figure 36. PC samples, printed Feb 25, 2016; close-up of samples 5, 6, and 7.

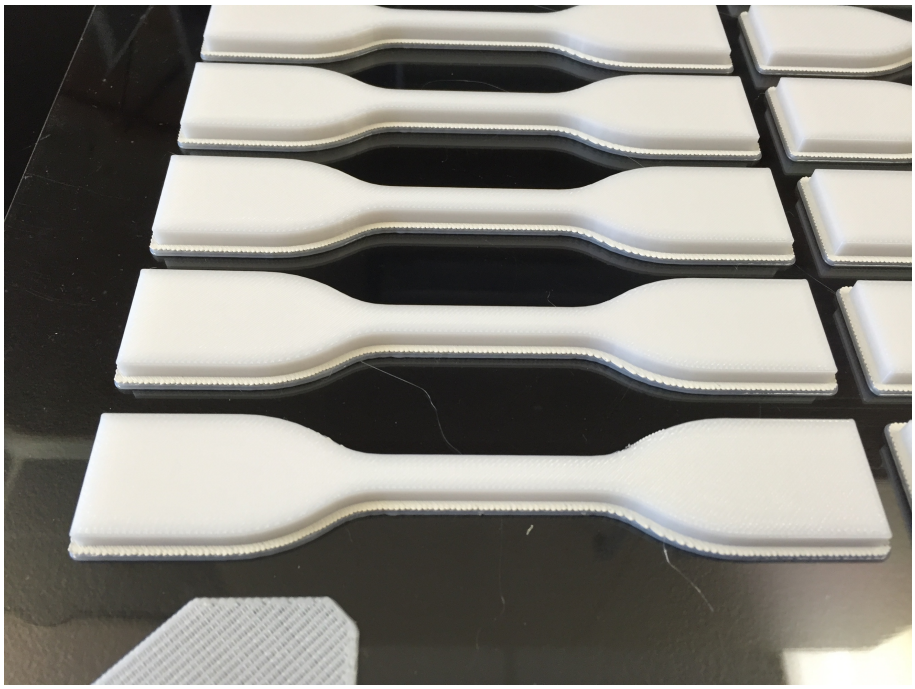

Figure 37. PC samples, printed Feb 25, 2016; close-up of samples 6, 7, and 8.

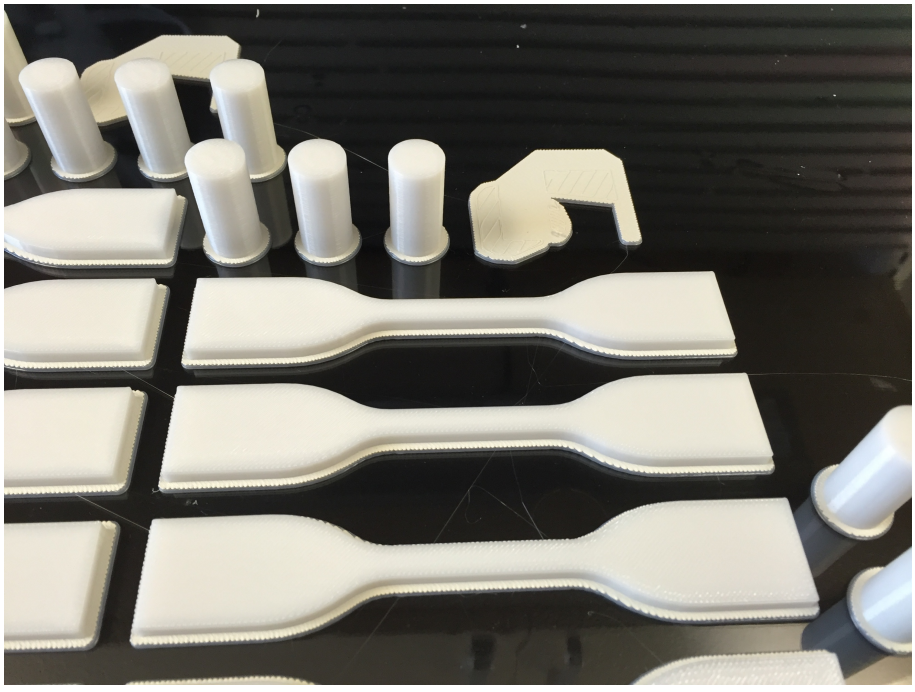

Figure 38. PC samples, printed Feb 25, 2016; close-up of samples 9, 10, and 11.

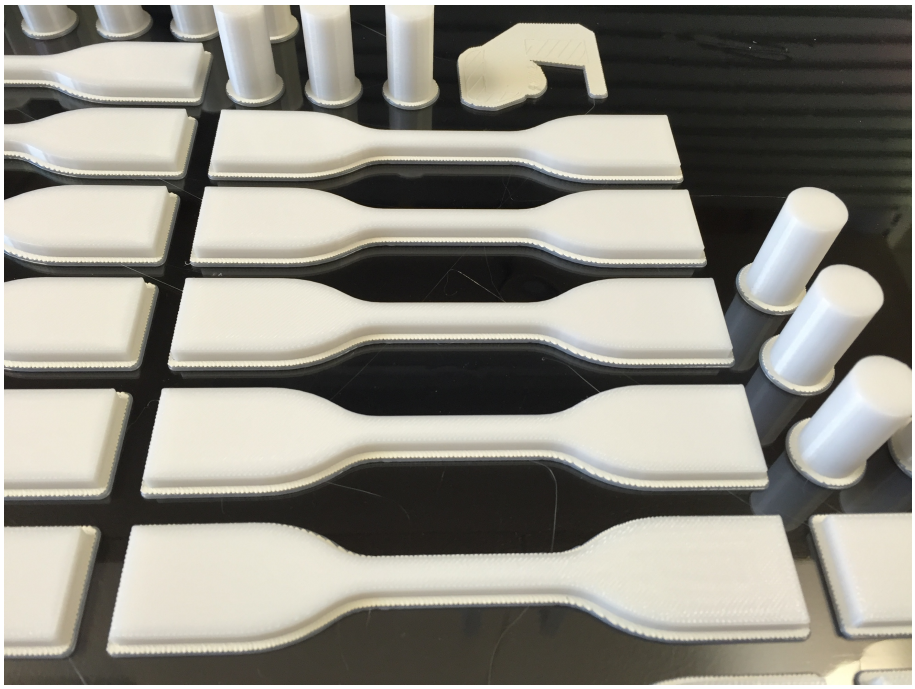

Figure 39. PC samples, printed Feb 25, 2016; close-up of samples 11, 12, and 13.

Figure 40. PC samples, printed Feb 25, 2016; close-up of samples 13, 14, and 15.

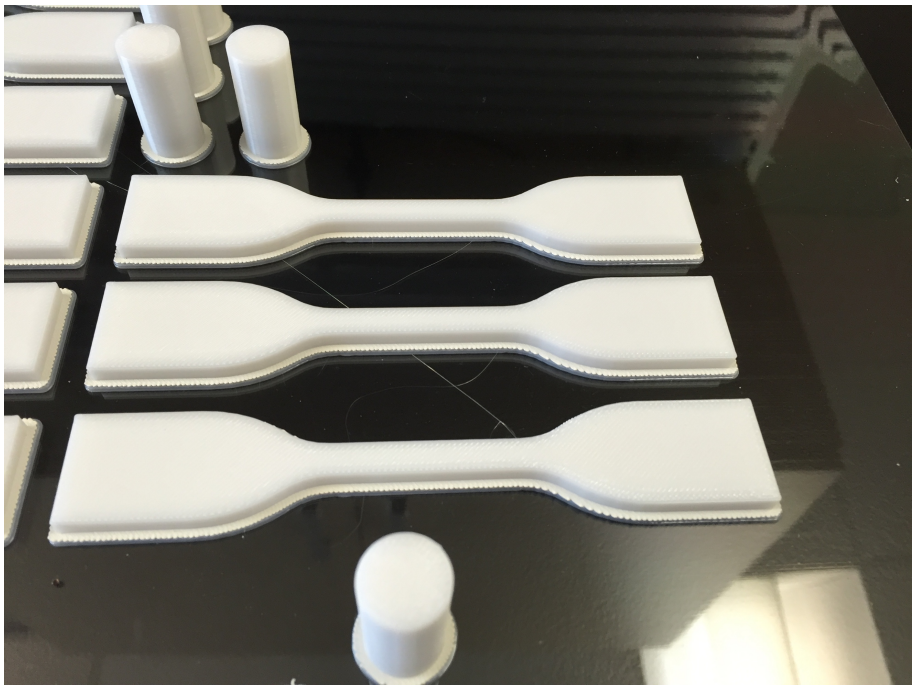

Figure 41. PC samples, printed Feb 25, 2016; close-up of samples 16, 17, and 18.

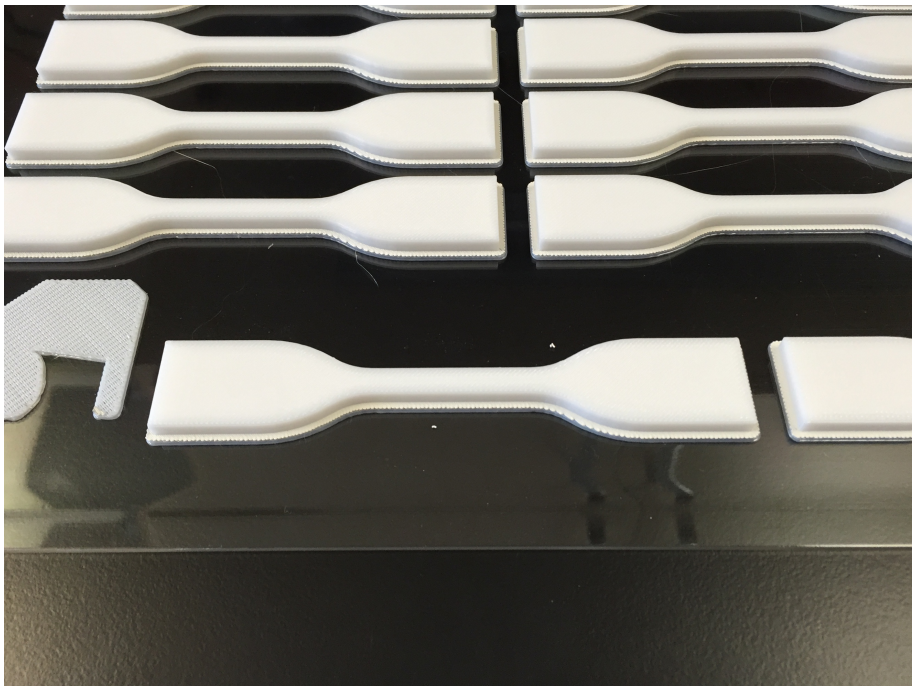

Figure 42. PC samples, printed Feb 25, 2016; close-up of sample 19.

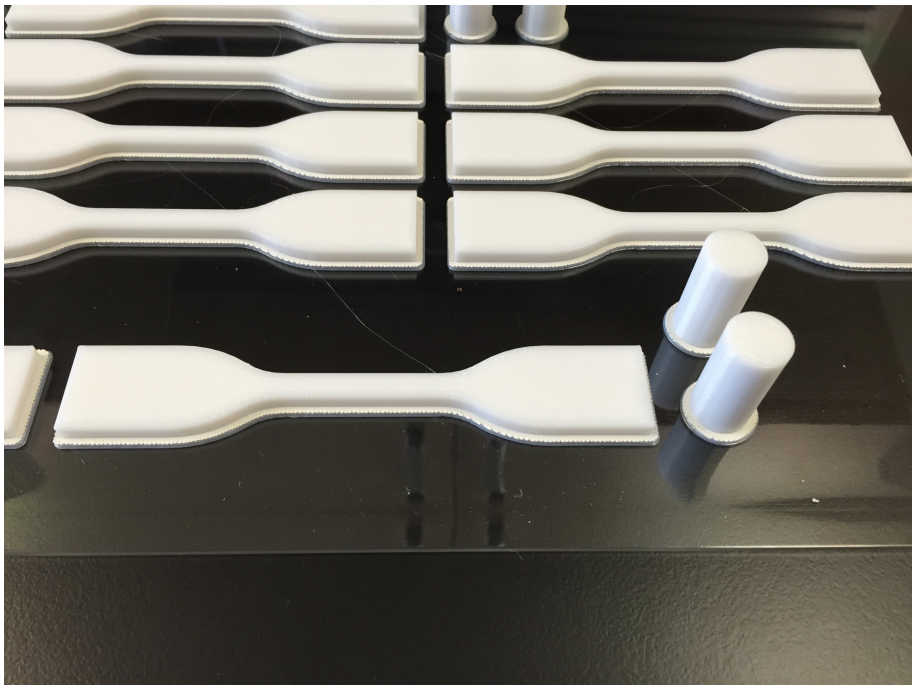

Figure 43. PC samples, printed Feb 25, 2016; close-up of sample 20.